

Defined matrices for epithelial organoid culture and disease modelling

Présentée le 8 octobre 2021

Faculté des sciences de la vie
Unité du Prof. Lutolf
Programme doctoral en chimie et génie chimique

pour l'obtention du grade de Docteur ès Sciences

par

Saba REZAKHANI

Acceptée sur proposition du jury

Prof. S. Gerber, présidente du jury
Prof. M. Lütolf, directeur de thèse
Prof. G. Schwank, rapporteur
Prof. L. Vallier, rapporteur
Prof. M. Bastings, rapporteuse

Be the change you want to see in the world.

-Mahatma Gandhi

Acknowledgements

The past 5 years were part of the journey I am pursuing to be the change I want to see in this world. I would have not been able to accomplish this without the help and support of the following people.

First, I am grateful to my thesis director and advisor **Prof. Matthias Lutolf**, who gave me the opportunity to join his laboratory of stem cell bioengineering (LSCB) in 2016. For the guidance and support, and for encouraging me to push my limits to reach my goals. Your insightful feedback helped me to sharpen my thinking and brought my work to a higher level.

Next, I would like to thank my thesis jury members: **Prof. Ludovic Vallier**, **Prof. Gerald Schwank**, **Prof. Maartje Bastings**, and **Prof. Sandrine Gerber** for their constructive comments and the great discussion.

I would also like to thank my collaborators on the liver project: **Prof. Kristina Schoonjans** for the biological insight and the guidance, **Giovanni Sorrentino** for his manner, for our fruitful discussions and for all he taught me during this project, and **Ece Yildiz** for helping with all the experiments, sharing the reagents, and for feeding the cells while I could not.

I am also deeply grateful to all the scientists and members of the EPFL facilities, without whom I could have not accomplished my PhD: **David Hacker** and **Jean-Philippe Gaudry** (Protein Expression Core Facility), **Diego Chiappe** (Proteomics Core Facility), **Bastien Mangeat**, and **Elisa Cora** (Gene Expression Core Facility), **Christian Iseli** and **Marion Leleu** (Bioinformatics Competence Center), The Bioimaging and Optics platform and **Jessica Sordet-Dessimoz** (Histology Core Facility, EPFL).

I would like to extend my sincere thanks to the three wonderful students that I had the opportunity to supervise for their Master's thesis: **Roxane Kreuter**, **Dominique Zemp**, and **Mina Blagojevic**. Those times that I worked with them, were among the most invaluable time of my PhD.

Also, a big thank you to our great secretary, Miss **Julia Prébandier**, for being very helpful with all the administrative tasks. Thank you, Julia!

I want to thank all our great lab managers who facilitated the lab routine and ensured our safety: **Evangelos Panopoulos**, **Stefanie Boy**, and **Lucie Tillard**.

I enjoyed every single moment of the past 5 years due to the presence of amazing LSCB lab members. I would like to offer my special thanks to them. Old members of LSCB (Chronological order): **Nikolce Gjorevski** for teaching me the organoid work, and for his critical feedbacks, **Gena Nikitin** for his help with chemistry and our interesting conversations, **Lura Kolb**, **Sylke Hoehnel**, **Sara Geraldo**, and **Sonja Giger** for all their support, **Nathalie Brandenburg** for our scientific discussion and providing me with the SUN plates, **Vincent Trachsel** for our lunch discussions,

Delphine Blondel for our collaboration and for being a cheerful member of the lab, **Andrea Manfrin** for being an amazing person and scientist and his valuable scientific feedback, **Mehmet Girgin** for understanding me as a person with similar cultural background and for answering my end of PhD-related questions, **Giuliana Rossi** for being understanding and supportive, for her therapeutic hugs and her critical feedback. Current members of LSCB: **Mike Nikolaev** for being my neighbor in the deserted space of LSCB, and for sharing organoids and materials whenever I needed, **Olga Mitrofanova** for all her help with human organoid culture and identifying the working antibodies, **Moritz Hofer** for being a genuine person and for his translating my thesis abstract (Moritz, now you know what is network defect in German!), **Tania Hübscher** for being an amazing neighbor for the past two years, for our jokes and for translating my thesis abstract, **Sophia Lee** for being understanding and supportive, **Francisco Lorenzo Martin** for his feedback and help with the RNA-seq analysis, **Devanjali Dutta** for her scientific feedback, **Nicolas Broguiere** for our scientific and political discussions, **Antonius Chrisnandy** for his good mood, patience, and good collaborations, **Bilge Elci** for being my liver organoid buddy, for her contagious laughter, and our great discussion and collaboration, **Julia Tischler** for being supportive and spreading the positive vibes around.

To **JiSoo Park** and **Stefano Vianello**, my family in Lausanne, my safe corner, and my precious friends, for their being in this world above everything else. Thanks, **JiSoo** for sharing this journey with me, for all our adventures, and for all your help. **Stefi**, thanks for being such a wonderful role model, for our interesting discussions, and for all your help with proof-reading my thesis.

To my amazing friends outside the lab who had to put up with my stress and complaints during the past years. **Azadeh**, thanks for all your support and for being all ear when I needed. **Mahtab**, thanks for being there for me during all the happy and sad moments of this journey. **Farzaneh** and **Hamedeh** thanks for all your support, and encouragement, for being my real friends in Switzerland, my family. **Bastien**, thanks for your help with translations and introducing me to good French literature and culture. Thanks, **Mojtaba**, for all the happy and sad moments, for your support that helped me to get to where I am, and to know myself better.

To my dearest **Jaakko**. Thanks for your presence, your support, your understanding, our discoveries, for being a source of inspiration, and for filling my heart with so much Lov and peace that no stress could kick in.

Last but not least I would like to thank my family for their constant love and support, without whom I could have not been where I am. My grandparents for their prayers and love. **Pouyan** and **Kavian** for being amazing and supportive brothers, and my safe corner in Switzerland. **Kavian**, I will not forget your help with cooking during the pre-thesis submission phase. My dearest mom, **Shirin**, I could have not hold myself together during the tough times without you - the most encouraging and caring mom in this world. My dearest dad, **Sirous**, you have always been my source of strength and independence, thanks for having my back through all these years. Dear mom, and dear dad I dedicate this thesis to you two! Thanks for everything.

Abstract

Advances in our understanding of the biology of stem cells and their niches have provided the necessary foundation to create *in vitro* complex self-organizing three-dimensional (3D) structures called organoids. While organoids represent a highly promising new class of biological model systems, the translational potential of these systems is currently limited by their dependence on animal-derived matrices, particularly Matrigel, an extracellular matrix (ECM) derived from mouse tumors. Apart from their immunogenicity and batch-to-batch variability, these matrices do not allow modulation of ECM composition and, accordingly, systematic adaptation of properties to specific cells and tissues. To address this issue, new biomaterial-based approaches have focused on the development of synthetic alternatives to Matrigel. This work focuses on the development of chemically defined matrices to elucidate the specific effects of ECM, with the goal of further increasing the translational relevance of epithelial organoids for regenerative medicine and disease modeling applications. Given the critical functionality of the intestine and the liver, and emergence of debilitating diseases due to damage to these organs, I have mainly focused on intestinal and liver organoids.

First, I developed a new family of synthetic poly(ethylene glycol) (PEG)-based hydrogels, so-called ‘low-defect thiol-Michael addition’ (LDTM) hydrogels, by modifying the conventional crosslinking strategy of existing PEG-co-peptide hydrogels formed by Michael addition of bis-cysteine peptides and vinyl sulfone-terminated PEG macromers. These mechanically tunable hydrogels are chemically defined and can be prepared with minimal batch-to-batch variability. They also allow the derivation of mouse and human intestinal organoids, the latter without any animal components. In addition, I have demonstrated a role of laminin in enhancing organoid derivation and patterning. Accordingly, I then investigated the possibility of replacing animal-derived laminin with its recombinant counterparts. I demonstrated that incorporation of full-length recombinant laminin into LDTM matrices enabled the formation of intestinal organoids in mice, albeit to a lesser extent than natural laminin. However, the minimal laminin fragment conferring integrin-binding properties was not sufficient to induce organoid budding alone.

Together with colleagues, I applied a similar biomaterial-based approach to culture organoids from liver ducts. Liver organoids were successfully expanded and maintained in a minimal ECM-like environment. The organoids showed remarkable sensitivity to the mechanical properties of hydrogels requiring activation of the SFKs/Yes-associated protein (YAP) axis, independent of actomyosin contractility. The use of synthetic matrices allowed the unprecedented establishment of biopsy-derived human liver organoids without the need for animal components at any step of the process, making this protocol fully compatible with clinical applications.

As the final step, I leveraged the modularity of synthetic matrices and derivation of liver ductal organoids in these matrices, to model some aspects of liver fibrosis – a global health problem

affecting millions of people, and for which organ transplantation is the only medical solution. I demonstrated the role of tissue stiffness, a feature usually neglected in fibrosis models, on a regenerative mechanism associated with liver fibrosis called ductular reaction (DR). Human ductal liver organoids showed reduced proliferative capacity in LDTM gels with stiffness values similar to those of fibrotic liver tissue. In addition, transcriptomic analysis revealed impaired stemness potential, as well as concomitant induction of inflammatory responses. Furthermore, I used organoid formation efficiency in LDTM gels as a proxy of progenitor-mediated liver regeneration, and tested the efficacy of some fibrosis-directed drugs on DR, the results of which indicated the importance of using human organoids and a minimal mechanically tunable matrix in assays for drug screening. Targeting the affected pathways and identifying molecular mechanisms through which cell-matrix interactions regulate ductular liver regeneration may facilitate strategies to improve this process and develop novel regenerative and antifibrotic therapies.

Overall, the newly developed hydrogels provide a reproducible, chemically defined environment that can be readily prepared with minimal batch-to-batch variability for multiple stem cell types and for organoid culture. Successful derivation of human intestinal and liver organoids in these matrices may open exciting prospects for clinical applications of organoids. In addition, the modularity of these matrices to mimic the ECM in pathological tissues, particularly the aberrant mechanical properties of fibrotic tissues, will enable the development of powerful disease models and predictive drug screening platforms and promote the development of new therapies.

Key words: extracellular matrix (ECM), hydrogel, poly(ethylene) glycol (PEG), thiol Michael-addition, network defect, stiffness, epithelial organoids, stem cell, clinical application, disease modelling

Résumé

Les dernières avancées dans la compréhension de la biologie des cellules souches et de leurs niches ont apporté les fondements nécessaires à la dérivation de structures tridimensionnelles complexes qui s'autoorganisent *in vitro*, les organoïdes. Même si les organoïdes représentent une nouvelle classe de modèles biologiques très prometteurs, le potentiel translationnel de ces modèles est actuellement limité par leur dépendance en matrices dérivées d'animaux, et en particulier en Matrigel, une matrice extracellulaire (MEC) provenant de tumeurs de souris. En plus de leur immunogénicité et de leurs problèmes de reproductibilité, ces matrices ne permettent pas de moduler la composition de la MEC et donc d'adapter ses propriétés aux besoins de tissus et de cellules spécifiques. Pour pallier à ce problème, de nouvelles approches basées sur les biomatériaux ont misé sur le développement d'alternatives synthétiques au Matrigel. Ce travail de thèse s'axe sur le développement de matrices définies chimiquement, dans le but de déterminer les effets spécifiques de la MEC et de continuer à améliorer la pertinence des organoïdes épithéliaux dans les applications translationnelles en médecine régénérative et dans la modélisation des maladies. Etant donné l'importance des intestins et du foie ainsi que des maladies liées aux dommages causés à ces organes, je me suis concentrée sur les organoïdes intestinaux et hépatiques.

Premièrement, j'ai développé une nouvelle famille d'hydrogels synthétiques basés sur le poly(éthylène) glycol (PEG), appelés hydrogels LDTM (pour « low-defect thiol-Michael addition ») en modifiant la stratégie conventionnelle de réticulation des hydrogels formés par addition de Michael entre les peptides bi-cystéinés et les terminaisons vinyl sulfone des macromères de PEG. Ces hydrogels modulables mécaniquement sont chimiquement définis et peuvent être préparés avec une variabilité minimale entre les lots. Ils supportent aussi la formation et la culture d'organoïdes intestinaux de souris et d'humain, ces derniers sans aucun besoin en composants dérivés d'animaux. J'ai, de plus, démontré le rôle joué par la laminine pour améliorer la formation et la structure de ces organoïdes. J'ai poursuivi en investiguant la possibilité de remplacer la laminine dérivée d'animaux par ses homologues recombinants. J'ai démontré que l'incorporation de la laminine recombinante de pleine longueur dans les matrices LDTM permet la formation d'organoïdes intestinaux de souris, mais moins efficacement que la laminine d'origine animale. Le fragment minimal de la laminine qui lui confère ses propriétés de liaison aux intégrines n'est en revanche pas suffisant pour induire la formation de structures de cryptes sur les organoïdes.

Dans le cadre d'une collaboration, j'ai appliqué une approche similaire et basée sur les biomatériaux pour la culture d'organoïdes du canal hépatique. Ces organoïdes de foie ont été propagés et maintenus avec succès dans un environnement imitant une matrice extracellulaire minimale. Les organoïdes ont montré une sensibilité remarquable aux propriétés mécaniques des hydrogels demandant l'activation de la voie de signalisation des protéine-tyrosine kinases de la famille Src (SFKs)/Yes-associated protein (YAP), indépendamment de la contractilité de l'actomyosine. L'utilisation de matrices synthétiques a permis le premier établissement d'organoïdes de

foie humain dérivés de biopsies sans utilisation de composés d'origine animale à aucune étape du processus, rendant ce protocole entièrement compatible pour des applications cliniques.

Finalement, j'ai utilisé la modularité des matrices synthétiques et les organoïdes de canal hépatique pour modéliser certains aspects de la fibrose du foie – un problème de santé global qui affecte des millions de personnes et pour lequel la seule solution est la transplantation. J'ai démontré le rôle de la rigidité du tissu, une composante souvent négligée dans les modèles de fibrose, sur un mécanisme de régénération associé à la fibrose du foie appelé réaction ductulaire. Les organoïdes de canal hépatique humains ont montré une capacité de prolifération réduite dans les gels LD TM avec une rigidité comparable à celle d'un foie fibrosé. Des analyses transcriptomiques ont également révélé une diminution de la formation des cellules souches, un potentiel de régénération des cholangiocytes réduit et une induction de réponses inflammatoires. Comme estimation de la régénération médiée par les cellules progénitrices, j'ai mesuré l'efficacité de la formation des organoïdes dans les gels LD TM et ainsi pu tester l'efficacité de certains médicaments contre la fibrose sur le mécanisme de réaction ductulaire. Le résultat de ces tests démontre l'importance d'utiliser des organoïdes humains et une matrice minimale et modulable pour les tests de médicaments. Identifier les mécanismes moléculaires affectés et cibler les voies par lesquelles les interactions entre la matrice et les cellules régulent la régénération des canaux hépatiques permettra de trouver de nouvelles stratégies pour améliorer cette dernière, sur lesquelles se baser pour développer ensuite de nouvelles thérapies.

Dans l'ensemble, les hydrogels développés dans le cadre de ce travail offrent un environnement reproductible et chimiquement défini. Ils peuvent être préparés rapidement, de manière reproductible et appliqués à différentes cultures de cellules souches et d'organoïdes. Le succès de la formation et du maintien des organoïdes intestinaux et hépatiques humains dans ces gels ouvre des perspectives intéressantes pour les applications cliniques. La possibilité de moduler ces matrices pour imiter la MEC de tissus malades, et en particulier de modéliser les propriétés mécaniques anormales des tissus fibrosés, permettra le développement de modèles de maladies et de tests de médicaments plus efficaces qui promouvront l'avènement de nouvelles thérapies.

Mots-clés : matrice extracellulaire (MEC), hydrogel, poly(éthylène) glycol (PEG), addition de Michael avec thiols, défauts de réticulation, rigidité, organoïdes épithéliaux, cellules souches, applications cliniques, modélisation de maladies.

Zusammenfassung

Fortschritte in unserem Verständnis von Stammzellen und deren sogenannten Nischen legten eine Grundlage für die Erschaffung von komplexen selbstorganisierten dreidimensionalen (3D) Zellstrukturen, die wir Organoide nennen. Während Organoide sich als eine vielversprechende neue Art biologischer Modellsysteme erweisen, ist eine umfassende Ausschöpfung deren Potenzials hinsichtlich klinischer Anwendungen begrenzt, insbesondere infolge der Abhängigkeit von Matrizen tierischer Herkunft wie beispielsweise Matrigel, eine extrazelluläre Matrix (EZM) die aus Tumoren von Mäusen gewonnen wird. Abgesehen von ihrer Immunogenität und Variabilität zwischen einzelnen Chargen erlauben diese Matrizen keine Modulation der EZM-Zusammensetzung und dementsprechend keine systematischen Anpassungen der Eigenschaften an bestimmte Zellen und Gewebe. Um dieses Problem anzugehen, konzentrierten sich diverse neue Ansätze basierend auf Biomaterialien auf die Entwicklung von Alternativen zu Matrigel. Diese Arbeit fokussiert sich auf die Entwicklung chemisch definierter Matrizen zur Ermittlung spezifischer Wirkungen von EZM-Komponenten mit dem Ziel, die translatorische Relevanz epithelialer Organoide weiter zu erhöhen, insbesondere für deren Anwendungen in der regenerativen Medizin und zur Modellierung von Krankheiten. Angesichts der zentralen Funktion des Darms und der Leber sowie des Auftretens schwerwiegender Krankheiten bei Schäden an diesen Organen habe ich mich hauptsächlich auf Darm- und Leberorganoide konzentriert.

Zunächst entwickelte ich eine neue Art synthetisch Hydrogele auf Polyethyleneglycol (PEG)-Basis, nämlich sogenannte LDTM-Hydrogele (*Eng.* für Low-defect thiol Michael-Addition), durch die Modifikation der konventionellen Vernetzungsstrategie bestehender PEG-Peptid-Hydrogele, welche durch Michael-Addition von Cystein-Peptiden und Vinylsulfon-terminierten PEG-Makromeren gebildet werden. Diese Hydrogele mit regulierbarer mechanischen Eigenschaften sind chemisch definiert und können mit minimaler Chargenvariabilität hergestellt werden. Sie ermöglichen des Weiteren die Erzeugung von Organoiden des Darms von Mäusen und Menschen, und dies bei menschlichen Organoiden sogar ohne zusätzliche tierische Bestandteile. Zudem habe ich gezeigt, dass Laminin zur Verbesserung der Erzeugung von Organoiden sowie deren Entwicklung von Organähnlichen Zellstrukturen beiträgt. Infolgedessen untersuchte ich dann die Möglichkeit, das von Tieren stammendes Laminin in Organoidkulturen durch sein rekombinantes Pendant zu ersetzen. Ich konnte aufzeigen, dass die Zugabe von rekombinantem Laminin in Vollängenform zu LDTM-Matrizen die Bildung von Maudarmorganoiden ermöglicht, wenn auch weniger gut als bei der Zugabe von natürlichem Laminin. Ein minimales Lamininfragment welches eine Integrin-Bindung ermöglicht, war jedoch nicht ausreichend um die typische Ausbuchtungen von Organoiden zu induzieren.

Einen analogen Ansatz auf Biomaterialienbasis habe ich mit Arbeitskollegen dann auf Kulturen von Lebergang-Organoiden angewendet. Solche Leberorganoide konnten erfolgreich expandiert und in einer minimalen EZM-ähnlichen Umgebung gehalten werden. Die Organoide zeigten eine

bemerkenswerte Sensitivität gegenüber den mechanischen Eigenschaften von Hydrogelen. Diese ist abhängig von der Aktivierung des SFKs/Yes-associated protein (YAP) Signalwegs und unabhängig von Actomyosinkontraktionen. Die Verwendung von synthetischen Matrizen ermöglichte die Etablierung von aus Biopsien stammenden menschlichen Leberorganoiden, ohne dass in irgendeinem Schritt des Prozesses tierische Komponenten erforderlich waren. Dadurch ist dieses Protokoll vollständig mit klinischen Anwendungen kompatibel.

Als letzten Schritt nutzte ich die Modularität synthetischer Matrizen und deren Erzeugungsmöglichkeiten von Lebergangorganoiden, um einige Aspekte der Leberfibrose zu modellieren. Millionen von Menschen betreffend, stellt Leberfibrose ein globales Gesundheitsproblem dar, mit Organtransplantation als bislang einzige medizinische Möglichkeit. Ich demonstrierte eine zentrale Rolle erhöhter Gewebesteifigkeit, ein Merkmal von Fibrose, das in Modellen häufig vernachlässigt wird. Die Steifigkeit beeinflusst insbesondere den als duktiläre Reaktion (DR) bezeichnete Regenerationsmechanismus in Leberfibrose. Humane Lebergang-Organoiden zeigten eine verringerte Proliferationskapazität in LDTM-Hydrogelen mit Steifheitswerten ähnlich jenem von fibrotischem Lebergewebe. Darüber hinaus ergab die transkriptomische Analyse eine beeinträchtigte Stammzellbildung und ein verringertes Regenerationspotential der Cholangiozyten sowie eine gleichzeitige Induktion von Entzündungsreaktionen. Des Weiteren verglich ich die Effizienz der Organoidbildung in LDTM-Hydrogelen und benutzte diese als Approximationswert für das Leberregenerationspotential von Vorläuferzellen. Diesbezüglich testete ich die Wirksamkeit einiger Antifibrotischer Medikamente gegen DR. Die Ergebnisse unterstrichen die Bedeutung der Verwendung menschlicher Organoiden und einer minimalen, mechanisch einstellbaren Matrix in Wirkstoffscreenings. Die Identifizierung molekularer Mechanismen in den Zell-Matrix-Wechselwirkungen, die die Lebergangregeneration regulieren und die gezielte Modulation der betroffenen Signalwege können neue Strategien von regenerativen antifibrotischen Therapien ermöglichen, die diesen Regenerationsprozess fördern.

Insgesamt bieten die neu entwickelten Hydrogele eine reproduzierbare, chemisch definierte Umgebung für die Organoidkulturen mehrerer Stammzelltypen, und können mit minimaler Chargenvariabilität hergestellt werden. Die erfolgreiche Erzeugung von menschlichen Darm- und Leberorganoiden in diesen Matrizen eröffnet Perspektiven für die klinische Anwendung von Organoiden. Weiter wird die Modularität dieser Matrizen zur Modellierung der EZM von pathologischem Gewebe wie die mechanischen Eigenschaften fibrotischer Gewebe verbessern, was wiederum die Entwicklung leistungsfähiger Krankheitsmodelle und prädiktive Wirkstoffscreening-Plattformen ermöglicht, um schlussendlich die Entwicklung neuer Therapien zu unterstützen.

Schlüsselbegriffe: Extrazelluläre Matrix (EZM), Hydrogel, Polyethyleneglycol (PEG), Thiol Michael-Addition, Netzwerkdefekte, Steifigkeit, Epitheliale Organoiden, Stammzellen, Klinische Anwendungen, Krankheitsmodelle.

Objective and Aims

Stem cells have the intrinsic ability to assemble into complex 3D structures when provided with a matrix and appropriate signaling cues. These self-organizing 3D structures, called organoids, can be derived from adult stem cells (ASC) or pluripotent stem cells (PSC) and mimic the cellular diversity, spatial organization, and functionality of their *in vivo* counterparts. Their organ-like make up and function therefore makes them a powerful tool for modeling tissue development and disease, drug screening, and cell therapy.

To date, considerable efforts have been made to identify soluble niche components, such as modulators of the Wnt signaling pathway, that are essential for organoid culture; however, the role of the solid extracellular matrix (ECM) as an essential element of the niche has yet to be elucidated. Indeed, current organoid cultures rely on Matrigel, an undefined basement membrane protein mixture composed of laminin, collagen IV, entactin, heparan sulfate, and numerous growth factors, as the 3D matrix. Notably, the ECM components and characteristics are difficult to manipulate in current *in vivo* and *in vitro* models. In addition, batch-to-batch variability, the risk of pathogen transmission, and the inability to modify their key physical and biochemical properties make this matrix unsuitable for clinical applications.

To address this major bottleneck, the overall goal of this thesis is to develop defined synthetic matrices for epithelial organoid culture and disease modeling. In the first chapter, I explain how to recreate the physical properties of the stem cell niche using biomaterial-based approaches, and in the following chapters, I demonstrate the development of defined matrices for the culture of intestinal and liver organoids and the modeling of disease as described below:

Aim 1: To develop a simple and fully synthetic matrix for epithelial organoid culture without the requirement of a crosslinking enzyme. By modifying the crosslinking strategy of conventional PEG-co-peptide hydrogels, I synthesize low defect thiol-Michael addition (LDTM) hydrogels that can be formed at low polymer content without losing their mechanical integrity.

Aim 2: To derive mouse and human intestinal and hepatic organoids in LDTM hydrogels. By adjusting the physical properties of the LDTM gels (Aim 1), and incorporating suitable ECM molecules, I demonstrate successful derivation of mouse and human intestinal and liver organoids.

Aim 3: To substitute animal-derived laminin as key ECM components with its recombinant counterpart. I explore the possibility of substituting animal-derived laminin with recombinant laminin fragments or full-length laminin.

Aim 4: To develop a human organoid-based tissue fibrosis model by modulating ECM mechanics. I use human liver organoids as an *in vitro* model of ductular reaction and study the effect of the fibrotic environment stiffness on this phenomenon.

Contents

Acknowledgements	i
Abstract	iii
Résumé	v
Zusammenfassung	vii
Objective and Aims	ix
Chapter 1 Introduction.....	1
Introduction.....	1
1.1 The extracellular matrix as a key instructive stem cell regulatory unit.....	2
1.2 Synthetic matrices as a means to deconstruct the native intestinal and hepatic ECM3	
1.3 Conclusion	14
1.4 References	15
Chapter 2 Low-defect thiol-Michael addition hydrogels as Matrigel substitutes for epithelial organoid derivation	19
2.1 Abstract	19
2.2 Introduction.....	20
2.3 Results and discussion	21
2.4 Conclusion	33
2.5 Materials and methods.....	34
2.6 References	38
2.7 Supplementary information.....	40
Chapter 3 Substituting animal-derived laminin in synthetic matrices for epithelial organoid culture	47
3.1 Abstract	47
3.2 Introduction.....	47
3.3 Results and discussion	48
3.4 Conclusion	53

3.5	Materials and methods.....	55
3.6	References	58
3.7	Supplementary information.....	60
Chapter 4	Mechano-modulatory synthetic niches for liver organoid derivation	65
4.1	Abstract	65
4.2	Introduction.....	66
4.3	Results and discussion	66
4.4	Conclusion	76
4.5	Materials and methods.....	77
4.6	References	82
4.7	Supplementary information.....	85
Chapter 5	Mechanically-controlled cultures of human ductal organoids unveil the role of tissue stiffness in ductular reaction	91
5.1	Abstract	91
5.2	Introduction.....	92
5.3	Results and discussion	93
5.4	Conclusion	98
5.5	Materials and methods.....	100
5.6	References	103
5.7	Supplementary information.....	105
Chapter 6	Conclusion and perspective	109
	Curriculum Vitae.....	115

Chapter 1 Introduction

Extracellular Matrix Requirements for Gastrointestinal Organoid Cultures

Rezakhani S^{1,2}, Gjorevski N¹, Lutolf MP^{1,2,*}

¹ Laboratory of Stem Cell Bioengineering, Institute of Bioengineering, School of Life Sciences, Ecole Polytechnique Fédérale de Lausanne (EPFL), 1015 Lausanne, Switzerland.

² Institute of Chemical Sciences and Engineering, School of Basic Sciences, EPFL, 1015 Lausanne, Switzerland.

* Correspondence: matthias.lutolf@epfl.ch

(Revised version has been published in Biomaterials 2021, <https://doi.org/10.1016/j.biomaterials.2021.121020>)

Introduction

The intestine and liver are the three main, solid tissues of the gastrointestinal tract that arise from the endoderm during development¹. They play a major role in digestion and metabolism, where the liver controls detoxification and urea production, and the intestine is responsible for digestive function, nutrient absorption, and waste removal². Given their critical functionality, debilitating diseases can arise due to damage to these organs. For example, in the intestine, infections, irritable bowel syndrome (IBS), inflammatory bowel disease (IBD), and colon cancer are common disorders. Although the liver has a remarkable regenerative capacity, chronic inflammation and scarring can still severely impair its function³, and cirrhosis and liver cancer account for 3.5% of all deaths worldwide⁴.

The importance of the gastrointestinal system to health and disease led to the development of different *in vitro* and *in vivo* models. Conventional *in vitro* models are based on cell lines or tissue explants, and *in vivo* animal models are all poor representatives of epithelial physiology. Fortunately, there was a breakthrough in recent years with the identification of intestinal stem cells (ISCs) and their niche⁵, which enabled researchers to expand single stem cells into three-dimensional (3D) cellular structures resembling the native intestine. These 3D structures that can self-organize under specific microenvironmental cues are called organoids⁶. They recapitulate

multiple biological parameters including the spatial organization of cells, cell-cell interactions, and cell-matrix interactions⁷.

By creating an artificial stem cell niche *in vitro*, which requires control over the physical extracellular matrix (ECM), chemical (signaling molecules), and cellular (differentiated cell types) environment, researchers could culture 3D structures recapitulating multiple aspects of different gastrointestinal tissues, such as the intestine⁵, and liver⁸. Current organoid systems mostly rely on biochemical signals and cell-cell interactions to control stem cell fate, but there are important elements to consider including the ECM, cell-ECM interaction, and biophysical signals that are still unknown. This is because current *in vitro* models rely on animal-derived Matrigel—an ill-defined gelatinous basement-membrane protein mixture composed of laminin, collagen IV, entactin, heparan sulfate, and numerous growth factors⁹—as the 3D matrix, and ECM components are difficult to manipulate in current *in vivo* and *in vitro* models.

Defining different ECM components for *in vitro* organoid culture is crucial for understanding their role *in vivo* in aspects such as development, function, repair, and disease. Here, I aim to define the ECM components required for intestinal and hepatic organoid culture and how biomaterial-based approaches can be used to identify different ECM properties for enhanced organoid culture.

1.1 The extracellular matrix as a key instructive stem cell regulatory unit

The ECM, a 3D non-cellular microenvironment that surrounds cells, is crucial for physiological tissue and organ function. Although the composition and organization of the ECM vary between organs, it is mainly composed of water, proteins (primarily collagen, elastin, fibronectin, and laminin), and polysaccharides. The ECM both provides support for tissue integrity and elasticity as well as transmits biochemical and biomechanical signals that regulate cell adhesion, migration, proliferation, differentiation, and survival^{10,11}. Just as cells secrete and remodel their surrounding ECM, so does the ECM shape and remodel cell identity. Thus, in many cases, the composition of the ECM becomes almost inseparable from the identity of the cell itself, and indeed, it is instructive and permissive to it.

This concept has been particularly successful in framing the "niche" for many stem cells of the adult body, in which the ECM, along with soluble niche factors, provides specific biophysical and biochemical environments that maintain stemness¹². Depending on the cell type, the ECM can either form a two-dimensional (2D) sheet-like basal lamina, as is the case for epithelial stem cells, or a highly hydrated 3D fibrillar polymer network that fully encompasses the cells¹³. Stem cell differentiation can also be directly affected by the stiffness and elasticity of the ECM¹⁴, as cells sense the external forces and respond to the environment as dictated by these qualities. Cell adhesion to the ECM through integrins, syndecans, and discoidin domain receptors results in signaling cascades that regulate gene expression¹⁰. Moreover, cellular behavior is modulated by the ECM through the storage and release of growth factors, such as epidermal growth factor (EGF), fibroblast growth factor (FGF), and other signaling molecules¹¹.

Therefore, when we think about introducing or re-introducing matrices *in vitro*, we have to consider both biological and mechanical factors. From a biological point of view, do we know the composition of the native matrix? Are there any unique isoforms that might inform the investigation? From a mechanical point of view, are we able to present such components in a structured way? Are we recapitulating the correct mechanical environment or are we instead only providing biological signaling decoupled from mechanics?

In the following, I will discuss these questions related to the ECM in the intestine and liver.

1.2 Synthetic matrices as a means to deconstruct the native intestinal and hepatic ECM

As scientists move to *in vitro* systems to study gastrointestinal tissues, expansion and differentiation protocols solely centered on soluble signaling factors and small-molecule modulators are slowly becoming obsolete as the representation of *in vivo*-like ECM features may also hold a similar transformative potential^{13,15}.

Intestinal and hepatic organoid cultures mainly rely on Matrigel⁹ and collagen as the 3D hydrogel matrix (**Table 1**). Although these culture systems have been important for identifying molecules and niche signals, such as Wnt/R-spondin to maintain stem cell maintenance and differentiation, they cannot manipulate ECM components and, subsequently, their effect on specific tissue. Instead, synthetic matrices that allow better control over the components can serve as an alternative model to deconstruct the physiological complexity of native environments and define their key instructive elements^{7,16,17}.

By incorporating signaling proteins from native ECMs through chemical or enzymatic crosslinking, an experimenter can modulate the biochemical and biophysical properties of these synthetic ECMs independently of each other and untangle the effect of different ECM components. For instance, we can provide these ligands by incorporating intact molecules (if they are big enough not to diffuse out of the matrix, e.g., laminin) or peptides into the synthetic hydrogels for 3D culture. The most commonly used peptides are fibronectin-derived peptide sequence RGD, the collagen-derived peptide GFOGER, or the laminin-derived peptides IKVAV and YIGSR.

Moreover, we can design biomaterials that allow matrix remodeling and degradation through different mechanisms. Cells secrete enzymes, like matrix metalloproteinase (MMP), that degrade the matrix, and by incorporating some MMP-sensitive specific amino acid sequences in the hydrogel (as a crosslinker or in the backbone), we can facilitate cell-mediated degradation^{18,19}. ECM degradation can also occur independently of cells; for example, some natural polymers like hyaluronan can be digested by enzymes²⁰, or synthetic hydrogels with ester groups in their backbone can be hydrolyzed over time²¹. In contrast to hydrolytically and enzymatically degradable linkages, photodegradable linkages allow precise spatial and temporal control over degradation and release²².

In the following, I will show how this approach is used to deconstruct the native intestinal, and hepatic ECM to rebuild defined matrices with minimal essential components for growing primary mouse and human epithelial organoids *in vitro*.

Table 1. 3D intestinal and hepatic organoid culture systems

Organoid type	Matrix	Cell type	Reference
Intestine	Matrigel	Mouse and Human ISC Human PSC Mouse ISC Minced murine intestine	Sato et al. ^{5,65} Spence et al. ⁶⁶ , Miyoshi et al. ⁶⁷ Ootani et al. ⁶⁸
	Collagen	Mouse and Human ISC	Jabaji et al. ^{69,70} , Tong et al. ⁷¹
	Alginate	Human PSC	Capeling et al. ⁷²
	Fibrin/Laminin	Mouse and human ISC	Broguiere et al. ³⁹
	Synthetic matrices	Mouse and human ISC	Gjorevski et al. ³⁵ , Rezakhani et al. ³⁶
		Human PSC and iPSC	Cruz-Acuña et al. ⁴⁰
	Recombinantly-engineered hydrogel	Minced murine intestine	Di Marco et al. ³⁸
Liver	Matrigel	Human iPSC	Takebe et al. ⁷³
		Mouse and human ductal fragment and single cells	Broutier et al. ⁸
		Mouse and human primary hepatocytes	Peng et al. ⁴⁹ , Hu et al. ⁴⁹
	Decellularized-ECM	Human fetal liver progenitor cells Human liver duct and fetal hepatocyte	Vyas, Baptista et al. ⁴⁶ Giobbe et al. ⁷⁴
	Fibrin/Laminin	Human ductal progenitor cells	Broguiere et al. ³⁹
	Synthetic matrices	Mouse and human ductal cells	Sorrentino, Rezakhani et al. ⁵⁰ , Ye et al. ⁵²

Intestine

ECM in intestinal epithelium

The intestinal epithelium is a highly dynamic system with an extremely high cellular turn-over rate. This fast renewal is driven by a process in which stem cells residing at the bottom of the crypt divide to give rise to transient amplifying cells, which then migrate up the crypt and undergo several rounds of division before differentiating into Paneth cells, absorptive enterocytes, mucus-secreting goblet cells, and hormone-secreting enteroendocrine cells. This process is tightly regulated and renews the epithelial layer every 4–5 days.

The intestinal epithelium is separated from the connective tissue and musculature by a basement membrane, which appears to play essential roles in the development and maintenance of the intestinal epithelium²³. For instance, differential spatial expression of laminin isoforms and their epithelial integrin receptors were observed along the crypt-villus axis during development and in the adult intestine^{24,25}. In the human small intestine, laminin-1 (111), as an upper crypt-villus form, and laminin-2 (211), as a lower crypt form, show complementary distribution; whereas, laminin-5 (332) is only restricted to the villus²⁶ (**Figure 1**). This distribution is different in rodents, as laminin-1 α chains are restricted to the crypt zone^{24,26}. Moreover, there are four different laminin-binding integrins expressed along the crypt-villus axis, and *in vitro* studies have revealed functional relationships between different laminin chains and specific intestinal cell functions²⁷.

Apart from laminins, it has been shown that the human intestinal epithelial basement membrane contains different collagen IV- α chains. They are differentially distributed throughout the subepithelial basement membrane, with $\alpha 1(\text{IV})$ and $\alpha 2(\text{IV})$ chains distributed along the entire crypt-villus axis, $\alpha 5(\text{IV})$ and $\alpha 6(\text{IV})$ chains restricted to the crypt, and $\alpha 3(\text{IV})$ and $\alpha 4(\text{IV})$ chains expressed on top of the villus region^{28,29} (**Figure 1**). Moreover, collagen IV interacts with collagen VI, which has been found as a *bona fide* basal lamina component in human intestinal epithelium and which is synthesized by crypt epithelial cells and regulates interactions between epithelial cell and fibronectin³⁰. Fibronectin and its receptor ($\alpha 5\beta 1$) were found mainly in the crypt region, and RGD-dependent adhesion and its role in maintaining human intestinal crypts have been discussed previously³¹. Besides laminin and collagen, it has been shown that heparin-sulfate, located on the basolateral surface of the intestinal epithelial cells, plays a critical role in crypt hemostasis³².

There are not many functional studies pinpointing the specific effect of ECM proteins due to their pleiotropic effects. There are some studies, though, that show how ECM remodeling affects the tissue architecture. For example, Mahoney *et al.* showed that a decrease in laminin $\alpha 5$ in a mouse model resulted in the deposition of colonic laminins, which transformed the small intestinal architecture to a colonic mucosal architecture³³. Similarly, blocking endogenous hyaluronic acid from binding to its receptors decreased intestinal length, villus height, and crypt depth, suggesting that it contributes to the regulation of normal intestinal growth³⁴.

Deconstructing intestinal ECM for organoid culture

The architecture and composition of the basement membrane is essential when it comes to the development and maintenance of the intestinal epithelium. As such, current organoid culture relies on Matrigel (**Table 1**), the solubilized basement-membrane extract from the Engelbreth-Holm-Swarm (EHS) mouse sarcoma, which is non-conductive to controlled modification and unsuitable for clinical applications.

Instead, Gjorevski *et al* used a bottom-up approach to deconstruct the complexity of this basement membrane in a defined manner *in vitro*³⁵ (**Figure 2A,E**). First, authors discovered that inert matrix backbones composed of enzymatically crosslinked poly(ethylene glycol) (PEG) failed to support ISC growth. To render these synthetic hydrogels bioactive, they incorporated different ECM components such as fibronectin, laminin-111, collagen IV, hyaluronic acid, and perlecan, which exist at the bottom of the intestinal crypts. They showed that intestinal colonies could form in the presence of any of these ECM components, though they ended up replacing full-length fibronectin with an RGD-peptide to induce adhesion sites in a minimal chemically defined matrix. PEG-RGD gels supported intestinal colony formation and multipotency. To learn how matrix stiffness affects intestinal organoids, they embedded ISCs in PEG gels containing 1 mM RGD and different elastic moduli.

They showed that there was an optimal stiffness (1.3 kPa) for ISC expansion, while colony formation efficiency was lower in either softer or stiffer matrices. They also looked at the effect of matrix remodeling on ISC behavior by embedding ISCs in PEG hydrogels harboring a mutated collagen I-derived sequence that can be cleaved by cell-secreted proteases. ISCs grown in proteolytically degradable matrices formed colonies with irregular shapes and attenuated *Lgr5* expression. Moreover, inflammation-related genes were upregulated in these matrices, which is reminiscent of pathological conditions that appear to be deleterious to ISC maintenance.

RGD-containing PEG gels supported intestinal colony formation but did not permit ISC differentiation and organoid formation when switched to a differentiation condition. When comparing the same condition in Matrigel by using nuclear YAP localization (an effector of the Hippo signaling pathway) as a readout, authors determined that *Lgr5*⁺-colonies thickened and buckled due to compression instead of budding. They reasoned that softer matrices that alleviate the accumulation of compressive forces would permit morphogenesis. Hence, they designed dynamic gels with a high initial stiffness for colony formation and subsequent softening over time through hydrolytic degradation for differentiation. Moreover, they found that matrix softening was not sufficient to induce budding in the presence of RGD only, indicating that an ECM component was still missing. Therefore, they incorporated laminin-111 as the key constituent of the intestinal basement membrane, and the final gels supported intestinal morphogenesis. By dissecting the ISC niche, Gjorevski *et al* studied the role of the ECM (adhesion, mechanical properties, remodeling) in ISC proliferation and differentiation, and they showed that different stages had specific ECM requirements.

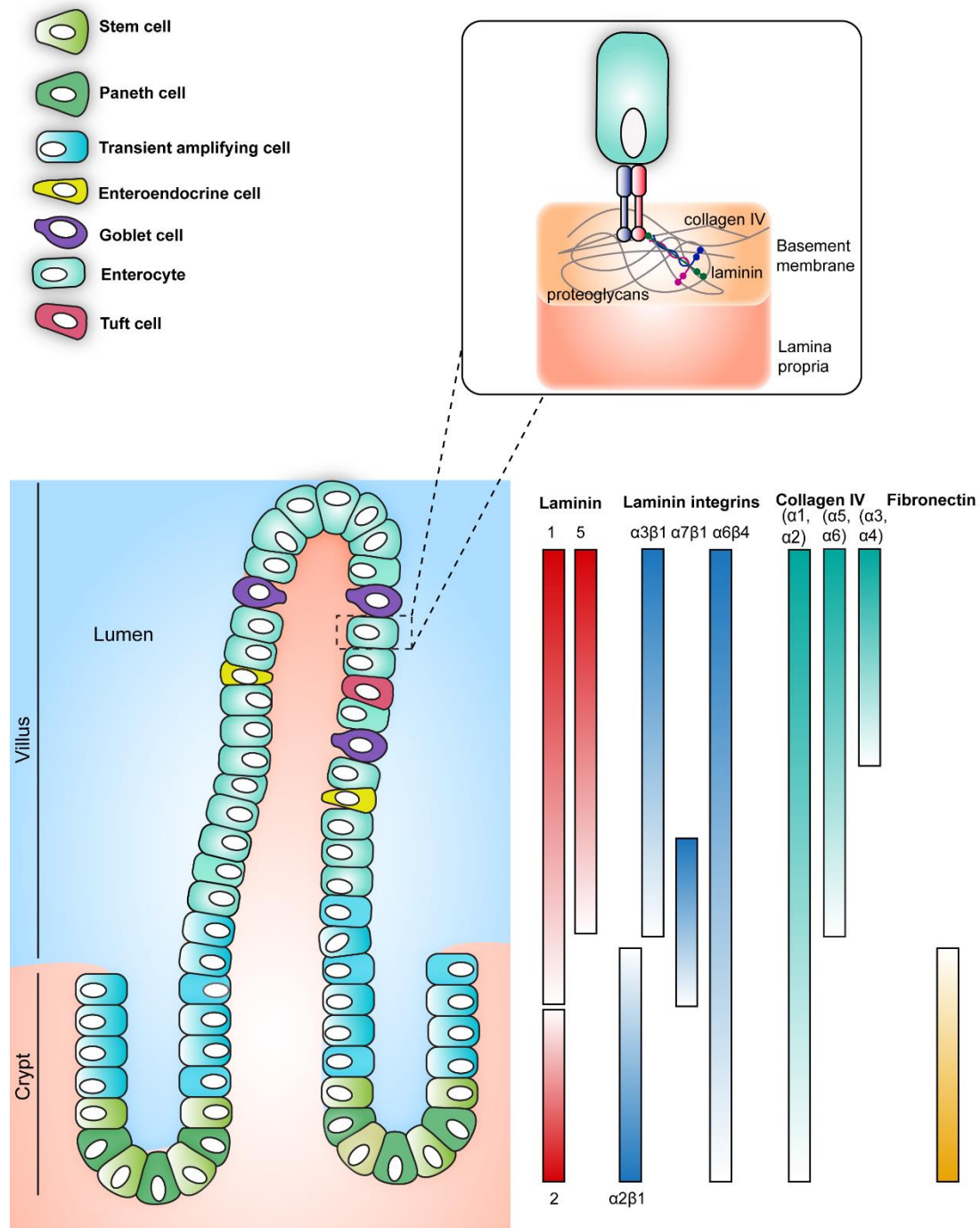


Figure 1. The architecture of small intestine *in vivo* and differential distribution of ECM components in the subepithelial basement membrane of human small intestine. Lgr-5⁺ intestinal stem cells reside at the bottom of the crypt and give rise to transient amplifying cells, which migrate up the crypt and differentiate into Paneth cells, enterocytes, goblet cells, and enteroendocrine cells. The intestinal epithelium is in direct contact with the basement membrane, which is mainly composed of laminin, collagen IV, and proteoglycans. The distribution pattern of different laminin isotypes and their receptors, along with collagen IV chains and fibronectin, are illustrated.

In the next chapter, I explain how I replaced the enzymatically crosslinked PEG hydrogels previously used for epithelial organoid culture³⁵ with a simpler, chemically crosslinked gel system³⁶. I modified the network architecture of conventional PEG-co-peptide hydrogels so that they could form with a low polymer content at a shear modulus of ~1.3 kPa, which is optimal for the expansion of primary ISCs into cystic polarized epithelial tissues (**Figure 2C,G**). Laminin-containing hydrolytically degradable hydrogels with gradual softening permitted mouse intestinal organogenesis. Additionally, only RGD was required to culture human intestinal organoids in these matrices without the need for any animal-derived components. Hernandez-Gordillo et al. also took advantage of the modularity of PEG-based hydrogels to investigate the cell-ECM parameters necessary for the culture of human intestinal enteroids (spherical cyst-like structures)³⁷. Inspired by the ISC niche, the authors included a collagen-derived peptide (GFOGER), recognized by integrin $\alpha 2\beta 1$ at the crypt base (**Figure 1**), and a fibronectin-derived peptide (PHSRN-K-RGD) in 8-arm PEG (20 kDa) gels with MMP-susceptible crosslinkers; they demonstrated the successful derivation of human duodenal and colon enteroids in gels supplemented with GFOGER peptide and not fibronectin-derived RGD (**Figure 2D,H**).

Moreover, additional studies tried to substitute Matrigel with a defined matrix that had similar mechanical properties. For example, DiMarco et al. developed a recombinantly engineered matrix with an elastin-like polypeptide backbone and identified the effect of matrix stiffness and adhesion on intestinal organoid formation³⁸. They showed that organoid formation efficiency in matrices with a stiffness of 180 Pa and an RGD concentration of 3.2 mM was similar to that measured in collagen I gels. Broguiere et al. also developed a matrix based on fibrin and the major component of Matrigel, laminin, to culture mouse and human intestinal organoids³⁹.

Cruz-Acuña *et al.* reported PEG-based hydrogels for culturing human intestinal organoids from human embryonic stem cell (ESC)- and induced pluripotent stem cell (iPSC)-derived spheroids⁴⁰ (**Figure 2B,F**). They used maleimide-terminated multi-arm PEG as the hydrogel backbone and protease-sensitive peptides as the crosslinker. They showed the effect of matrix stiffness and the incorporation of adhesive peptides on human intestinal organoid viability. Hydrogels of 3.5% (w/v) and 4% (w/v) polymer density with an elastic modulus of less than 100 Pa showed better viability. While RGD-functionalized hydrogels maintained organoid viability similar to Matrigel, laminin-derived peptides (IKVAV, AG73) and a collagen-mimetic (GFOGER) peptide reduced organoid viability. Moreover, they illustrated that matrix degradability was required for prolonged organoid survival.

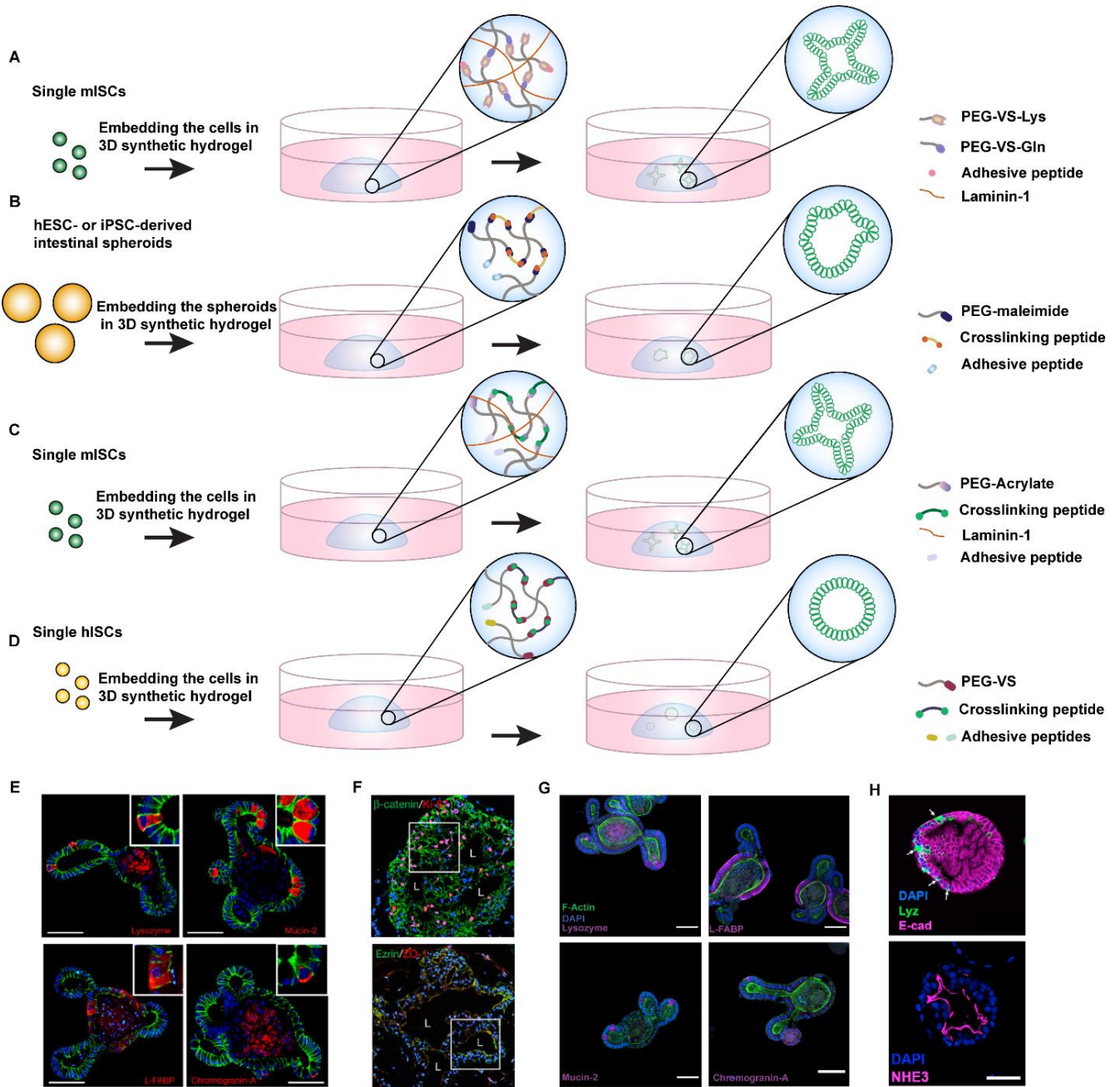


Figure 2. Synthetic matrices have been engineered to elucidate different ECM properties required for intestinal organoid culture. Gjorevski et al. used enzymatically crosslinked PEG hydrogels containing laminin-1 and RGD peptide to culture mouse intestinal organoids from single mouse intestinal stem cells³⁵ (A,D). Cruz-Acuña et al. developed RGD-containing PEG-based hydrogels to culture human intestinal organoids from human ESC- and iPSC-derived spheroids⁴⁰ (B,F). Rezakhani et al. cultured mouse and human intestinal organoids in chemically-crosslinked hydrogels, the latter in absence of any animal-derived laminin-1(C,G)³⁶. Hernandez-Gordillo et al. have demonstrated the derivation of human duodenal and colon enteroids in PEG gels supplemented with GFOGER peptide(D,H)³⁷.

Liver

The hepatic extracellular matrix

The liver is composed of many lobules, each containing a central vein, portal triad (portal vein, hepatic artery, and biliary duct), and in between, single sheets of hepatocytes that are separated by sinusoids that carry blood from the portal triads to the central vein⁴¹ (**Figure 3**). Each of these three different zones are surrounded by specific ECM molecules that regulate specific cell functions.

In a normal liver, the ECM comprises less than 3% of the relative area and approximately 0.5% of the weight^{42,43}. The dense, interstitial ECM is restricted to the capsule, around large vessels, and in the portal triad, while the perisinusoidal matrix is composed of both an interstitial and a basement membrane-like low-density ECM. This configuration is ideally suited for facilitating the rapid bidirectional exchange of macromolecules normally taking place between the plasma and hepatocytes and highlights the role of a hepatic ECM in this process⁴⁴. The strategic position of the perisinusoidal matrix explains why quantitative or qualitative changes in the ECM may significantly influence hepatic function⁴³.

Collagen types I, III, IV, and V are the most abundant proteins found in the hepatic ECM⁴⁵. While type IV collagen, in association with laminin and entactin-nidogen and in conjunction with proteoglycans form a low-density, basement membrane-like material along the sinusoid wall, collagen types I, III, and V, the major constituents of fibrillar collagen, are confined mainly to the portal tract and central vein wall. Moreover, this regional specificity in the ECM has been shown in a recent study⁴⁶ in which the authors seeded human fetal liver progenitor cells in a decellularized liver scaffold, and observed that after the cells and ECM self-assembled into 3D organoid structures, bile ducts were surrounded by laminin and collagen IV, whereas the hepatocytes were mostly surrounded by collagen I and fibronectin (**Figure 3**).

Deconstructing the ECM for ductal organoid culture

Lgr5⁺ cells replenish and repair the tissue cells in the intestine, whereas Lgr5⁺ cells are not expressed in the healthy liver and appear near bile ducts only upon injury⁴⁷. Although oval cells or EpCAM/Sox9-expressing ductal cells have long been regarded as bi-potential facultative stem/progenitor cells, the *in vivo* relevance of the oval cell-driven regenerative response, as well as its cell-of-origin, have remained controversial⁴⁸. Broutier et al. have described a long-term culture of bile-duct-derived bipotent progenitor cells from mouse and human liver⁸. In these culture systems, EpCAM⁺ biliary cells differentiate into expandable cystic bipotent progenitor cells with ductal characteristics. However, no spontaneous hepatocytic differentiation occurs, and the *in vivo* transplantation efficiency of these organoids is poor compared with primary hepatocytes. Recently, the long-term culture of primary mouse hepatocytes, which retain many morphological and functional properties of hepatocytes, has been described by the Nusse⁴⁹ and Clevers⁴⁸ labs.

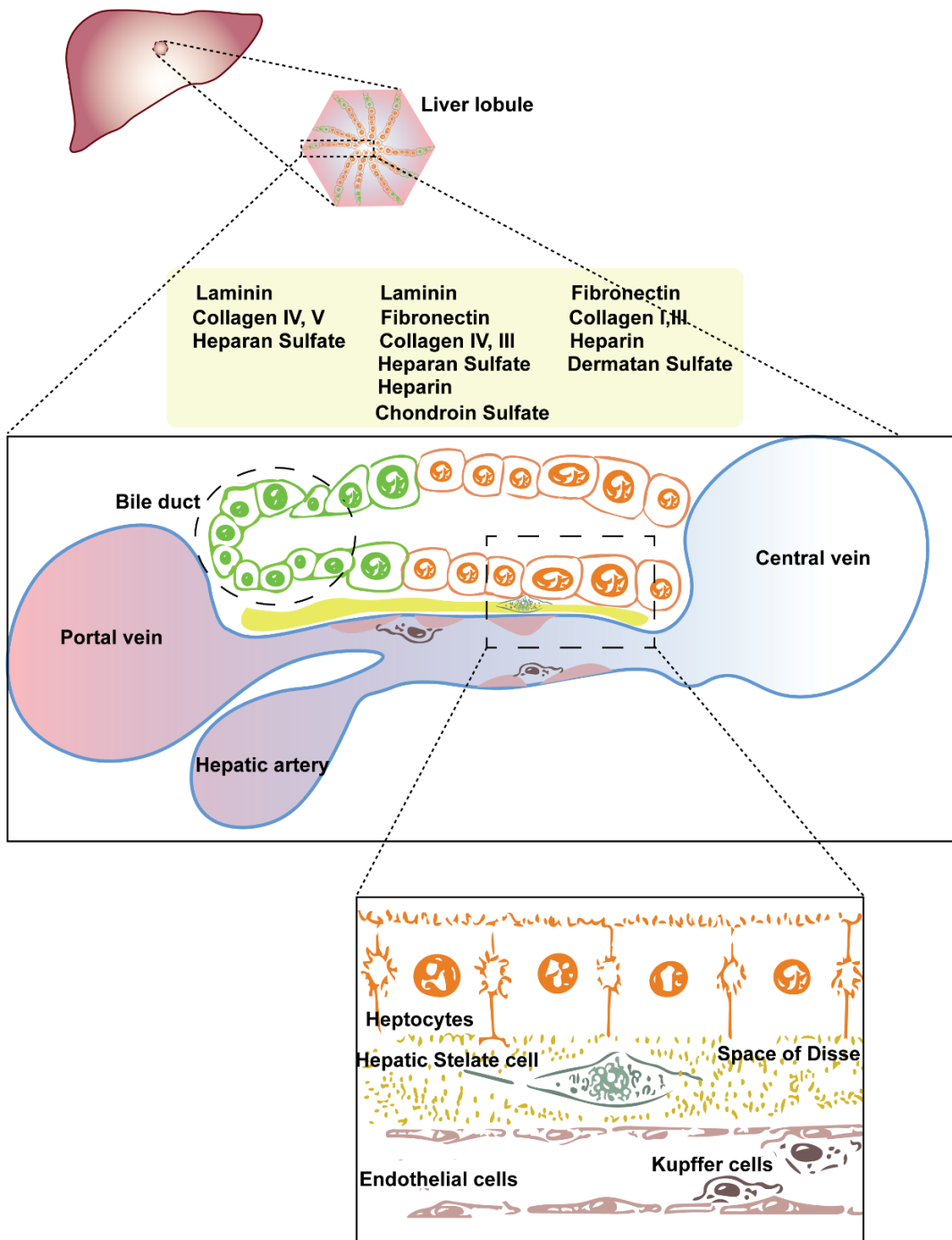


Figure 3. The architecture of the liver *in vivo* and differential distribution of ECM components in the Space of Disse. The liver is composed of lobules, and each lobule is composed of a central vein, portal triad (consists of portal vein, hepatic artery, and biliary duct), and in between: single sheets of hepatocytes that secrete bile salts to the bile duct, which is lined with cholangiocytes. With increasing distance from the portal triads, there is gradual increase in the amounts of fibrillar collagens, fibronectin, chondroitin sulfate, and dermatan sulfate proteoglycans.

Similar to other organoid types, liver organoids have also been generated in Matrigel. However, as explained before, different parts of the liver are surrounded by different ECM molecules, so having an optimized matrix for ductal or hepatocyte organoids would result in a more physiologically relevant culture. In Chapter 4, I explain how together with collaborators, I applied a similar strategy to hepatic organoids⁵⁰ and cultured ductal organoids first in an inert PEG with a stiffness that matched the physiological stiffness of the liver ($\approx 1.3 \text{ kPa}$ ⁵¹). Then, I incorporated key ECM proteins found in the native liver into the ductal region, such as laminin-111, collagen IV, and fibronectin, and obtained similar results by replacing fibronectin with its minimal integrin recognition peptide RGDSPG (**Figure 4A,C**). The organoids derived in PEG-RGD gels could be differentiated into hepatocytes; however, the maturity is still far behind primary hepatocytes (even in Matrigel culture), and we speculate that the inclusion of collagen to imitate the physiological niche would enhance hepatocyte differentiation. Moreover, I showed the successful derivation of human liver organoids in these hydrogels without any animal-derived components at any step of the process. Recently, Ye et al. developed a thermo-reversible hydrogel based on poly(isocyanopeptides) (PIC) and laminin-111 as the major components of the hepatic basement membrane and stiffness, similar to Matrigel. These hydrogels allowed derivation of human ductal organoids⁵² (**Figure 4B,D**).

Deconstructing the ECM in diseased tissues

We discussed the ECM of the healthy intestine and liver, and how to use the modularity of synthetic matrices to mimic the physiological ECM. However, the ECM remains an overlooked component of these tissues in disease, which is surprising considering the dynamic structure and constant remodeling of the ECM, wherein cells are constantly synthesizing, degrading, and reassembling its components. As an example of this importance, MMPs and adamalysins (ADAMs) play the main role in ECM component cleavage, while tissue inhibitors of metalloproteinase (TIMPs) inhibit the activity of MMPs to avoid extensive degradation¹¹. This process is tightly controlled, and during injury and disease processes, matrix deposition and turnover can be highly altered from the homeostatic condition. In other words, dysregulation of ECM composition, structure, and stiffness contributes to several pathological conditions, such as fibrosis and cancer¹¹. Our understanding of the protein composition of the ECM in normal and pathological tissue has recently increased due to the emergence of mass-spectrometry-based proteomics⁷⁰, and this is highly important to consider while developing disease models. Bridging the gap between conventional 2D models and *in vivo* animal models, human organoids provide unique opportunities to study human diseases⁷¹. In the following, we will discuss how the ECM of the intestine, and liver changes during the disease process and how we can apply this information to build more realistic organoid models. Inflammatory bowel diseases (IBD), such as Crohn's disease (CD), and ulcerative colitis (UC), are the major gastrointestinal disorders affecting more than 3 million people in western countries⁷². Common features of IBD are tissue damage and alteration of tissue architecture, which is mostly mediated by MMPs, specifically MMP9⁷³. Degradation products of hyaluronan, collagen, and laminin have been shown to induce inflammation, and circulating levels of collagen, laminin, and vimentin fragments correlate with subtypes of IBD⁷⁴.

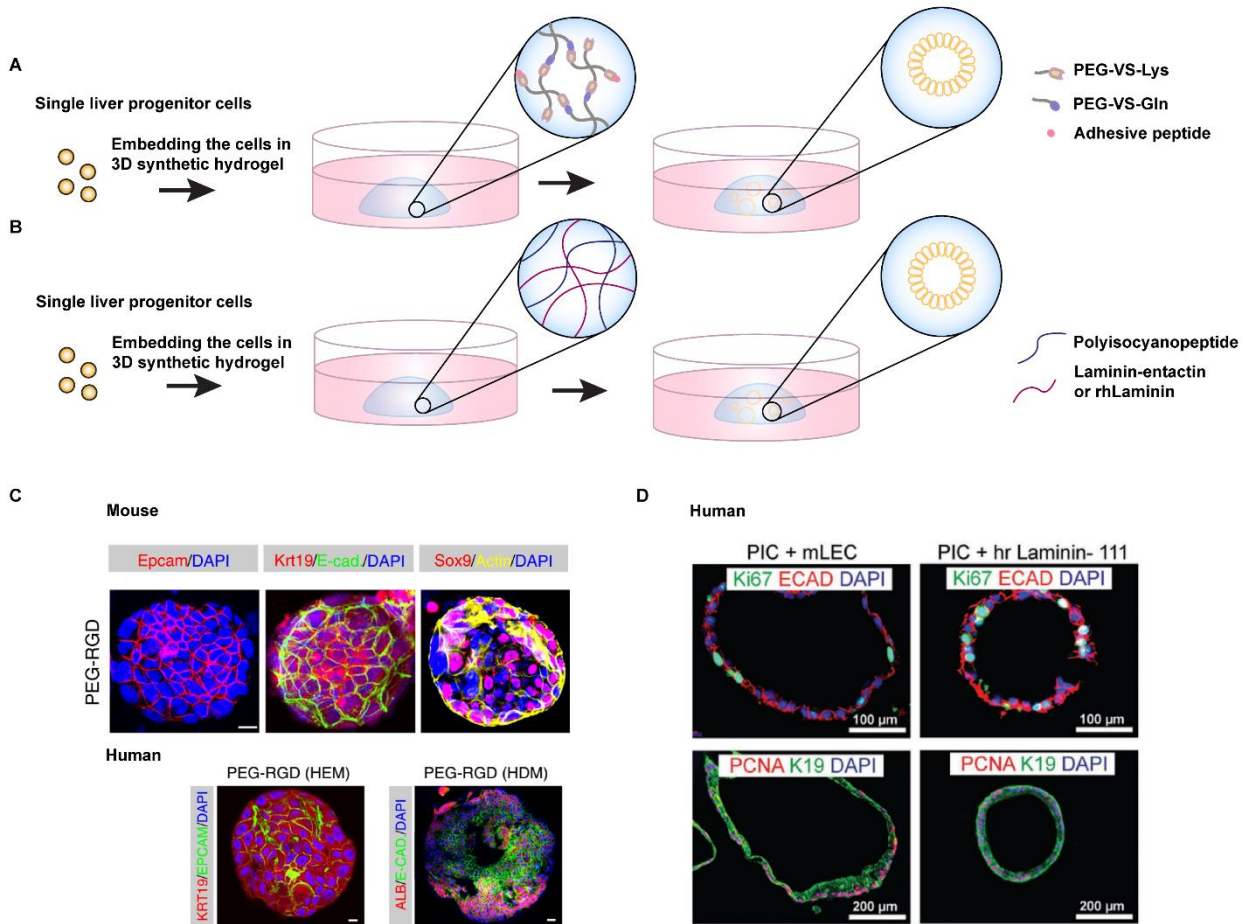


Figure 4. Synthetic matrices have enabled the generation of liver organoids in the absence of animal-derived components. Sorrentino and Rezakhani *et al.* used enzymatically-crosslinked PEG hydrogels containing the RGD peptide to culture mouse and human liver ductal organoids from ductal stem/progenitor cells⁵⁰ (A,C). Scale bars for the first row: 25 μm , and for the second row: 10 μm . Ye *et al.* derived human liver ductal organoids in thermoreversible PIC/laminin gels⁵² (B,D).

Furthermore, alterations in basement membrane composition include an increase in collagen IV and V expression, while the altered expression of the $\alpha 1$, $\alpha 2$, and $\alpha 3$ subunits of laminin has been noted in the inflamed segments of the small intestine in CD, in which laminin-2 in the intestinal crypts is replaced by laminin-1 and laminin-5^{75,76}. As a complication of IBD, intestinal fibrosis is associated with an up to six-fold increase in ECM stiffness (16.7 kPa vs 2.9 kPa⁷⁷). Therefore, it is important to consider the differences in ECM stiffness and composition for modeling IBD.

As any chronic liver disease is characterized by a change in both the quantity and composition of the ECM, the liver ECM plays a crucial role in liver diseases. Indeed, as a direct effect of aberrant ECM deposition in the fibrotic liver, tissue stiffness increases over time and severely compromises its function⁷⁸. In a fibrotic liver, total collagen content increases by three- to tenfold, and the perisinusoidal low-density ECM is gradually replaced by a high-density ECM due to the accumulation of fibrillar collagens (types I and III), and an electron-dense basement membrane that shifts from basal membrane-type proteoglycans (heparan sulfate) to interstitial-type proteoglycans (dermatan sulfates and chondroitin sulfates).⁴⁵ This subendothelial accumulation of collagen,

termed capillarization of the sinusoid, is associated with the disappearance of endothelial-cell pores (fenestrations), and the subsequent impaired hepatocyte function is characteristic of liver injury⁷⁹. In contrast to the increase in collagen I and III depositions, laminin-521, which maintains characteristics of quiescent rat hepatic stellate cells (HSCs) in the Space of Disse⁸⁰ during homeostasis, was markedly reduced in an old rat⁸¹. Moreover, it has been shown that impaired mechanosensing via integrin $\alpha 5/\beta 1$ in HSCs contributes to the age-related reduction of ECM (laminin-521) and hepatic growth factor release that may affect liver regeneration⁸¹. Therefore, it is very important to include collagen I and III in hepatic organoid culture when modeling liver fibrosis. Additionally, as the stiffness of the liver increases during fibrosis, it is important to culture organoids in a matrix with the stiffness of fibrotic tissue. In chapter 4, and 5, I show how I generated hydrogels with a stiffness matching that of the fibrotic tissue⁵¹ and cultured mouse and human liver ductal organoids in those matrices. I observed a significant impairment of organoid formation in these hydrogels⁵⁰, and liver organoids had reduced expression of hepatic progenitor markers, an upregulation of genes involved in the cellular response to hepatic injury, and an increase in the expression of matrix metalloproteases⁵⁰.

1.3 Conclusion

In addition to longer-ranged diffusible signals, crosslinked ECM molecules are essential and thus, somewhat underappreciated components of organoid systems, such as those of the intestine and liver. I discussed emerging biomaterial-based approaches that can be used to elucidate the specific effects of the ECM, with the aim of further increasing the physiological sophistication and translational relevance of organoid models. In parallel with identifying individual ECM species that steer organoid morphogenesis and potentially also organ development, function, and repair *in vivo*, it would be insightful to further deconstruct the known molecular players and the mechanistic underpinnings of their effects.

1.4 References

1. Dedhia PH, Bertaux-Skeirik N, Zavros Y, et al. Organoid Models of Human Gastrointestinal Development and Disease. *Gastroenterology* 2016;150:1098–1112.
2. Wells JM, Spence JR. How to make an intestine. *Development* 2014;141:752–760.
3. Cordero-Espinoza L, Huch M. The balancing act of the liver: tissue regeneration versus fibrosis. *J Clin Invest* 2018;128:85–96.
4. Asrani SK, Devarbhavi H, Eaton J, et al. Burden of liver diseases in the world. *J Hepatol* 2019;70:151–171.
5. Sato T, Vries RG, Snippert HJ, et al. Single Lgr5 stem cells build crypt-villus structures in vitro without a mesenchymal niche. *Nature* 2009;459:262–5.
6. Fatehullah A, Tan SH, Barker N. Organoids as an in vitro model of human development and disease. *Nat Cell Biol* 2016;18:246–254.
7. Yin X, Mead BE, Safaee H, et al. Engineering Stem Cell Organoids. *Stem Cell* 2016;18:25–38.
8. Broutier L, Andersson-Rolf A, Hindley CJ, et al. Culture and establishment of self-renewing human and mouse adult liver and pancreas 3D organoids and their genetic manipulation. *Nat Protoc* 2016;11:1724–1743.
9. Kleinman HK, Martin GR. Matrigel: Basement membrane matrix with biological activity. *2005;15:378–386.*
10. Frantz C, Stewart KM, Weaver VM. The extracellular matrix at a glance. *J Cell Sci* 2010;123:4195–4200.
11. Bonnans C, Chou J, Werb Z. Remodelling the extracellular matrix in development and disease. *Nat Rev Mol Cell Biol* 2014;15:786–801.
12. Moore KA, Lemischka IR. Stem cells and their niches. *Science (80-)* 2006;311:1880–1885.
13. Lutolf MP, Blau HM. Artificial stem cell niches. *Adv Mater* 2009;21:3255–3268.
14. Engler AJ, Sen S, Sweeney HL, et al. Matrix Elasticity Directs Stem Cell Lineage Specification. *Cell* 2006;126:677–689.
15. Brassard JA, Lutolf MP. Engineering Stem Cell Self-organization to Build Better Organoids. *Cell Stem Cell* 2019;24:860–876.
16. Gjorevski N, Ranga A, Lutolf MP. Bioengineering approaches to guide stem cell-based organogenesis. *Development* 2014;141:1794–804.
17. Murrow LM, Weber RJ, Gartner ZJ. Dissecting the stem cell niche with organoid models: an engineering-based approach. *Development* 2017;144:998–1007.
18. West JL, Hubbell JA. Polymeric biomaterials with degradation sites for proteases involved in cell migration. *Macromolecules* 1999;32:241–244.
19. Lutolf MP, Raeber GP, Zisch AH, et al. Cell-responsive synthetic hydrogels. *Adv Mater* 2003;15:888–892.
20. Girish KS, Kemparaju K. The magic glue hyaluronan and its eraser hyaluronidase: A biological overview. *2007;80:1921–1943.*
21. Zustiak SP, Leach JB. Hydrolytically Degradable Poly (Ethylene Glycol) Hydrogel Scaffolds with Tunable Degradation and Mechanical Properties. *2010:1348–1357.*
22. Kloxin AM, Kasko AM, Salinas CN, et al. Photodegradable hydrogels for dynamic tuning of physical and chemical properties. *Science (80-)* 2009;324:59–63.
23. Beaulieu J-F. *Extracellular Matrix Components and Integrins in Relationship to Human Intestinal Epithelial Cell Differentiation*. 1997.
24. Simon-assmann P, Duclos B, Orian-rousseau V, et al. Differential Expression of Laminin Isoform and alfa6-beta4 Integrin Subunits in the Developing Human and Mouse Intestine. *Dev Dyn*

- 1994;201:71–85.
25. Dydensborg AB, Teller IC, Basora N, et al. Differential expression of the integrins $\alpha 6\beta 4$ and $\alpha 6\beta 4$ along the crypt–villus axis in the human small intestine. *Histochem Cell Biol* 2009;131:531–536.
26. Beaulieu JF, Vachon PH. Reciprocal expression of laminin A-chain isoforms along the crypt-villus axis in the human small intestine. *Gastroenterology* 1994;106:829–839.
27. Teller IC, Auclair J, Herring E, et al. Laminins in the developing and adult human small intestine: Relation with the functional absorptive unit. *Dev Dyn* 2007;236:1980–1990.
28. Simoneau A, Herring-Gillam FE, Vachon PH, et al. Identification, distribution, and tissular origin of the $\alpha 5(IV)$ and $\alpha 6(IV)$ collagen chains in the developing human intestine. *Dev Dyn* 1998;212:437–447.
29. Sato H, Naito I, Momota R, et al. The differential distribution of type IV collagen α chains in the subepithelial basement membrane of the human alimentary canal. *Arch Histol Cytol* 2007;70:313–323.
30. Groulx JF, Gagné D, Benoit YD, et al. Collagen VI is a basement membrane component that regulates epithelial cell-fibronectin interactions. *Matrix Biol* 2011;30:195–206.
31. Benoit YD, Groulx J-F, Gagné D, et al. RGD-Dependent Epithelial Cell-Matrix Interactions in the Human Intestinal Crypt. *J Signal Transduct* 2012;2012:1–10.
32. Yamamoto S, Nakase H, Matsuura M, et al. Heparan sulfate on intestinal epithelial cells plays a critical role in intestinal crypt homeostasis via Wnt/ -catenin signaling. *AJP Gastrointest Liver Physiol* 2013;305:G241–G249.
33. Mahoney Z, Stappenbeck T, Miner J. Laminin $\alpha 5$ influences the architecture of the mouse small intestinal mucosa. *J Cell Sci* 2008;121:2493–2502.
34. Riehl TE, Ee X, Stenson WF. Hyaluronic acid regulates normal intestinal and colonic growth in mice. *Am J Physiol Gastrointest Liver Physiol* 2012;303:G377–G388.
35. Gjorevski N, Sachs N, Manfrin A, et al. Designer matrices for intestinal stem cell and organoid culture. *Nature* 2016;539:560–564.
36. Rezakhani S, Gjorevski N, Lutolf MP. Low-Defect Thiol-Michael Addition Hydrogels as Matrigel Substitutes for Epithelial Organoid Derivation. *Adv Funct Mater* 2020;30:1–12.
37. Hernandez-Gordillo V, Kassis T, Lampejo A, et al. Fully synthetic matrices for in vitro culture of primary human intestinal enteroids and endometrial organoids. *Biomaterials* 2020;254:120125.
38. DiMarco RL, Dewi RE, Bernal G, et al. Protein-engineered scaffolds for in vitro 3D culture of primary adult intestinal organoids. *Biomater Sci* 2015;3:1376–1385.
39. Broguiere N, Isenmann L, Hirt C, et al. Growth of Epithelial Organoids in a Defined Hydrogel. *Adv Mater* 2018;30.
40. Cruz-Acuña R, Quirós M, Farkas AE, et al. Synthetic hydrogels for human intestinal organoid generation and colonic wound repair. *Nat Cell Biol* 2017:1–6.
41. Gordillo M, Evans T, Gouon-Evans V. Orchestrating liver development. *Dev* 2015;142:2094–2108.
42. Bedossa P, Paradis V. Liver extracellular matrix in health and disease. *J Pathol* 2003;200:504–515.
43. Kleinman HK, Malinda KM, Ponce ML. Extracellular matrix. *Inflamm Dis Blood Vessel* 2000:29–36.
44. Martinez-Hernandez A, Amenta PS. The hepatic extracellular matrix. *Virchows Arch A Pathol Anat Histopathol* 1993;423:77–84.
45. Rojkind M, Giambrone MA, Biempica L. Collagen Types in Normal and Cirrhotic Liver. *Gastroenterology* 1979;76:710–719.
46. Vyas D, Baptista PM, Brovold M, et al. Self-assembled liver organoids recapitulate hepatobiliary organogenesis in vitro. *Hepatology* 2018;67:750–761.
47. Huch M, Dorrell C, Boj SF, et al. In vitro expansion of single Lgr5+ liver stem cells induced by Wnt-

- driven regeneration. *Nature* 2013;494:247–50.
48. Hu H, Gehart H, Artegiani B, et al. Long-Term Expansion of Functional Mouse and Human Hepatocytes as 3D Organoids. *Cell* 2018;175:1591-1606.e19.
 49. Peng WC, Logan CY, Fish M, et al. Inflammatory Cytokine TNF α Promotes the Long-Term Expansion of Primary Hepatocytes in 3D Culture. *Cell* 2018;175:1607-1619.e15.
 50. Sorrentino G, Rezakhani S, Yildiz E, et al. Mechano-modulatory synthetic niches for liver organoid derivation. *Nat Commun* 2020;11:1–10.
 51. Yin M, Woollard J, Wang X, et al. Quantitative assessment of hepatic fibrosis in an animal model with magnetic resonance elastography. *Magn Reson Med* 2007;58:346–353.
 52. Ye S, Boeter JWB, Mihajlovic M, et al. A Chemically Defined Hydrogel for Human Liver Organoid Culture. *Adv Funct Mater* 2020;30.
 53. Taha IN, Naba A. Exploring the extracellular matrix in health and disease using proteomics. *Essays Biochem* 2019;63:417–432.
 54. Kim J, Koo B. Human organoids: model systems for human biology and medicine. *Nat Rev Mol Cell Biol* 2020;21.
 55. Kaplan GG. The global burden of IBD: From 2015 to 2025. *Nat Rev Gastroenterol Hepatol* 2015;12:720–727.
 56. O’Shea NR, Smith AM. Matrix metalloproteases role in bowel inflammation and inflammatory bowel disease: An up to date review. *Inflamm Bowel Dis* 2014;20:2379–2393.
 57. Petrey AC, la Motte CA de. The extracellular matrix in IBD. *Curr Opin Gastroenterol* 2017;33:234–238.
 58. Li ACY, Thompson RPH. Basement membrane components. *J Clin Pathol* 2003;56:885–887.
 59. Bouatrouss Y, Herring-Gillam FE, Gosselin J, et al. Altered expression of laminins in Crohn’s disease small intestinal mucosa. *Am J Pathol* 2000;156:45–50.
 60. Johnson LA, Rodansky ES, Sauder KL, et al. Matrix stiffness corresponding to strictured bowel induces a fibrogenic response in human colonic fibroblasts. *Inflamm Bowel Dis* 2013;19:891–903.
 61. Herrera J, Henke CA, Bitterman PB, et al. Extracellular matrix as a driver of progressive fibrosis Find the latest version : Extracellular matrix as a driver of progressive fibrosis. 2018;128:45–53.
 62. S. L. Friedman. The cellular basis of hepatic fibrosis: Mechanisms and treatment strategies. *New England Journal of Medicine* 1990;323:1120–1123.
 63. Rohn F, Kordes C, Castoldi M, et al. Laminin-521 promotes quiescence in isolated stellate cells from rat liver. *Biomaterials* 2018;180:36–51.
 64. Rohn F, Kordes C, Buschmann T, et al. Impaired integrin $\alpha 5/\beta 1$ -mediated hepatocyte growth factor release by stellate cells of the aged liver. *Aging Cell* 2020:1–17.
 65. Sato T, Stange DE, Ferrante M, et al. Long-term Expansion of Epithelial Organoids From Human Colon, Adenoma, Adenocarcinoma, and Barrett’s Epithelium. *Gastroenterology* 2011;141:1762–1772.
 66. Spence JR, Mayhew CN, Rankin SA, et al. Directed differentiation of human pluripotent stem cells into intestinal tissue in vitro. *Nature* 2011;470:105–109.
 67. Miyoshi H, Stappenbeck TS. In vitro expansion and genetic modification of gastrointestinal stem cells in spheroid culture. *Nat Protoc* 2013;8:2471–2482.
 68. Ootani A, Li X, Sangiorgi E, et al. Sustained in vitro intestinal epithelial culture within a Wnt-dependent stem cell niche. *Nat Med* 2009;15:701–706.
 69. Jabaji Z, Sears CM, Brinkley GJ, et al. Use of Collagen Gel as an Alternative Extracellular Matrix for the *In Vitro* and *In Vivo* Growth of Murine Small Intestinal Epithelium. *Tissue Eng Part C Methods* 2013;19:961–969.
 70. Jabaji Z, Brinkley GJ, Khalil HA, et al. Type I collagen as an extracellular matrix for the in vitro

- growth of human small intestinal epithelium. PLoS One 2014;9:1–9.
71. Tong Z, Martyn K, Yang A, et al. Towards a defined ECM and small molecule based monolayer culture system for the expansion of mouse and human intestinal stem cells. Biomaterials 2017;154:e17–e19.
 72. Capeling MM, Czerwinski M, Huang S, et al. Nonadhesive Alginate Hydrogels Support Growth of Pluripotent Stem Cell-Derived Intestinal Organoids. Stem Cell Reports 2019;12:381–394.
 73. Takebe T, Sekine K, Enomura M, et al. Vascularized and functional human liver from an iPSC-derived organ bud transplant. Nature 2013;499:481–484.
 74. Giobbe GG, Crowley C, Luni C, et al. Extracellular matrix hydrogel derived from decellularized tissues enables endodermal organoid culture. Nat Commun 2019;10.

Chapter 2

Low-defect thiol-Michael addition hydrogels as Matrigel substitutes for epithelial organoid derivation

Saba Rezakhani^{1,2}, Nikolce Gjorevski¹, Matthias P. Lutolf^{1,2*}

¹Laboratory of Stem Cell Bioengineering, Institute of Bioengineering, School of Life Sciences, Ecole Polytechnique Fédérale de Lausanne (EPFL), 1015 Lausanne, Switzerland.

² Institute of Chemical Sciences and Engineering, School of Basic Sciences, EPFL, 1015 Lausanne, Switzerland.

*E-mail: matthias.lutolf@epfl.ch

(Published in Advanced Functional Materials, 2020

<https://doi.org/10.1002/adfm.202000761>)

2.1 Abstract

Due to their selective crosslinking chemistry and well-defined mechano-biochemical characteristics, hydrogels crosslinked by thiol-Michael addition reactions have garnered immense interest for 3D cell culture applications. These hydrogels are typically formed via end-linking of bis-cysteine oligopeptides and branched f-functional ($f \geq 3$) poly(ethylene glycol) (PEG). Unfortunately, this gel design accumulates excessive structural defects at a solid content below $\sim 10\%$ (w/v) due to diluted bi-functional components reacting intra-molecularly to form primary loops that compromise the gels' mechanical integrity and lead to excessive swelling. These limitations restrict the suitability of the gels for challenging cell culture applications, such as the growth of organoids. Here, we report low-defect thiol-Michael addition (LDTM) hydrogels based on novel building blocks designed towards minimizing structural defects. Compared to the conventional gels, LDTM gels can be generated at an at least two-fold lower solid content, while still incorporating high concentrations of bioactive ligands (~ 3 mM). LDTM gels promote the efficient development of fully patterned mouse intestinal organoids as well as human intestinal organoids, the latter in the absence of any animal-derived components. We thus provide powerful alternatives to the gold-standard Matrigel, which is expensive and too variable for robust organoid development, facilitating translational applications of organoids.

2.2 Introduction

Owing to their structural and functional similarity to native tissues, organoids, which are miniaturized multicellular tissues formed via stem cell self-organization,¹ have sparked interest for their application in disease modeling, drug screening, and regenerative medicine.^{2,3} Organoids can be derived from multi- or pluri-potent stem cells via three-dimensional (3D) cell culture, which currently requires Matrigel, a reconstituted basement membrane extract, which is isolated from tumor tissues grown in mice and provides a highly bioactive scaffold rich in laminin-111.⁴ However, Matrigel has an extremely complex and undefined composition.⁵ The batch-to-batch variability, risk of pathogen transfer, and inability to modify its key physical and biochemical properties make this matrix unsuitable for clinical applications. For such complex 3D cell culture applications as organoid development, chemically derived, synthetic matrices are necessary.

Pioneering efforts in biomaterial development for organoid culture have focused on identifying synthetic alternatives for Matrigel.^{6–8} Our laboratory has demonstrated that epithelial organoids can be derived from mouse or human intestinal⁹ and liver¹⁰ stem and progenitor cells in PEG hydrogels crosslinked via human Factor XIIIa, a natural transglutaminase¹¹. These organoid culture matrices were functionalized with adhesion peptides, in some cases also laminin-111⁹, and were formulated at an optimal shear modulus (G') of ~ 1.3 kPa.^{9,10} These enzymatically crosslinked PEG matrices have served as an important starting point to define the key requirements for epithelial stem cell expansion, tissue growth, and subsequent organoid development, revealing for example an important role of gel stiffness in controlling multiple steps of *in vitro* organogenesis. However, the complexity of the hydrogel crosslinking chemistry, as well as high costs and batch-to-batch variability associated with the crosslinking enzyme FXIIIa, arguably limits its broader applicability. Therefore, we set out to adopt this concept to a simpler and more robust hydrogel crosslinking chemistry based on Michael addition reactions between thiols and vinyl sulfone - a highly modular “click” reaction.¹² Of note, it has been previously demonstrated that hydrogels composed of maleimide-terminated 4-arm PEG and matrix metalloprotease (MMP)-sensitive bis-cysteine peptides promote the generation of human pluripotent stem cell (hPSCs)-derived intestinal organoids.¹³ However, organoid derivation in these matrices required pre-aggregation of hPSC expanded on a Matrigel layer, and it was thus not possible to generate organoids from a single cell in a chemically defined system.

Although thiol-Michael addition hydrogels are widely considered as nearly ideal networks that can be formed with a well-defined molecular architecture and bio-functionality, they suffer from structural defects at low solid content.^{14,15} That is to say, in a “real” PEG-co-peptide network, intramolecular crosslinks occurring between two functional groups of the same macromer lead to the formation of primary loops.¹⁶ Such imperfections have an adverse effect on the mechanical properties of a network, and lead to excessive swelling, because they decrease the concentration of its elastically active chains^{16,17}, and they are more likely to occur at the low polymer content, that is, below $\sim 10\%$ (w/v), typically required for *in vitro* tissue formation. Zhong and colleagues¹⁸ quantified the impact of “loop” defects on polymer network elasticity and derived a real elastic network theory (RENT) that describes how loop defects affect bulk elasticity: $G = G_0 (1 - \frac{3}{8} \phi_\lambda)$, where G_0 is the modulus of an ideal network with no defects and G is the modulus of the real

network. This theory reveals the direct impact of primary loops on the shear modulus, indicating that higher shear moduli can be achieved by decreasing first-order network defects. To minimize network defects, Shikanov *et al.*¹⁵ have reported improved crosslinking densities of PEG-co-peptide hydrogels formed from acrylate-terminated 4-arm PEG and a tri-functional, rather than a bi-functional, cysteine-bearing peptide linker¹⁹. Using the same network design, Kim *et al.* investigated the effect of biomodification and PEG functionality on the final network properties²⁰. Accordingly, an increased PEG functionality resulted in a higher degree of bioactive modification, in turn resulting in a better behavior of encapsulated cells. However, despite these improvements, no robust hydrogel formation was achieved below 4% (w/v) solid content, a range that is typically required to achieve the biologically relevant stiffness ranges required for organoid culture.

To address these shortcomings, we herein modified the conventional crosslinking strategy of PEG-co-peptide hydrogels formed by Michael addition of bis-cysteine peptides and vinyl sulfone (VS)-terminated PEG macromers (PEG-VS)^{14,21}, such as to substantially reduce network defects and therefore enhance the gel's physicochemical properties at low solid content. We refer to these matrices as low-defect thiol-Michael addition (LDTM) hydrogels. We demonstrate that LDTM gels provide excellent scaffolds for mouse and human intestinal organoid derivation. In particular, mouse intestinal stem cells (ISCs) were found to undergo colony formation and crypt formation with efficiencies close to those of Matrigel, the gold standard organoid culture system. Moreover, we for the first time achieve the derivation of human intestinal organoids in the absence of any animal-derived components such as Matrigel-derived laminin-111. Overall, these cost-effective, chemically defined hydrogels can be easily produced with minimal batch-to-batch variability and may thus open up exciting avenues for the clinical application of organoids.

2.3 Results and discussion

Conventional thiol-Michael addition gel architectures do not promote stem cell expansion and organoid derivation

We first tested whether the enzymatically crosslinked PEG hydrogels that we had previously utilized for epithelial organoid culture^{9,10} could be potentially replaced with a simpler, chemically crosslinked gel system. To this end, we generated cell-adhesive, RGD (Arg-Gly-Asp)-modified^{22–24} PEG-co-peptide hydrogels, crosslinked via end-linking of bis-cysteine oligopeptides and 4- or 8-arm VS-terminated PEG macromers (termed here ‘conventional PEG-PEP gels’)¹⁴, at a shear modulus of ~1.3 kPa, optimal for the expansion of primary ISCs into cystic polarized epithelial tissues. To achieve this targeted stiffness, we used a PEG content of 5% and 4% (w/v) for 4-arm or 8-arm PEG macromers, respectively. Surprisingly, and in contrast to control culture conditions (Matrigel and FXIII-crosslinked gels), encapsulated single mouse ISCs embedded in these conventional thiol-Michael addition hydrogels did not promote the formation of polarized ISC colonies, even across a relatively large range of shear moduli between 200 Pa and 1.6 kPa (**Figure S1**). Although some colonies were formed in softer matrices, the extent of colony formation was far below that of Matrigel. Of note, Acuña *et al.* have similarly reported that hydrogels with a polymer (PEG-4MAL) content ranging from 3.5% to 4% supported early- to late-stage organoid

transformation, whereas culture in hydrogels formed at higher polymer concentrations resulted in greatly decreased viability.¹³

Design and synthesis of low-defect thiol-Michael addition (LDTM) hydrogels

We hypothesized that the failure to support ISC-based epithelial colony formation in conventional PEG-co-peptide (PEG-PEP) gels (**Figure S1**) could be related to their relatively high polymer content necessary to compensate for the high swelling caused by network imperfections, with this failure occurring either directly or indirectly (**Figure 1A**). The imperfections in these gels are primarily introduced when the bifunctional peptides react with multi-arm PEG intra-molecularly to form ‘primary loops’ (**Figure 1A**). To address this problem and minimize the level of network defects in conventional PEG-PEP gels, we conceived a hydrogel crosslinking scheme based on pre-reacted building blocks that could not engage in primary loop formation (**Figure 1B**). In this scheme, we predicted that using a 10-fold excess of thiols over VS would guarantee an efficient coupling, leaving unreacted thiol residues for further crosslinking. To this end, we first pre-reacted the bis-cysteine oligopeptides with 4- and 8-arm PEG-VS macromers via Michael-addition, generating tetra- and octa-thiol PEG macromers (**Figure 1B**, step 1), which were purified and then reacted with 4-arm or 8-arm PEG-VS (mol. wt. 20 kDa and 40 kDa) to form LDTM hydrogels (**Figure 1B**, step 2). Indeed, Ellman’s assay²⁵ on tetra- and octa-thiol containing PEG macromers performed before and after treatment with the reducing agent TCEP (tris[2-carboxyethyl]phosphine) confirmed no significant difference in thiol concentration between the two conditions, revealing an absence of disulfide-bond formation in the newly formed macromers (**Figure S2A**). ¹H-NMR measurements confirmed an almost complete functionalization of multi-arm PEGs with peptides (**Figure S2B**).

We then assessed whether the newly synthesized macromers (**Figure 1B**) could be used to form hydrogels via Michael addition reaction. Because of the well-known dependency of physicochemical gel properties on the stoichiometric ratio of functional groups¹⁴, we formulated hydrogels (at fixed solid content of 3% and without RGD) at five different stoichiometric ratios of VS to SH groups (r , ranging from 0.67 to 1.67) (**Figure S3**). The gels with the highest shear modulus and lowest swelling ratio, respectively, were formed at $r \approx 0.8$, consistent with conventional PEG-PEP hydrogels¹⁴. As expected, increasing the PEG functionality from 4- to 8-arms influenced both the swelling and elastic behavior, wherein 8-arm PEG-based hydrogels had a higher shear modulus and swelled significantly less compared to those generated from 4-arm PEG (**Figure S3**).

LDTM gels form at unusually low solid content and high ligand concentration

We next sought to compare the swelling ratios, mechanical properties, and functionalization with bioactive ligands of conventional PEG-PEP hydrogels and LDTM gels for both 4-arm and 8-arm PEG gels (**Figure 2**). These experiments revealed striking differences between the gel types directly related to the different network designs: Across all concentrations tested, LDTM gels had a higher

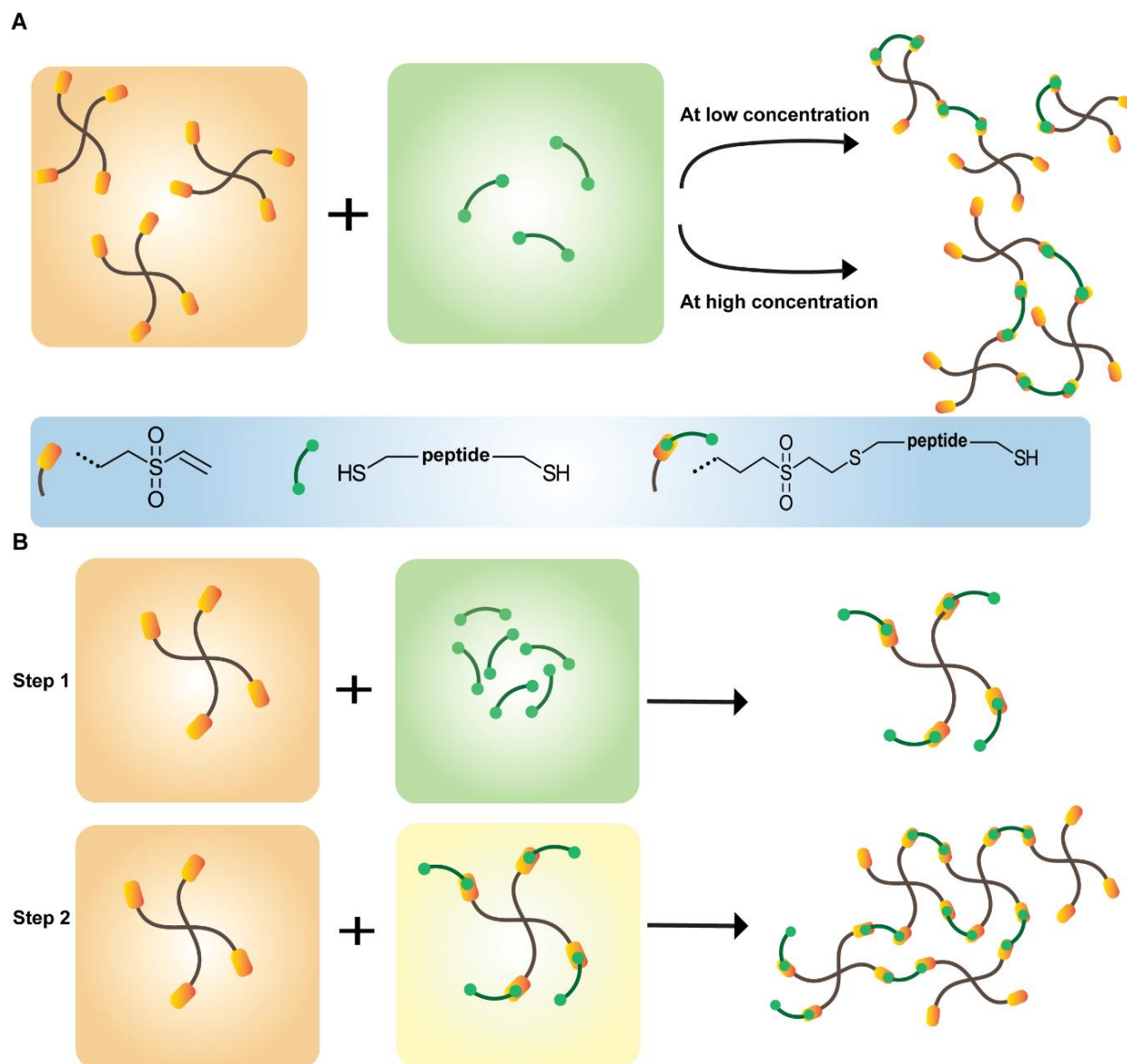


Figure 1. Concept and chemistry. A) Crosslinking of 4-arm PEG macromers with bifunctional peptides. At high polymer concentrations, all crosslinks are elastically active, whereas at low polymer concentrations, primary loop formation due to intramolecular crosslinking between two functional groups on the same precursor decreases the number of elastically active chains in the network. B) Gel precursor synthesis (step 1) and synthesis scheme for the stepwise copolymerization of 4-arm PEG-VS macromers with PEG macromers containing tetra-thiol peptides (step 2).

shear modulus (**Figure 2A,B**), swelled less (**Figure 2C,D**), and maintained better network integrity when functionalized with the cell adhesion peptides RGD (**Figure 2E-H**). Indeed, LDTM gels could be formed at an unusually low solid content of ~1.25% (w/v), in contrast to conventional PEG-PEP gels that did not form below 2% (w/v).

The incorporation of bioactive ligands such as these RGD peptides into hydrogels can compromise the gels crosslinking density because ligand incorporation via thiol residues occurs through the same Michael addition chemistry and therefore competes with crosslinking via VS groups.

However, modifying the conventional macromer structure according to **Figure 1B** allowed us to markedly increase the degree of bioactivity of the hydrogels, particularly at very low solid content (**Figure 2E-H**). Indeed, 4- and 8-arm PEG hydrogels formulated at ~3% (w/v) with tetra- and octa-thiol macromers allowed us to incorporate up to 2 and 3 mM of RGD, respectively, without losing their mechanical integrity, whereas traditional gels already became too soft ($G' < 50$ Pa) when functionalized with 1 mM of RGD. The robust and reproducible presentation of cell-adhesive ligands is another major advantage of the synthetic gel system compared to Matrigel, which offers no direct control over the concentration and identity of cell-binding ligands. Indeed, a proteomics analysis showed only ~53% similarity between batches of two Matrigel manufacturers.⁵

To get some insights into the non-ideal characteristics of our newly formulated gels and the effect of the macromer structure modification on crosslinking density, we calculated the concentration of elastically active chains using a modified Flory-Rehner equation¹⁴. As shown in **Figure S4**, LDTM gels have higher concentration of elastically active chains compared to conventional PEG-PEP hydrogels.

LDTM gels support mouse ISC colony formation

With fully defined synthetic hydrogels able to form at unusually low solid content, we next tested those gels for their potential to derive epithelial organoids. Previous work in our lab has extensively characterized the growth requirements of mouse ISCs, normally located at the bottom of intestinal crypts *in vivo*, within synthetic matrices.⁹ ISCs can be cultured *in vitro* and self-organize into intestinal organoids bearing crypt-villus structures containing stem cells and differentiated cells^{26,27}. To test whether LDTM hydrogels could support the expansion of single ISCs into polarized epithelial colonies, similar to what we had reported for matrices crosslinked via the transglutaminase FXIIIa,⁹ we encapsulated dissociated mouse ISCs into RGD-modified 4- and 8-arm LDTM gels of varying stiffness. Whereas conventional PEG-PEP gels did not support ISC colony formation (**Figure 3A,D**), LDTM hydrogels with the same stiffness supported the formation of epithelial colonies (**Figure 3B,E**). After four days of culture, we observed maximal colony formation efficiency in the gels (containing 1mM RGD) with shear moduli of ~1 kPa, indicating an effect of matrix stiffness on ISC proliferation and colony formation efficiency (**Figure 3C,F**).

When switched to differentiation culture conditions to promote organoid formation, epithelial colonies grown in 4- and 8-arm LDTM hydrogels did not support the formation of organoids, that is, epithelia that harbor outward-protruding crypt-like structures. This is in line with our previous experiments on organoid formation in PEG hydrogels crosslinked via Factor XIIIa, revealing a requirement for matrix softening to ~ 200Pa for triggering crypt formation and thus complete organoid development.⁹ To verify that the absence of budding in LDTM hydrogels was due to the high stiffness of the gels and not a loss of stem-cell potential, intestinal colonies were transferred to Matrigel after four days of culture. In this more permissive microenvironment, ISCs gave rise to fully developed organoids bearing crypts (**Figure 3G,H**), thus demonstrating that organoid-formation potential was not lost in relatively stiff LDTM gels.

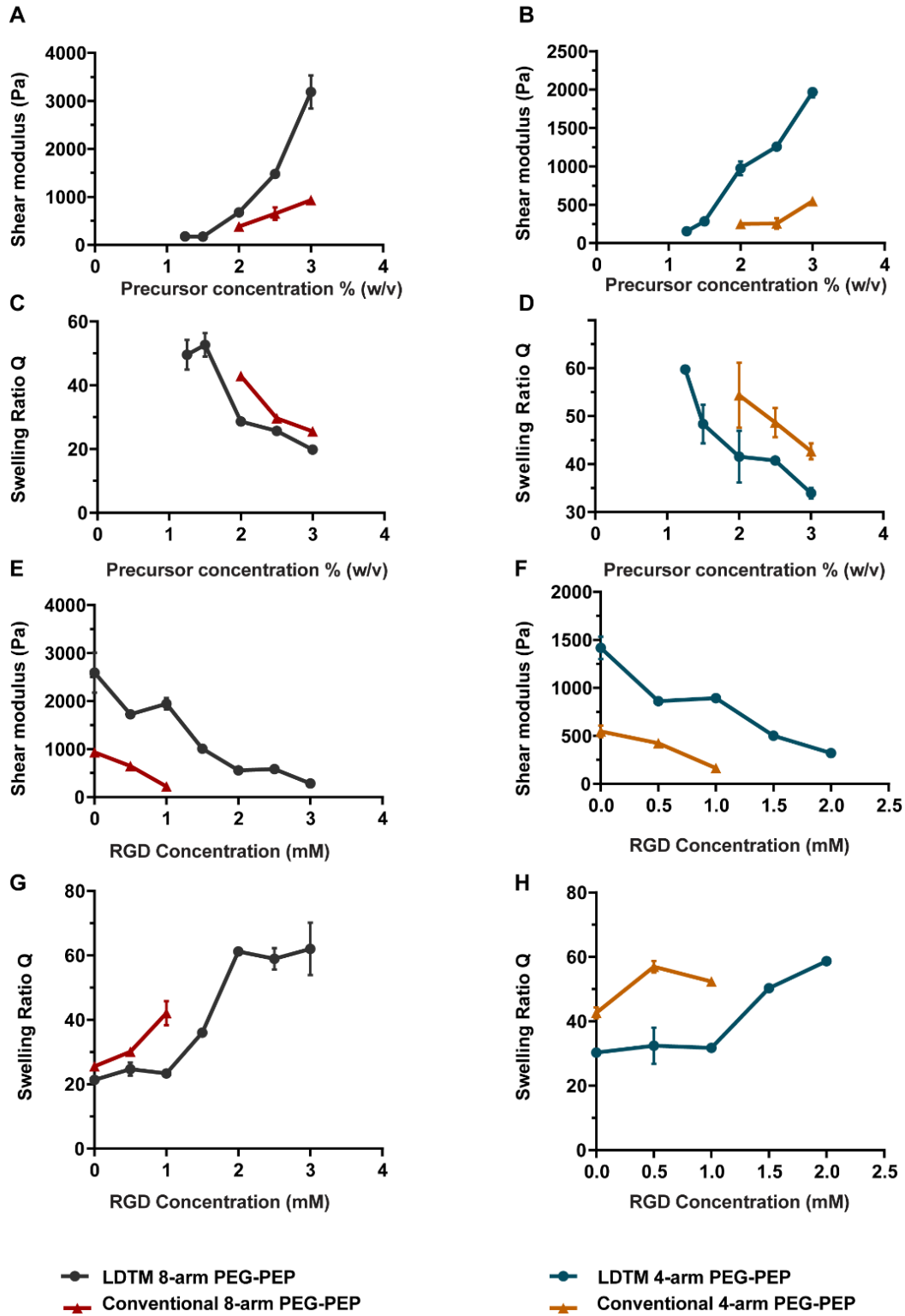


Figure 2. Network characterization. A, B) 4- and 8-arm LDTM hydrogels (no RGD) have a higher shear modulus and (C, D) lower swelling ratios compared to conventional PEG-PEP gels. (E-H) Shear moduli and swelling ratios of hydrogels formed at 3% (w/v) and at $r = 0.8$ as a function of RGD concentration. All data are reported as mean \pm S.D. ($n = 3$)

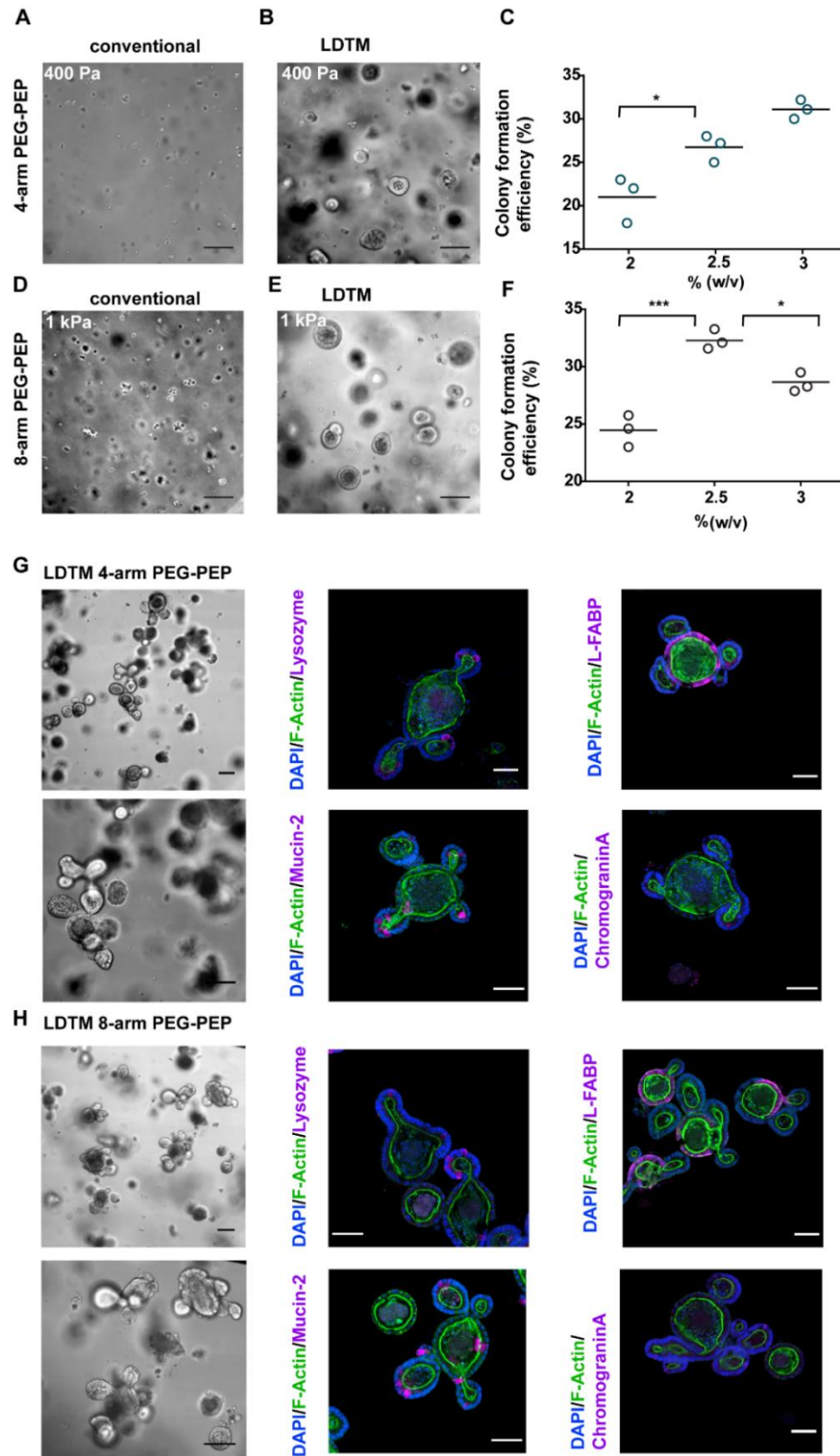


Figure 3. Stem cell expansion and demonstration of multipotency. **A, B, D, E)** ISC colony formation in conventional and LDTM 4-arm and 8-arm PEG hydrogels (2.5%(w/v), 1 mM RGD) after four days of culture in expansion medium. **C, F)** Quantification of colony formation efficiency in LDTM hydrogels. **G, H)** Colonies expanded in 4- and 8-arm LDTM hydrogels formed organoids containing differentiated intestinal cells after transplantation in Matrigel. Scale bars for bright-field images: 100 μ m and for immunostaining images: 50 μ m.

Hydrolytically degradable LDTM gels support complete organoid morphogenesis

To design a chemically defined, low swelling PEG matrix that would permit both ISC expansion and organoid formation in one step, we took advantage of our published strategy of inducing continuous, gradual softening via chemical degradation⁹. To this end, we formulated networks comprising various ratios of peptide-functionalized 4- and 8-arm PEG-Acrylate (termed ‘D-PEG’), allowing gel softening via ester hydrolysis, and thus providing a dynamic and softer environment conducive to *in vitro* organogenesis (**Figure 4A**). Indeed, 4-arm LDTM hydrogels containing 100% D-PEG (2.5% (w/v)) were found to provide an optimal, relatively stiff environment for initial ISC colony formation, and, through gradual softening over four days, to promote budding and organoid formation after switching to differentiation medium (**Figure 4B-E**). In contrast, the other tested gels, being the 4-arm LDTM hydrogels containing 50% D-PEG (2.5% (w/v)) and both 50% and 100% D-PEG-containing 8-arm LDTM hydrogels (2.5% (w/v)), did not reach an optimal stiffness after four days of expansion, and therefore did not permit organoid formation.

Peptide-free LDTM gels promote efficient organoid culture

The above LDTM gel formulations contained an MMP-sensitive peptide linker such as to facilitate organoid passaging via enzymatic gel degradation. However, the optimal gel formulation for organoid derivation (**Figure 4D,E**) was fully hydrolytically degradable (*i.e.* composed of 100% D-PEG), thus allowing organoid passaging without the need for enzymatic degradability. Consequently, we tried to generate a linker peptide-free system that could be considerably simpler and cheaper. We thus substituted the peptide-containing PEG macromer with multi-arm PEG-thiol (**Figure 5A**). Strikingly, hydrogels formed via Michael addition reaction between 8-arm PEG-Acr and PEG-thiol (3% (w/v), $r \approx 1$) supported the initial ISC colony formation (**Figure 5B**) and, upon softening via ester hydrolysis, allowed complete organoid development (**Figure 5C,D**).

Then, we systematically compared the two LDTM gel types with previously developed FXIIIa-based gels⁹ at the same initial stiffness and softening profile, as well as with Matrigel, in terms of ISC colony and organoid formation efficiencies. ISC culture in the different synthetic matrices resulted in similar colony formation efficiencies (**Figure 5E**). Interestingly, in the peptide-free LDTM gels, a lower number of colonies gave rise to organoids (**Figure 5F**). Taken together, these data show that our LDTM hydrogels sustain ISC growth and, when formed with hydrolytically degradable macromers, can accommodate epithelial tissue budding and complete organoid development, even in an inexpensive peptide-free system.

Human ISC expansion and differentiation in the absence of animal-derived components

We next assessed whether LDTM matrices could also support the derivation of clinically relevant human epithelial organoids. To do so, we first encapsulated single cells obtained from human small intestinal and colon organoids in RGD-containing 8-arm LDTM hydrogels (2.5% (w/v)) and cultured them in human intestinal organoid culture medium²⁸.

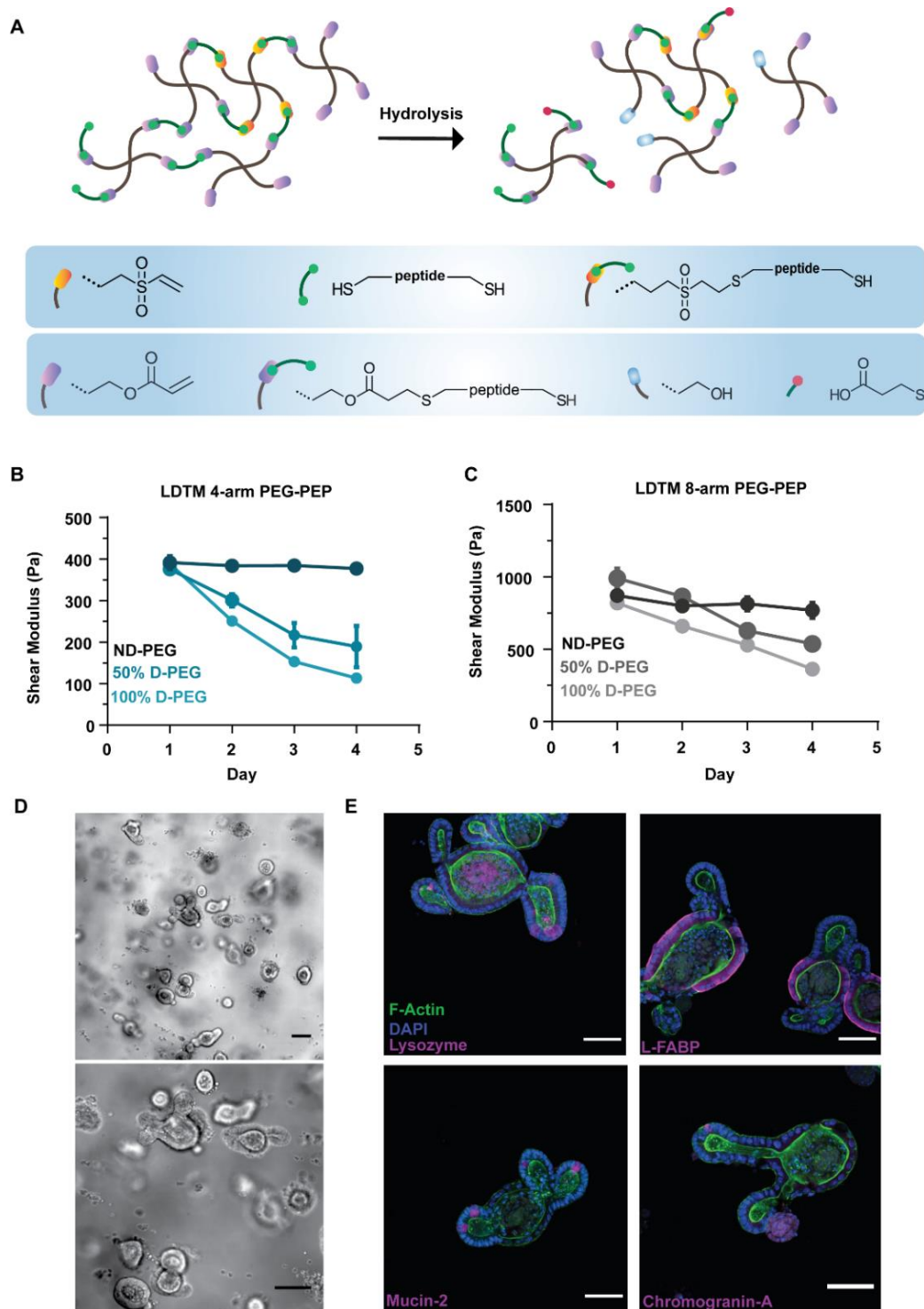


Figure 4. Dynamic matrices for organoid formation in one step. **A)** Schematic illustrating the ester hydrolysis of LDTM hydrogels containing peptide-functionalized PEG-Acr and PEG-VS macromers. **B), C)** Softening rate in 4- and 8-arm LDTM hydrogels (2.5%, 1 mM RGD) with different ratios of PEG-Acr to PEG-VS over 4 days of culture (from non-degradable [ND-PEG] to fully degradable [100% D-PEG]). **D)** 4-arm LDTM 100% D-PEG (2.5%, 1 mM RGD) permits efficient intestinal organoid formation. **E)** Immunostaining of Paneth cells (lysozyme), goblet cells (mucin-2), enterocytes (L-FABP), and enteroendocrine cells (chromogranin-A) in the formed organoids. All data are reported as mean \pm S.D. ($n = 3$). Scale bars for bright-field images: 100 μ m and for immunostaining images: 50 μ m.

Individual cells proliferated to give rise to cystic colonies after three days of culture, which was that same as in the Matrigel gold standard (**Figure 6**). Importantly, we found that laminin-111 was not necessary for colony formation as colony formation potential in RGD-only gels was not different, at least based on a visual inspection, than in gels modified with laminin-111²⁹ or the E8 fragment of laminin-511³⁰ (**Figure S5A**). Immunostaining for Ki-67 showed that human ISC colonies formed in RGD-functionalized LDTM gels contained proliferative cells (**Figure S5B**). Moreover, quantitative PCR (qPCR) revealed the expression of stem/progenitor markers in cystic colonies grown in LDTM gels to similar levels than in Matrigel (**Figure S5C,D**).

Recently, Sato *et al.* modified the culture conditions for human ISCs to promote improved organoid formation, that is, the co-emergence of stem/progenitor and differentiated cell types,³¹ as opposed to the conventional protocol that biases the system towards undifferentiated cells. Therefore, to test whether LDTM gels would support both the self-renewal and multi-lineage differentiation capacity of human ISCs into organoids, we encapsulated single human ISCs in RGD-only containing 8-arm PEG-VS LDTM hydrogels (2.5% (w/v)). After 10 days of culture, we observed thick epithelial colonies that formed budding structures upon transfer of colonies to Matrigel, confirming that LDTM hydrogels support stemness of human ISCs (**Figure S6A,B**).

Next, we hypothesized that hydrolytically degradable LDTM hydrogels that soften gradually (**Figure 4B,C**) could accommodate epithelial budding and organoid development similar to what is seen in mouse intestinal organoids. Strikingly, in hydrolytically degradable LDTM matrices composed of 3% (w/v) 4-arm D-PEG, we observed a similar organoid phenotype as in Matrigel, with tissues simultaneously harboring Ki-67-expressing proliferative cells and differentiated cell types, such as Goblet and Paneth cells (**Figure 7A,B**). The inclusion of laminin-111 in these hydrolytically degradable LDTM matrices further improved organoid formation capacity (**Figure S6C**), even affording serial passaging (**Figure S6D**).

These data demonstrate that LDTM hydrogels provide a chemically defined environment for the culture of human intestinal organoids without the requirement of animal-derived components, and thus could overcome the current roadblock for successful translation of organoid technology from the lab to the clinic.

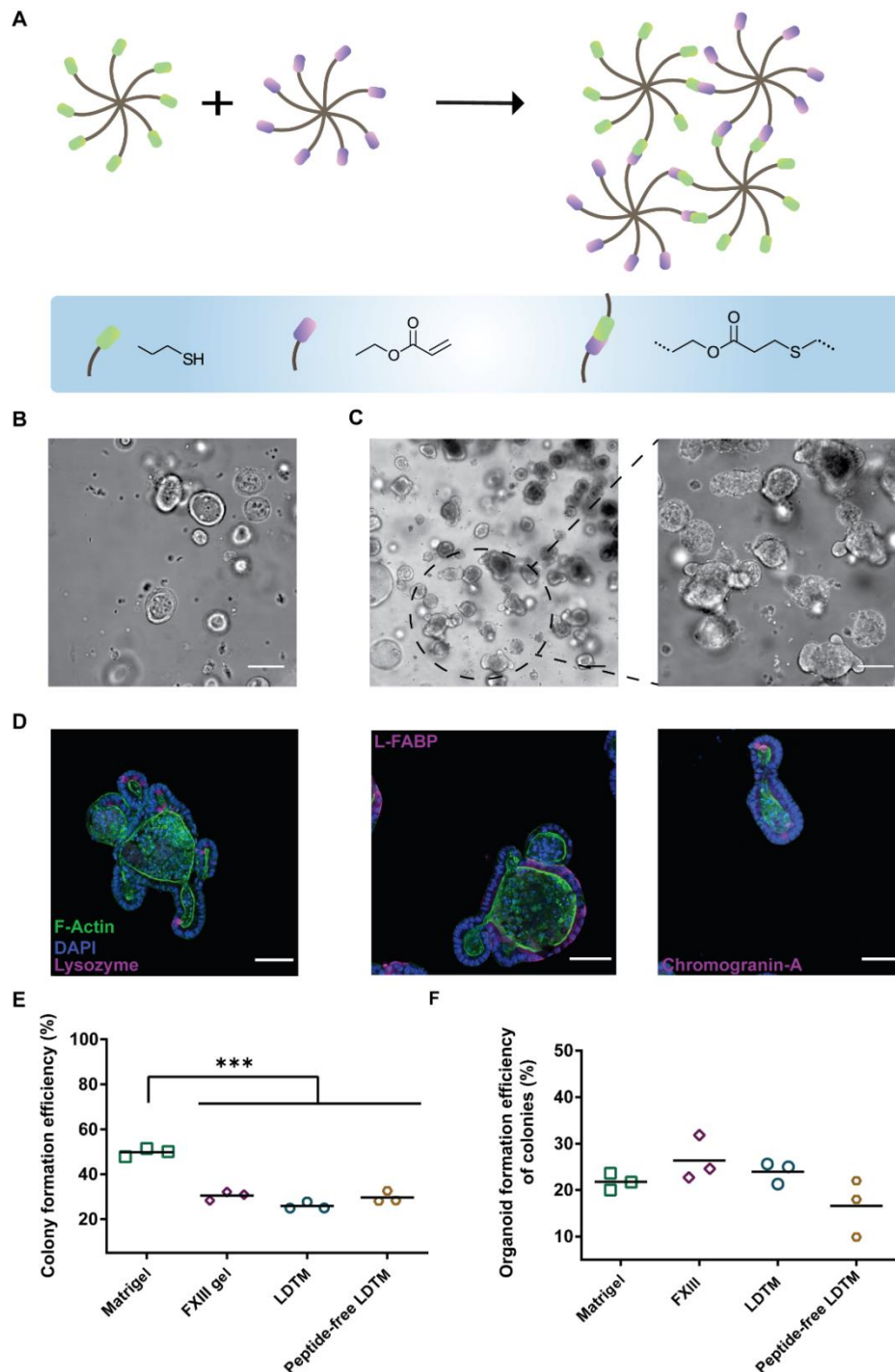


Figure 5. Peptide free LDTM hydrogels for mouse intestinal organoid formation. **A)** Schematic illustrating the Michael-addition reaction between acrylate- and thiol-functionalized 8-arm PEG. **B)** After four days of culture in proliferation medium, single mISCs form epithelial colonies (3% (w/v), 1 mM RGD). **C)** Round colonies could bud out and form organoids two days after switching to differentiation medium. Scale bars, 100 μ m **D)** Immunostaining of Paneth cells (lysozyme), enterocytes (L-FABP), and enteroendocrine cells (chromogranin-A) in the formed organoids. Scale bars, 50 μ m. **E)** Colony formation efficiency of ISC embedded in Matrigel, FXIII gels, LDTM, and peptide-free LDTM matrices. **F)** Percentage of the colonies that form organoids. Individual data points derived from $n = 3$ experiments and means are shown.

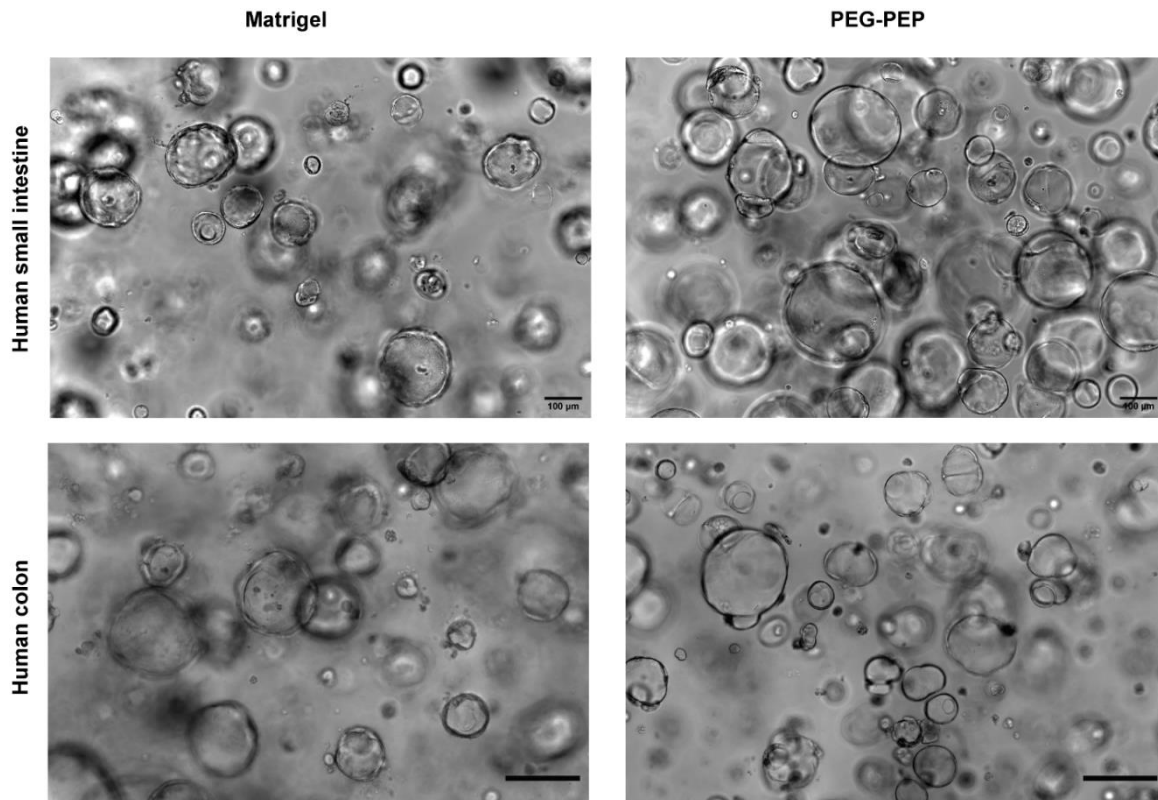


Figure 6. LDTM hydrogels support the expansion and colony formation of human intestine and colon stem cells. Single cells derived from human intestine and colon organoids previously generated in Matrigel were encapsulated in 8-arm LDTM gels (2.5%(w/v)) functionalized with 1 mM RGD, and cystic colonies were formed three days after embedding. Scale bars, 100 μm .

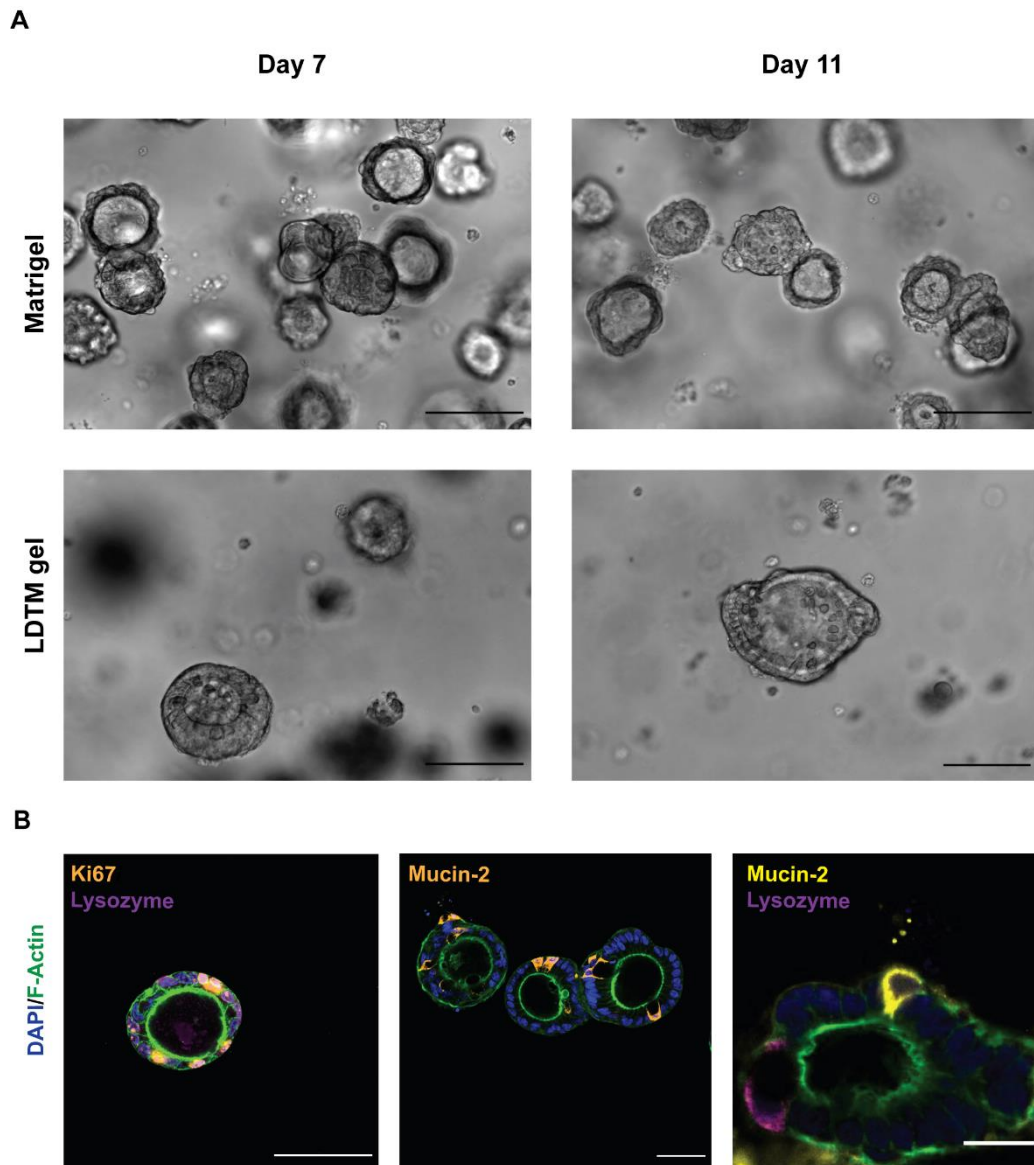


Figure 7. LDTM hydrogels support human intestinal organoid culture. Single cells derived from human intestinal organoids previously generated in Matrigel with modified culture conditions were encapsulated in Matrigel and 4-arm PEG-Acr LDTM gels (3% (w/v), 1 mM RGD). **A)** Organoids were formed after one week of culture. Scale bars, 100 μ m. **B)** Organoids encapsulated in LDTM gels contained proliferative and differentiated cells. Scale bars, 50 μ m.

2.4 Conclusion

Michael-addition click reactions between vinyl sulfone- or acrylate-terminated multi-arm PEG macromers and thiol-containing multi-arm PEG-peptide macromers allowed the formation of hydrogels at unusually low solid content and with higher bioactive ligand concentration than what can be achieved in existing systems. Increasing the precursors' functionality minimized structural imperfections and resulted in lower gel swelling and higher stiffness compared to traditional PEG-co-peptide formulations based on bis-cysteine peptides. We demonstrated the successful derivation of both mouse and human intestinal organoids in such simplified hydrogel formulations, wherein the human organoid derivation contained only the adhesion peptide RGD. These chemically crosslinked hydrogels do not depend on the use of an enzyme such as the transglutaminase Factor XIIIa¹¹, which is expensive and thus difficult to translate to the clinic. To our knowledge, the LDTM hydrogels introduced here are the first reported hydrogel system for the expansion of human small intestinal and colon organoids without the presence of any mouse tumor-derived component at any step of the process. LDTM hydrogels thus provide a reproducible, chemically defined environment that can be easily produced with minimal batch-to-batch variability for multiple stem cell types and for organoid culture. We believe that the ease of formation and low cost of these hydrogels may open particularly exciting perspectives for clinical applications of organoids.

2.5 Materials and methods

Hydrogel Components

Vinylsulfone-functionalized 4- and 8-arm PEG (4-arm PEG-VS 20 kDa, and 8-arm PEG-VS 40 kDa) were purchased from NOF, and acrylate-functionalized 4- and 8 arm PEG (4-arm PEG-Acr 20 kDa, 8-arm PEG-Acr 40 kDa) and thiol-functionalized 8-arm PEG (8-arm PEG-SH, 40 kDa) were purchased from Jenkem Technology. The peptide Ac-GCRE-*GPQGIWGQ*-ERCG-NH₂ (mol wt 1773.97 g mol⁻¹) with matrix metalloproteinases (MMPs) sensitive sequence (in italics) was obtained from Biomatik. The adhesion peptide Ac-GRCGRGDSPG-NH₂ (mol wt 1002.04 g/mol) was purchased from GL Biochem. To synthesize the tetra- and octa-thiol containing PEG macromers, multi-arm PEG-VS or PEG-Acr and peptides (SH/Vs or SH/Acr=10) were dissolved in triethanolamine (0.3M, pH 8.0), and reacted for 2 h at room temperature under inert atmosphere (drop-wise addition of PEG macromers to excess of peptides). The reaction solution was dialyzed (Snake Skin, MWCO 10K, PIERCE) against ultrapure water (pH<7) for 4 days at 4°C, and the final product was lyophilized. The lyophilized product was dissolved in water to make 10% precursor solutions.

Quantification of thiols and disulfides in PEG precursors

To verify the potential presence of disulfide bonds in the PEG precursors, thiol concentration was measured, before and after Tris(2 carboxyethyl)phosphine (TCEP, Thermo Scientific, 20491) treatment, using Ellman's assay based on the instruction from the supplier (Thermo Scientific, 22582). To reduce disulfide bonds, TCEP was dissolved in NaCO₃ (500 mM, pH=9), and added at 20X excess to the precursor solution and reacted for 1 hour at room temperature. TCEP-reduced precursors were passed through the Ziba Spin desalting column (Thermo Scientific, 89882) before measuring the concentration of thiols using Ellman's assay.

Hydrogel Formation

Conventional PEG-PEP hydrogels were formed by Michael type addition of di-thiol containing peptide on multi-arm PEG-VS and LDTM PEG-PEP hydrogels were formed by Michael type addition of tetra- and octa-thiol containing PEG precursors onto multi-arm PEG-VS. To make hydrogel networks of desired final PEG content, proper volumes of 10% (w/v) PEG-VS and peptides in 0.3 M triethanolamine, and 10% (w/v) synthesized macromers in water were mixed in different stoichiometric ratios. For example, to make 160 μ L of LDTM PEG-VS hydrogels (2.5% (w/v)), taking into account each precursors' densities, 22.13 μ L of synthesized octa-thiol containing PEG macromer, 20.37 μ L of PEG-VS and 27.5 μ L of water or cell culture medium were mixed. PEG-PEG matrices were formed by Michael type addition of thiol-functionalized 8-arm PEG on acrylate-terminated 8-arm PEG at equal stoichiometric ratio of functional groups. For cell encapsulation, the spare volume was used to incorporate dissociated ISCs, 300 mM TEA buffer, RGD containing peptide and natural mouse laminin-111 (Thermo Fisher Scientific) or Laminin-511 E8 fragment (Amsbio). Gels casted on PDMS-coated 24 well-plate were allowed to crosslink by incubation at 37°C for 10-20 min.

Equilibrium Swelling in Water

To calculate the swelling ratios (Q and Q') of hydrogels, 25 μL of gels were synthesized and weighed in air and ethanol before and after swelling in deionized water using a density determination kit. The volume of the dry polymer was determined based on the mass of the freeze-dried network and the density of the polymer in the dry state (taken as the density of PEG, 1.12 g cm^{-3}). Q and Q' were calculated as the ratio of gel volume after swelling to the volume of dry polymer and to the volume of the gel after crosslinking respectively.

Rheological Measurements of Swollen Networks

Shear modulus (G') of hydrogels was measured by performing small-strain oscillatory shear measurements on a Bohlin CVO 120 rheometer with plate-plate geometry. Briefly, 1-1.4 mm thick hydrogel discs were prepared and allowed to swell in water or cell culture medium for 24 hrs. The mechanical response of the hydrogels sandwiched between the parallel plates of the rheometer was recorded by performing frequency sweep (0.1-10 Hz) measurements in a constant strain (0.05) mode at room temperature.

Culture of mouse and human intestinal organoids

Murine intestinal crypts were isolated from 5–10-week-old heterozygous *Lgr5-eGFP-IRES-CreERT2* mice (Jackson Laboratory), as described previously and embedded in Matrigel (BD Biosciences; growth factor reduced, phenol red-free formulation).⁹ Human small intestinal organoids were generously provided by the Clevers lab, Hubrecht Institute, Netherlands. Human colon organoids were generously provided by the Schwank lab, University of Zurich, Switzerland. Single cells from dissociated mouse and human intestinal organoids grown in Matrigel were added to the hydrogels precursor solution and cast in 20- μL droplets at the bottom of wells in PDMS-coated 24-well plates. After polymerization (20-30 min, 37°C), the gels were overlaid with 600 μl of mISC expansion medium (Advanced DMEM/F12 containing Glutamax (Gibco), HEPES, penicillin-streptomycin, B27, N2 (Invitrogen) and $1 \times 10^{-6} \text{ M}$ N-acetylcysteine (Sigma)), supplemented with growth factors, including EGF ($50 \times 10^{-9} \text{ g ml}^{-1}$; R&D), Noggin ($100 \times 10^{-9} \text{ g ml}^{-1}$; produced in-house) and R-spondin ($1 \times 10^{-6} \text{ g ml}^{-1}$; produced in-house), and small molecules, including CHIR99021 ($3 \times 10^{-6} \text{ M}$; Millipore) and valproic acid (10^{-3} M ; Sigma) and conventional hISC expansion medium (Advanced DMEM/F12 containing Glutamax (Gibco), HEPES, penicillin-streptomycin, B27, N2 (Invitrogen) and 10^{-3} M N-acetylcysteine (Sigma), rWnt3a ($100 \times 10^{-9} \text{ g ml}^{-1}$; Time Bioscience), Noggin ($100 \times 10^{-9} \text{ g ml}^{-1}$; produced in-house) and R-spondin ($1 \times 10^{-6} \text{ g ml}^{-1}$; produced in-house), $10 \times 10^{-3} \text{ M}$ nicotinamide (Sigma), $10 \times 10^{-9} \text{ M}$ Gastrin (Tocris Bioscience), $500 \times 10^{-9} \text{ M}$ A83-01 (Tocris Bioscience), $10 \times 10^{-9} \text{ M}$ SB202190 (Sigma) and $10 \times 10^{-6} \text{ M}$ Blebbistatin (StemCell Technologies) or modified human organoid culture medium which contains conditioned medium (from L-WNR cell line)³², $10 \times 10^{-9} \text{ M}$ Gastrin (Tocris Bioscience), $500 \times 10^{-9} \text{ M}$ A83-01 (Tocris Bioscience), rhIGF ($100 \times 10^{-9} \text{ g ml}^{-1}$, Biolegend) and rhFGF-basic ($50 \times 10^{-9} \text{ g ml}^{-1}$, Peprotech). For single-cell culture, thiazovivin (2.5 μM ; Stemgent) was included in the medium during the first two days. Broad-spectrum protease inhibitor, GM6001, was added to the medium while embedding the cells in peptide-containing PEG hydrogels. The growth factors were replenished every two days, and the full medium was changed every 4 days. To induce mouse

intestinal organoid formation, the medium was removed, and the gels were washed with PBS, and medium containing EGF, Noggin, and R-spondin was added. To transfer colonies expanded in PEG hydrogels to Matrigel, gels were detached from the bottom of the plates using the tip of a metal spatula and transferred to 15-ml Falcon tube containing 1 ml of Dispase (1 mg ml⁻¹, Thermo Fisher Scientific). After 10-20 minutes enzymatic digestion, the reaction was quenched using 10% FBS containing 1 mM EDTA, washed with cold basal medium and centrifuged for 3 min at 800 rpm.

Quantification of ISC colony formation efficiency

Phase-contrast z-stacks images (20X) were collected through the entire thickness of the PEG gels at 4 different locations across the drops (Nikon Eclipse Ti) after 3 days of culture in expansion medium. The Cell Counter plugin in ImageJ (NIH) was used to quantify the number of single cells, irregularly shaped colonies, and lumen-containing colonies in each image. Colony formation efficiency was calculated by the ratio of lumen-containing colonies over the sum of colonies and single cells. To count the number of colonies in Figure S1, an all-in-focus image was produced from a series of z-stack images of each condition using Nikon's NIS-Elements software (EDF macro plugin).

Immunofluorescence analysis

Organoid staining was performed as described previously⁹. Briefly, intestinal organoids in Matrigel or PEG-Acr gels (almost degraded by the time organoids were formed) were fixed with 4% paraformaldehyde (PFA) in PBS (30 min, room temperature). After fixation, organoids were collected, centrifuged (800 r.p.m., 5 min), washed with ultra-pure water and pelleted. Next, the organoids were spread on glass slides and left to dry out to attach. Attached organoids were rehydrated with PBS, permeabilized with 0.2% Triton X-100 in PBS (1 h, room temperature) and blocked (10% goat serum in PBS containing 0.01% Triton X-100) for at least 3 h. Subsequently, mouse organoid samples were incubated with primary antibodies against lysozyme (1:50; Thermo Fisher Scientific PA1-29680), mucin-2 (1:50; Santa Cruz sc-15334), chromogranin-A (1:50; Santa Cruz sc-13090), L-FABP (1:50; Santa Cruz sc-50380) diluted in blocking buffer (overnight at 4 °C) and human organoid samples were incubated with ki67 (1:100 abcam ab16667), mucin-2 (1:100, BD Biosciences 555926) and lysozyme (1:100, GeneTex GTX72913). After washing with PBS for at least 3 h, samples were incubated with secondary antibody (1:1000 in blocking solution) Alexa 647 goat- α -rabbit (Invitrogen), or Alexa 568 donkey- α -mouse (Thermo Fisher Scientific A-31571), or Alexa 647 donkey- α -rabbit (Thermo Fisher Scientific, A-31573), phalloidin-Alexa 488 (1:100, Invitrogen) and DAPI (Thermo Fisher Scientific). Following extensive washing, stained organoids were imaged in confocal (Zeiss LSM 700) mode.

Quantitative real-time PCR (qPCR)

Human intestinal organoids grown in Matrigel or PEG gels were dissociated as described above, and RNA was extracted using an RNeasy Micro Kit (Qiagen). cDNA was synthesized using the iScript cDNA Synthesis Kit (Bio-Rad). qPCR was carried out using the Power SYBR Green PCR Master Mix (Applied Biosystems) and the primers listed in Table S1.

Statistical analysis

Statistical analyses were performed using GraphPad Prism 8.0 software. One-way ANOVA followed by a Bonferroni's multiple comparison test were used.

Acknowledgements

We thank G. Nikitin (EPFL) for help with the NMR measurements and D. Pioletti (EPFL) for rheometer use. This work was funded by the EU Horizon 2020 research programme INTENS (<http://www.intens.info/>) (#668294-2), the National Center of Competence in Research (NCCR) Bio-Inspired Materials, the Personalized Health and Related Technologies (PHRT) Initiative (PHRT - PM/PH Research Project Proposal 2017) from the ETH Board, and the Swiss National Science Foundation (SNSF) research grant 310030_179447.

2.6 References

1. Lancaster MA, Knoblich JA. Organogenesis in a dish: Modeling development and disease using organoid technologies. *Science* (80-) 2014;345:1247125–1247125.
2. Clevers H. Modeling Development and Disease with Organoids. *Cell* 2016;165:1586–1597.
3. Rossi G, Manfrin A, Lutolf MP. Progress and potential in organoid research. *Nat Rev Genet* 2018;19:671–687.
4. Kleinman HK, Martin GR. Matrigel: Basement membrane matrix with biological activity. *2005*;15:378–386.
5. Hughes CS, Postovit LM, Lajoie GA. Matrigel: a complex protein mixture required for optimal growth of cell culture. *Proteomics* 2010;10:1886–1890.
6. Brassard JA, Lutolf MP. Engineering Stem Cell Self-organization to Build Better Organoids. *Cell Stem Cell* 2019;24:860–876.
7. Kratochvil MJ, Seymour AJ, Li TL, et al. Engineered materials for organoid systems. *Nat Rev Mater* 2019;4:606–622.
8. Enemchukwu NO, Cruz-Acuña R, Bongiorno T, et al. Synthetic matrices reveal contributions of ECM biophysical and biochemical properties to epithelial morphogenesis. *J Cell Biol* 2016;212:113–124.
9. Gjorevski N, Sachs N, Manfrin A, et al. Designer matrices for intestinal stem cell and organoid culture. *Nature* 2016;539:560–564.
10. Sorrentino G, Rezakhani S, Yildiz E, et al. Mechano-modulatory synthetic niches for liver organoid derivation. *Nat Commun* 2020;11:1–10.
11. Ehrbar M, Rizzi SC, Schoenmakers RG, et al. Biomolecular hydrogels formed and degraded via site-specific enzymatic reactions. *Biomacromolecules* 2007;8:3000–3007.
12. Nair DP, Podgórski M, Chatani S, et al. The Thiol-Michael addition click reaction: A powerful and widely used tool in materials chemistry. *Chem Mater* 2014;26:724–744.
13. Cruz-Acuña R, Quirós M, Farkas AE, et al. Synthetic hydrogels for human intestinal organoid generation and colonic wound repair. *Nat Cell Biol* 2017:1–6.
14. Lutolf MP, Hubbell J a. Synthesis and Physicochemical Characterization of End-Linked Poly (ethylene glycol) -co-peptide Hydrogels Formed by Michael-Type Addition. *Biomacromolecules* 2003;4:713–722.
15. Shikanov A, Smith RM, Xu M, et al. Hydrogel network design using multifunctional macromers to coordinate tissue maturation in ovarian follicle culture. *Biomaterials* 2011;32:2524–2531.
16. Metters A, Hubbell J. Network formation and degradation behavior of hydrogels formed by Michael-type addition reactions. *Biomacromolecules* 2005;6:290–301.
17. Zhou H, Woo J, Cok AM, et al. Counting primary loops in polymer gels. *Proc Natl Acad Sci U S A* 2012;109:19119–19124.
18. Zhong M, Wang R, Kawamoto K, et al. Quantifying the impact of molecular defects on polymer network elasticity. *Science* (80-) 2016;353:1264–1268.
19. Pratt AB, Weber FE, Schmoekel HG, et al. Synthetic Extracellular Matrices for in Situ Tissue Engineering. *Biotechnol Bioeng* 2004;86:27–36.
20. Kim J, Kong YP, Niedzielski SM, et al. Characterization of the crosslinking kinetics of multi-arm poly(ethylene glycol) hydrogels formed via Michael-type addition. *Soft Matter* 2016;12:2076–2085.
21. Lutolf MP, Raeber GP, Zisch AH, et al. Cell-responsive synthetic hydrogels. *Adv Mater* 2003;15:888–892.
22. Hersel U, Dahmen C, Kessler H. RGD modified polymers: Biomaterials for stimulated cell adhesion and beyond. *Biomaterials* 2003;24:4385–4415.

23. Raeber GP, Lutolf MP, Hubbell JA. Molecularly Engineered PEG Hydrogels: A Novel Model System for Proteolytically Mediated Cell Migration. *Biophys J* 2005;89:1374–1388.
24. Fittkau MH, Zilla P, Bezuidenhout D, et al. The selective modulation of endothelial cell mobility on RGD peptide containing surfaces by YIGSR peptides. *Biomaterials* 2005;26:167–174.
25. Elbert DL, Hubbell JA. Conjugate addition reactions combined with free-radical cross-linking for the design of materials for tissue engineering. *Biomacromolecules* 2001;2:430–441.
26. Sato T, Vries RG, Snippert HJ, et al. Single Lgr5 stem cells build crypt-villus structures in vitro without a mesenchymal niche. *Nature* 2009;459:262–5.
27. Sato T, Clevers H. Growing Self-Organizing Mini-Guts from a Single Intestinal Stem Cell: Mechanism and Applications. *Science* (80-) 2013;340:1190–1194.
28. Sato T, Stange DE, Ferrante M, et al. Long-term Expansion of Epithelial Organoids From Human Colon, Adenoma, Adenocarcinoma, and Barrett's Epithelium. *Gastroenterology* 2011;141:1762–1772.
29. Beaulieu, Vachon, JF P. Reciprocal Expression of Laminin A-Chain Isoforms Along the. *Gastroenterology* 1994;106:829–839.
30. Mahoney Z, Stappenbeck T, Miner J. Laminin $\alpha 5$ influences the architecture of the mouse small intestinal mucosa. *J Cell Sci* 2008;121:2493–2502.
31. Fujii M, Matano M, Toshimitsu K, et al. Human Intestinal Organoids Maintain Self-Renewal Capacity and Cellular Diversity in Niche-Inspired Culture Condition. *Cell Stem Cell* 2018;23:787-793.e6.
32. Miyoshi H, Stappenbeck TS. In vitro expansion and genetic modification of gastrointestinal stem cells in spheroid culture. *Nat Protoc* 2013;8:2471–2482.

2.7 Supplementary information

Table S1. Primers used for qPCR analysis of human intestinal gene expression

Human gene	Forward primer	Reverse primer
hLGR5	GAGTTACGTCTTGCGGGAAC	TGGGTACGTGTCTTAGCTGATTA
hOLFM4	GCTCTGAAGACCAAGCTGAAA	GAAAACCCTCTCCAGTTGAGC
hSox9	AAGAACAAGCCGCACGTCA	TCTCGCTCTCGTTCAGAAGTC
hEphB2	CAAGCTCTACTGTAACGGGGA	GTTGATGGGACAGTGGGTACA
hMuc2	TGTGTACCAACTCCTCCCAAG	GCGTGTTCGTAATGGAACAGAT
hNHE3	GACTGCGTGAAGGGCATAGT	CAGGTAGGAGATGATGAACACG
hK20	TGGTCGCGACTACAGTGCATA	GAAGTCCTCAGCAGCCAGTT

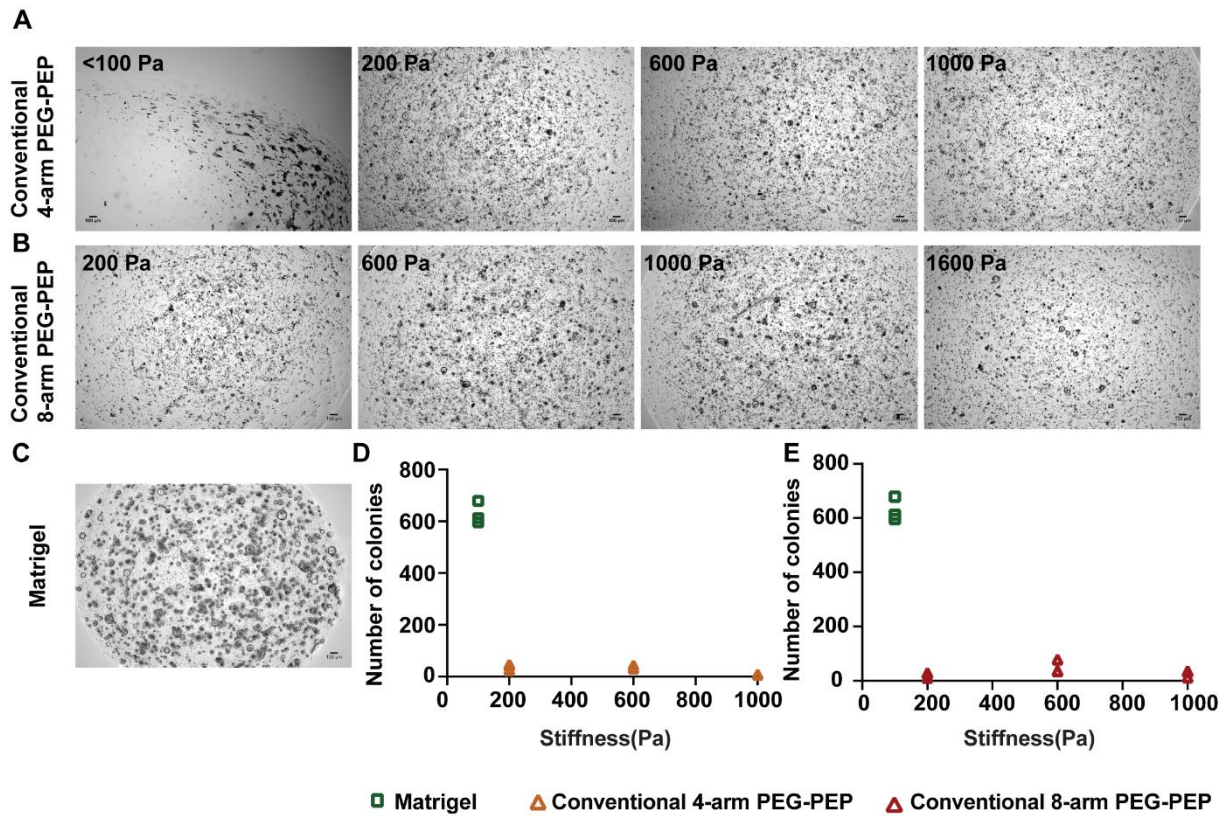
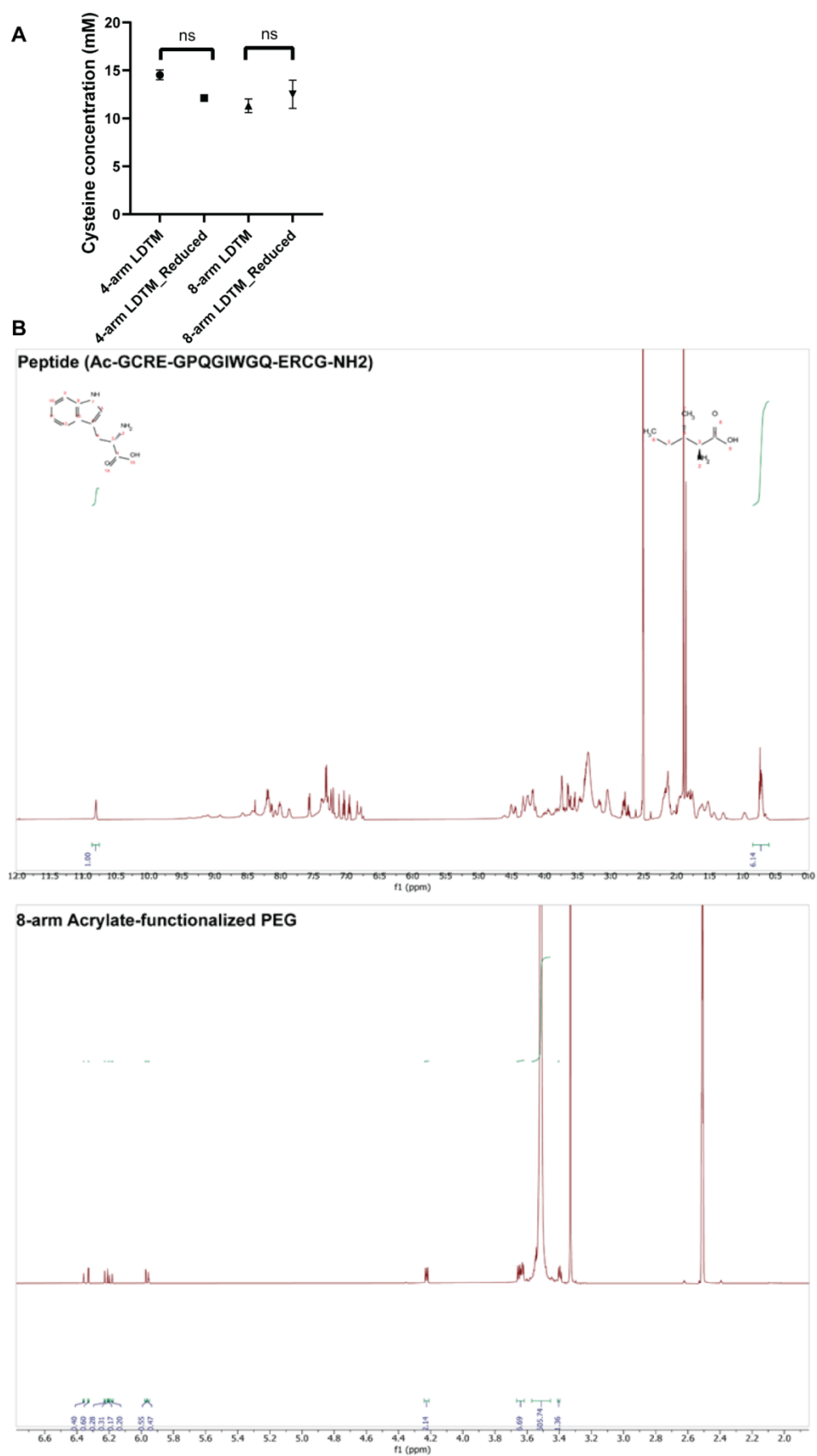


Figure S1. Conventional PEG-PEP hydrogels do not support mouse intestinal colony formation at different stiffnesses. A, B, C) Dissociated single mouse ISCs were encapsulated in conventional PEG-PEP hydrogels of varying stiffness, as well as Matrigel used as control. Bright-field images were taken through the thickness of the gel, and one all-in-focus image was created after 4 days of culture in expansion medium. Scale bars, 100 μ m. **D)** The number of colonies was scored in each condition (n=3).



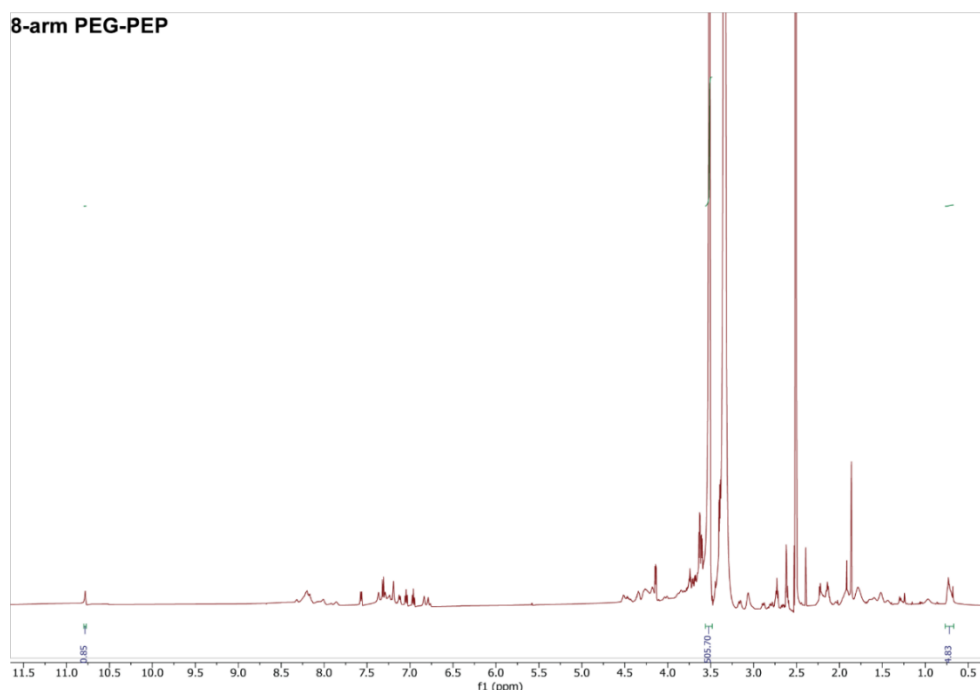


Figure S2. A) No difference in thiol concentration was observed in peptide-functionalized macromers before and after treatment with the reducing agent TCEP, revealing an absence of disulfide-bond formation in the newly formed macromers. **B)** ^1H NMR of the different precursors. ^1H NMR of crosslinking peptide, 8arm-PEG-Acrylate, and peptide-functionalized PEG. Dimethyl sulfoxide (DMSO) was used as solvent to perform the ^1H NMR. The functionalization of the final precursor was calculated based on the ratio of the integrals of the NH peak of tryptophan in the peptide (δ 10.80 (q, J = 4.7, 4.0 Hz, 1H) over OCH₂ from PEG (δ 3.51, s, 505H).

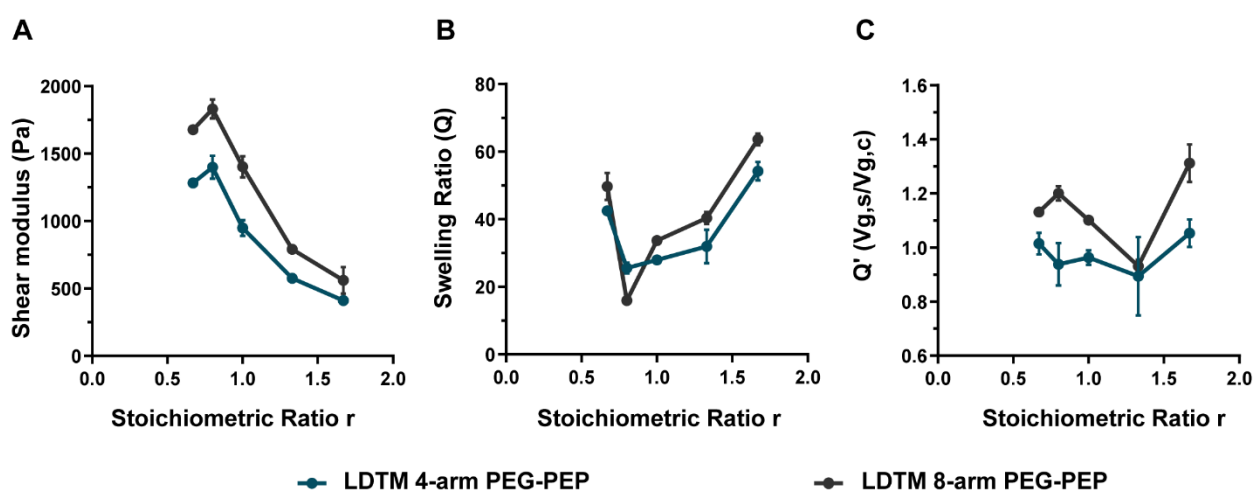


Figure S3. Effect of stoichiometric ratio of functional groups on macroscopic network properties. 4-and 8-arm LDTM hydrogels (3% (w/v), no RGD) with maximum (A) shear moduli and lowest (B) swelling ratios formed at the stoichiometric ratio of VS to SH groups (r) equal to 0.8 corresponding to 25% excess of thiol groups. (C) The ratio of swollen to nascent (just after crosslinking) hydrogel volume ($V_{g,s}/V_{g,c}$). All data are reported as mean \pm S.D. (n = 3).

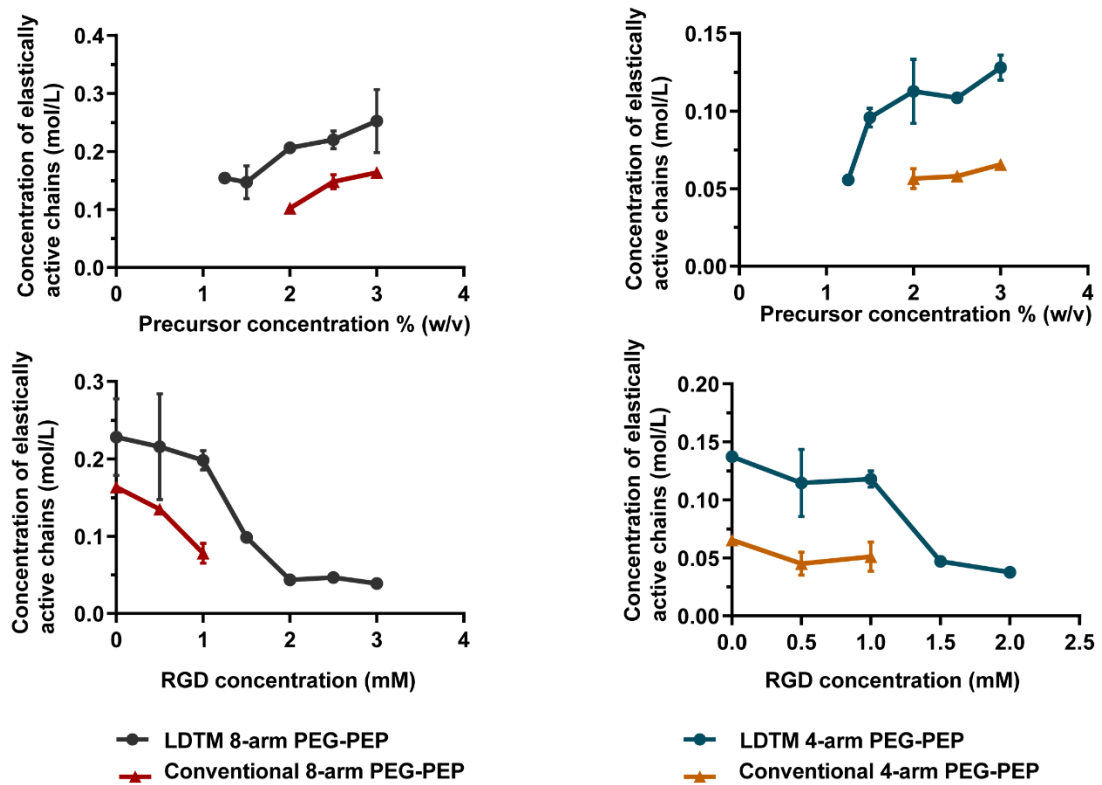


Figure S4. The concentration of elastically active chains as a function of precursor and RGD concentration. A, B) LDTM PEG hydrogels have a higher concentration of elastically active chains comparing to conventional PEG-PEP gels. C, D) Higher concentration of elastically active chains in LDTM PEG hydrogels (3% (w/v), $r=0.8$) allowed incorporation of up to 2mM and 3 mM RGD. All data are reported as mean \pm S.D. ($n = 3$).

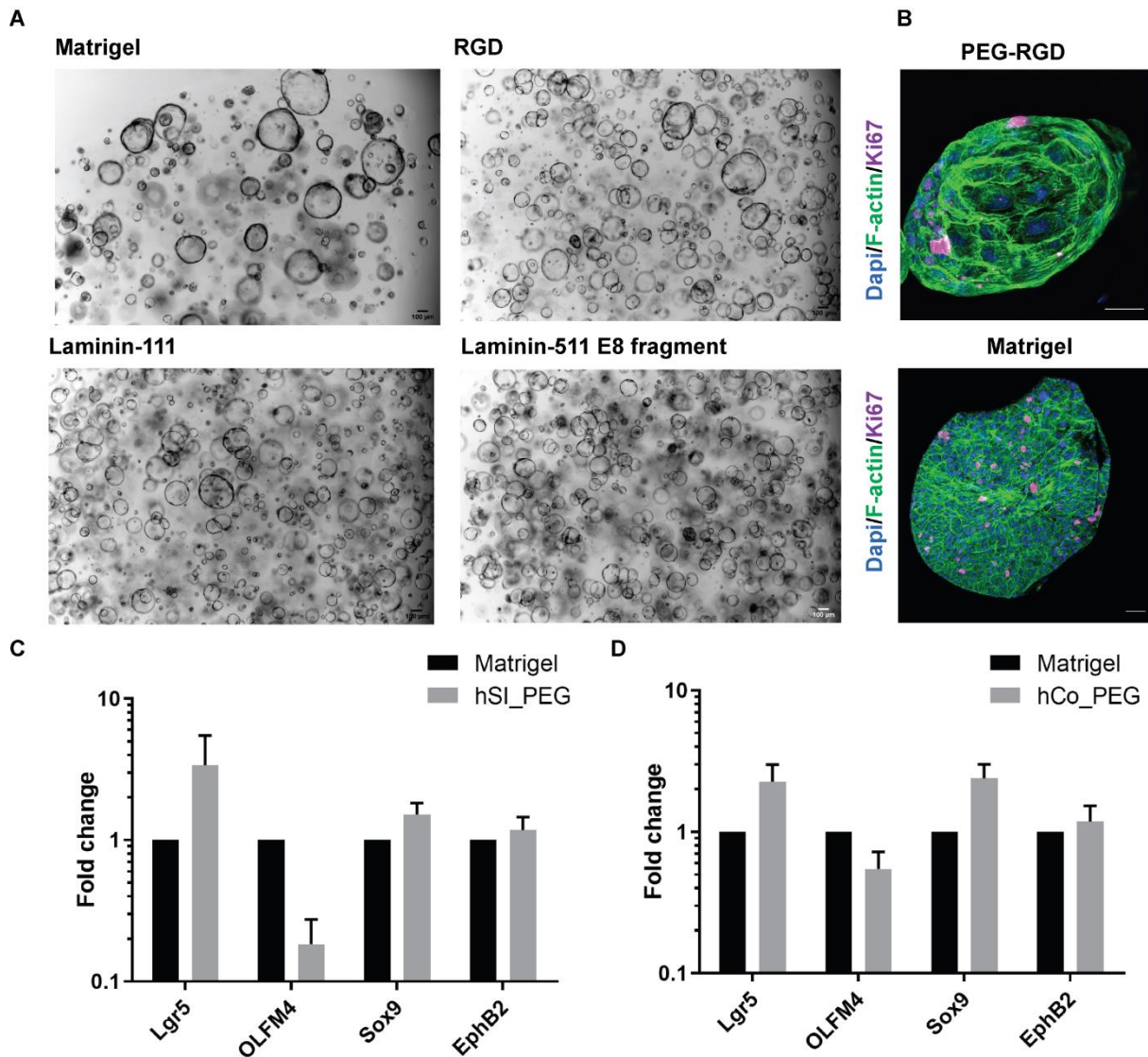


Figure S5. Human intestinal and colon organoids cultured in LDTM gels compared to Matrigel. **A)** Human intestinal colonies in LDTM gels supplemented with different ECM components and Matrigel after 6 days of culture in expansion medium. **B)** Immunostaining of human intestinal colonies after 6 days in the synthetic ECM and Matrigel showing proliferative cells (ki67) Scale bars, 50 μ m. **D)** Gene expression was measured by quantitative polymerase chain reaction (qPCR) in Matrigel and LDTM gels after one week of culture. Gene expression data ($2^{\Delta\Delta Ct}$) was normalized to GAPDH. All data are reported as mean \pm S.D. (n = 3).

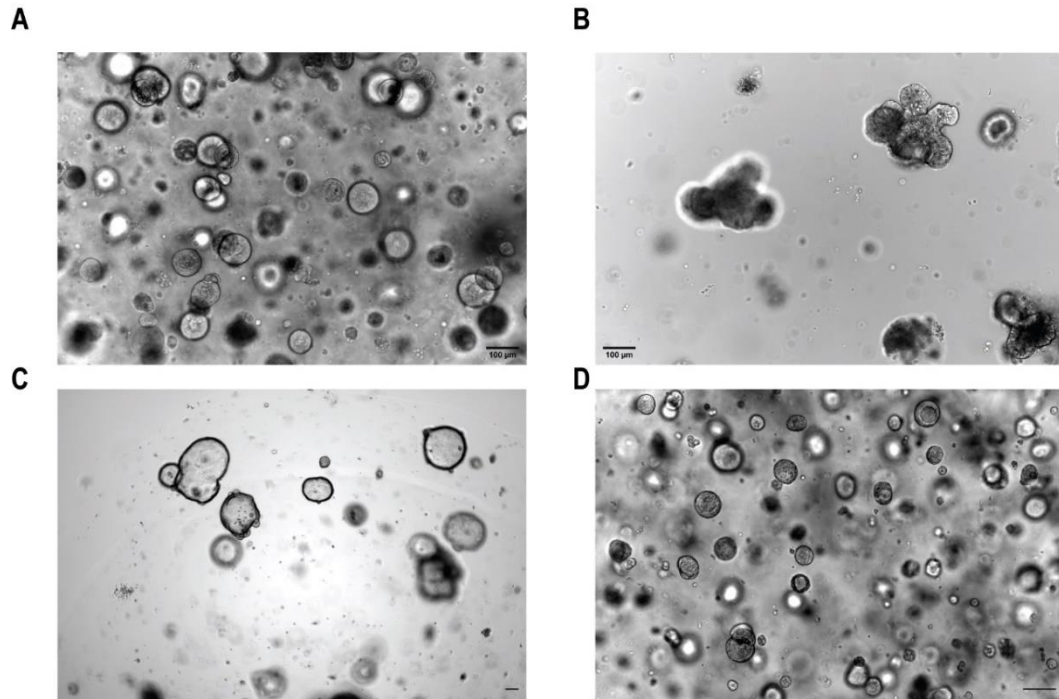


Figure S6. LDTM hydrogels support stemness of human intestinal stem cells. **A)** Human intestinal colonies in 8-arm LDTM gels (2.5% (w/v), 1 mM RGD) after 10 days of culture **B)** Human intestinal colonies form budding structures after transplantation in Matrigel. **C)** Human intestinal organoids in 4-arm PEG-Acr LDTM (3% (w/v), 1 mM RGD, 0.3 mg/ml laminin) after 10 days of culture. **D)** Human intestinal organoids can be passaged in LDTM gels. Scale bars, 100 μm.

Chapter 3

Substituting animal-derived laminin in synthetic matrices for epithelial organoid culture

Saba Reza khani^{1,2}, Matthias P. Lutolf^{1,2*}

¹Laboratory of Stem Cell Bioengineering, Institute of Bioengineering, School of Life Sciences, Ecole Polytechnique Fédérale de Lausanne (EPFL), 1015 Lausanne, Switzerland.

² Institute of Chemical Sciences and Engineering, School of Basic Sciences, EPFL, 1015 Lausanne, Switzerland.

*E-mail: matthias.lutolf@epfl.ch

(Manuscript in preparation)

3.1 Abstract

Epithelial organoids are most efficiently grown from matrices derived from mouse tumors, whose poorly defined composition, batch-to-batch variability, and immunogenicity limit clinical application. Some synthetic polymer-based matrices now allow expansion of mouse and human intestinal stem cells; however, organoid patterning still depends on incorporation of animal laminin 111- the major component of Matrigel - as a biochemical cue. Here, we investigate the possibility of replacing animal laminin with its recombinant counterpart. We show that incorporation of full-length recombinant laminin 111 into synthetic poly(ethylene glycol) (PEG)-based hydrogels enables intestinal organogenesis, albeit to a lesser extent than in natural laminin-containing gels. Furthermore, we show that the recombinant E8 fragment of laminin-111, the minimal fragment that confers integrin-binding activity, promotes intestinal organoid bulging in synthetic PEG gels. Our results suggest that the role of laminin as an integrin-binding motif is necessary but not sufficient for mouse intestinal organoid formation and that further efforts to incorporate other basement membrane components may be required to achieve greater efficiency.

3.2 Introduction

Organoids are *ex vivo* three-dimensional (3D) cellular structures formed by stem cell self-organization under specific microenvironmental cues¹. Organoids recapitulate multiple biological parameters of the organ of reference, including spatial organization of heterogeneous tissue-specific cells, cell-cell interactions, and cell-matrix interactions². Although stem cells are the main

biological component of the organoid system, the behavior of stem cells is controlled by their native microenvironment, termed niche³. The interplay among biochemical and mechanical signals by the extracellular matrix (ECM), cell-cell interactions, and soluble factors is key to the role of the niche on organoid development. Currently, organoid culture relies on Matrigel—an ill-defined gelatinous basement-membrane protein mixture composed of laminin, collagen IV, entactin, heparan sulfate, and numerous growth factors—as the 3D matrix.⁴ However, its batch-to-batch variability, risk of pathogen transfer, and inability to modify its key physical and biochemical properties make this matrix unsuitable for clinical applications

Recently, substantial effort in biomaterial development for organoid culture has focused on identifying synthetic alternatives for Matrigel.^{5–8} We have recently demonstrated successful derivation of mouse and human intestinal organoids in Low-Defect Thiol-Michael Addition (LDTM) hydrogels, the latter in absence of any animal-derived components.⁹ Moreover, we identified the pivotal role of laminin in intestinal organoid patterning, in agreement with previous results from Gjorevski *et al.*¹⁰

Despite such developments, the laminin used in these experiments is derived from Matrigel and therefore carries over many of its limitations including batch to batch variability and risk of pathogen transfer. To address this shortcoming and to obtain a fully-defined, synthetic organoid culture system, we tried to substitute natural laminin with recombinant human laminin which can be produced *in vitro*. We demonstrated mouse intestinal organoid formation in presence of recombinant laminin, albeit with low efficiency. Since full-length laminins are large heterotrimeric proteins (~ 800 kDa), and mass production of these recombinant proteins is still very difficult, as the next step we further examined whether fragments within laminin-111 can serve as surrogates for the full protein in supporting organoid growth. Our results indicate that incorporation of a shortened version of the integrin-binding domain of laminin-111 (E8 fragment) could lead to the formation of bulged organoids but was not sufficient for organoid budding.

3.3 Results and discussion

Organoid formation in laminin-only matrices

Multiple studies implicate laminin-111 as an indispensable component of organoid cultures, whether as a major constituent of Matrigel or as added to synthetic hydrogel matrices^{10,12,13}. We also observed that the inclusion of laminin in hydrolytically degradable matrices results in a higher appearance of Paneth cells (**Supplementary Figure 1**) which indicate the onset of symmetry breaking¹⁴. Moreover, we observed that increasing the concentration of laminin enhances culture condition, with an upper limit on the concentration of tethered factors (laminin and RGD) incorporated in the hydrogels. To test whether we could culture organoids in laminin-only gels, we seeded single mouse intestinal stem cells (mISCs) that had been previously cultured in Matrigel, in laminin-111 (6mg/ml concentration). After four days of culture in expansion medium, organoids were formed and these could be serially passaged in laminin gel, just as can be done in Matrigel (**Figure 1A**). Immunostaining confirmed the presence of differentiated cells in the organoids

(**Figure 1B**). Next, to have a less expensive defined matrix, we sought to verify the lower concentration limit at which laminin gels can still form. At 3 mg/ml laminin formed a loose and unstable network (**Figure 1C**). To stabilise the gel at such low protein concentrations, we added FXIIIa as a transglutaminase enzyme, Tris buffer, and provided an amine-donor PEG precursor at 1% (w/v). Indeed, Aeschlimann *et al* demonstrated that tissue transglutaminases play a role in the stabilization of the basement membrane¹⁶, and early studies have shown the role of Ca^{2+} in the self-aggregation of laminin-nidogen complex¹⁵. The laminin-nidogen complex was shown to contain glutamine residue(s), which act as amine acceptor site(s) in tissue transglutaminase-catalyzed cross-linking, and reaction with the isolated constituents of the complex revealed that the site(s) are located in nidogen alone. Under these modified conditions, laminin gel at 3 mg/ml could form a stable gel suitable for organoid derivation (**Figure 1D**).

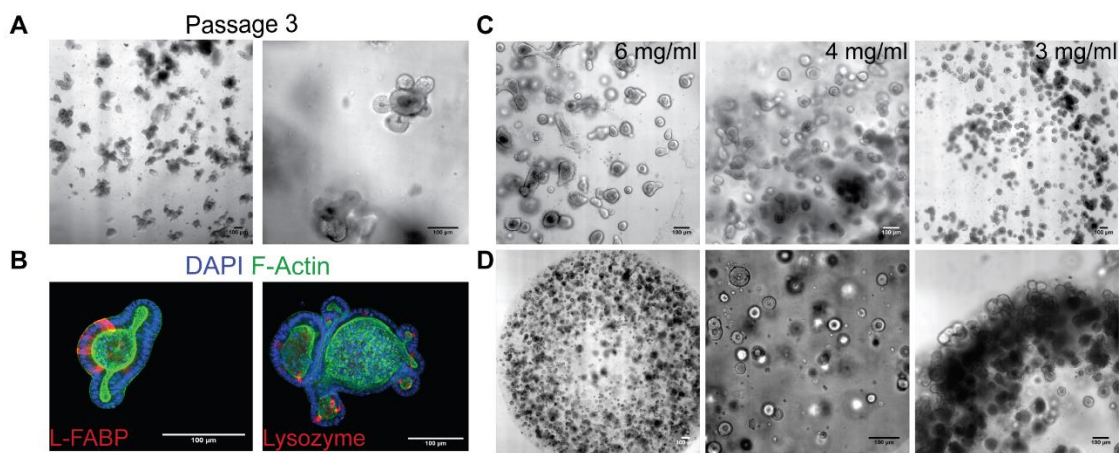


Figure 1. The modified laminin-entactin complex can form a gel at low concentrations. **A)** Single mISCs can be cultured and passaged in laminin gels (6 mg/ml). **B)** Organoids cultured in laminin gels (6 mg/ml) contain differentiated cells (enterocytes and Paneth cells). **C)** Laminin at 3 mg/ml a loose and unstable network. **D)** Addition of transglutaminase FXIIIa in presence of Ca-containing buffer and amine-donor PEG precursor, results in the formation of a more stable laminin gel at 3 mg/ml. Scale bar: 100 μm .

Replacing natural laminin with its recombinant counterpart

Ideally, the niche environment of organoids grown in culture would be of defined chemical composition. As such, we evaluated the possibility of replacing natural laminin with recombinant one. Recombinant laminin is commercially available at a stock concentration of 100 $\mu\text{g/ml}$, that is, 10 times less than the stock concentration of natural laminin that we typically use for mouse intestinal organoid culture (1 mg/mL). Accordingly, we first concentrated the recombinant laminin to 2.5 mg/ml and tested its bioactivity in our organoid culture. While single mISCs do not survive in an inert PEG gel¹⁰, intestinal stem cell colonies did form in LDTM gels in presence of recombinant laminin and without any other biochemical cues; confirming the bioactivity of the concentrated protein (data not shown). Next, we included both the recombinant protein and RGD peptide in the hydrogels. Both natural and recombinant laminins resulted in significant formation of intestinal colonies compared to the RGD-only control (**Figure 2A,B**). After two days of culture in

differentiation condition, most of the colonies in the gel containing natural laminin formed budding structures, yet only bulged structures were observed in the cystic colonies grown in the gels with recombinant laminin (**Figure 2C**). A minority of these bulging colonies formed buds the following day (**Figure 2D**). **Figure 2F**, shows the percentage of budding, bulging and cystic organoids in LDTM gels in presence of natural and recombinant laminin. To further assess the function of recombinant laminin in supporting intestinal organogenesis, we used a microcavity assay as a readout. Indeed, Brandenburg *et al*¹⁷ have demonstrated that mouse intestinal organoids can form in microcavity arrays when exposed to laminin-111. Our results with the microcavity arrays confirmed the results of 3D culture. Notably, single mISCs exposed to recombinant laminin could form few colonies after two days of culture; however, they could not form any organoids as in the conditions with Matrigel or natural laminin (**Supplementary Figure 2**).

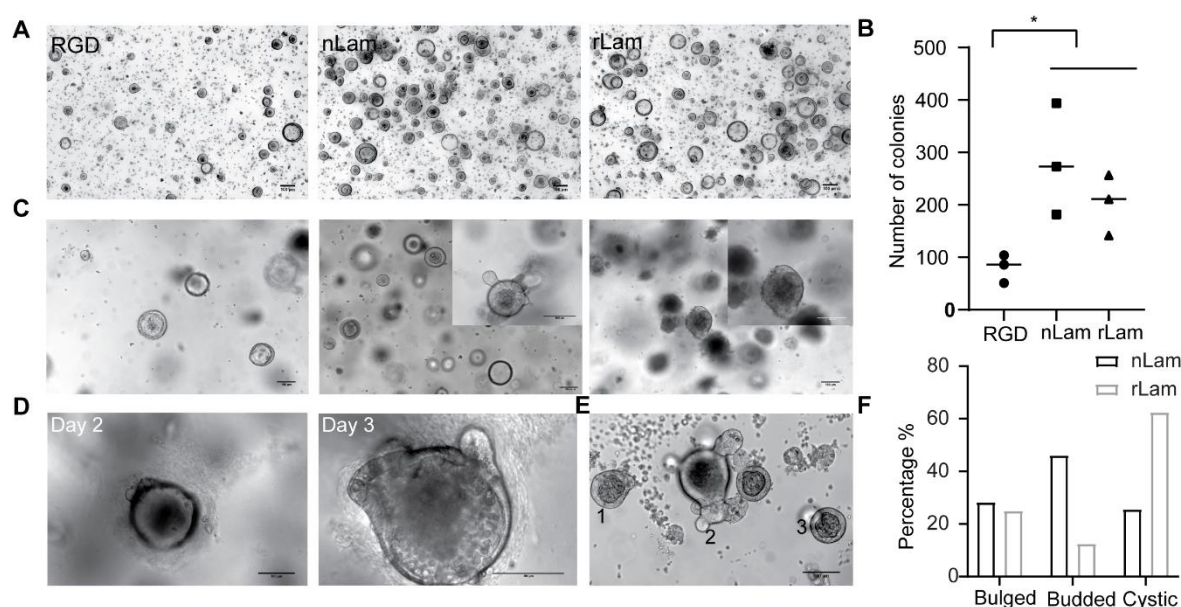


Figure 2. Mouse intestinal organoids form in LDTM gels in presence of recombinant laminin with lower efficiency. **A)** Colony formation of mISCs in LDTM gels containing RGD, natural laminin (nLam), and recombinant laminin (rLam) after 4 days of culture in expansion medium. **B)** Colony formation efficiency in LDTM gels containing RGD only, nLam, or rLam. **C)** Appearance of bud- and bulge-bearing organoids in LDTM gels containing nLam and rLam, respectively after 2 days of culture in differentiation medium. **D)** Formation of budding structures in LDTM gels containing recombinant laminin after 3 days of culture in differentiation medium. **E)** Representative image of bulged (**1**), budded (**2**), and cystic (**3**) organoids in LDTM gel containing nLam. **F)** Percentages of bulged, budded and cystic organoids in LDTM gels containing nLam or rLam. 39 and 24 organoids were counted for nLam and rLam conditions, respectively and percentage of bulged, budded and cystic structures were determined based on their morphology.

Incorporation of protease-resistant laminin fragments in LDTM gels

The concentration of recombinant laminin has low yield and it is therefore expensive to obtain high quantities of recombinant laminin at high concentration. Hence, we explored the possibility of

producing laminin fragments (as opposed to the whole protein) that may still support organoid formation.

Ott and Timpl *et al*^{18,19} have investigated production of different laminin fragments by digestion protocols. Laminin fragment-8 (E8), representing the terminal half of the long arm of laminin, consists of a rod-like segment and a complex globular domain²⁰. Disulfide-rich laminin fragment E1, consists of three rod-like segments originating from the center of the short arms of laminin. Fragment E4 corresponds to the three short arms of laminin. Fragment E3 has also been identified as a major heparin-binding domain in laminin²¹ (**Figure 3A**). Following Ott and Timpl's fragmentation protocol, we digested natural laminin with elastase for 24 hours at 37°C. Three main fragments were recovered after two steps of chromatography of affinity-based Heparin Sepharose and size exclusion chromatography columns (**Supplementary Figure 3**). SDS-PAGE electrophoresis revealed the presence of similar bands (25, 50 and 250 kDa) to what recovered by Timpl *et al* (**Supplementary Figure 4**).

To gain further insight into the molecular composition of each recovered fragment, we performed proteomic analysis on seven different bands of SDS-PAGE corresponding to 250 kDa and 50 kDa fragments recovered from the flow-through and the eluate of the size exclusion chromatography column, and 25 kDa fragments recovered from the eluate of the size exclusion chromatography column (**Figure 3B**). Results confirmed that the 250 kDa bound fragment corresponded to the short arms of laminin, similar to what called fragment 1 in Ott *et al*¹⁸. The 50, and 25 kDa fragments corresponded to the globular domain of the long arm of α chain (fragment E3) (**Supplementary Figure 5**), and the LG4, and LG5 domains of the α chain, respectively.

Next, to test the activity of the recovered fragments, we cultured mouse ISCs in LDTM gels containing them. To chemically tether the fragments to the gels, we first measured the thiol content of each fragment using Ellman's assay. Given that the measured thiol concentration was low, we further modified amine groups in the protein into thiol functionalities using Traut's reagent. Such thiolated fragments were then incorporated into the gels. While cystic colonies could form in gels containing different fragments (**Figure 4A**), only bulged organoids formed in the condition containing the 50kDa fragment (**Figure 4B,C**). It is important to mention that the recovered fragments were more diluted than the natural laminin stock concentration we usually use, and some of the material was further lost during the process of thiolation and filtering through desalting columns. Moreover, several studies^{22–25} underscore the requirement for all three laminin chains for their integrin-binding activity, while the 50, and 25 kDa fragments are only expected to contain the globular domain of the α chain. To test whether the addition of C terminus of β and γ chains in these fragments could improve organoid formation, and to also have a higher concentration of fragments to incorporate in LDTM hydrogels, we thus tried to use the recombinantly-produced integrin-binding domain of laminin.

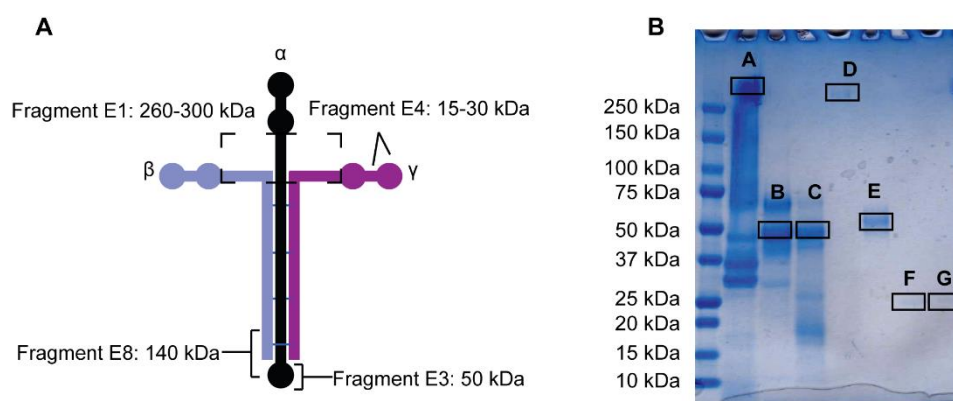


Figure 3. Derivation of laminin fragments by protease digestion. **A)** Schematic of different fragments identified by Ott and Timpl et al^{18,19}. **B)** SDS-PAGE (Coomassie blue-stained) of digested different fractions recovered from the flow-through and eluate of SEC chromatography that were further characterized by LC-MS. **C)** Cystic colonies were formed in LDTM gels containing different fragments; however, only bulged organoids were formed in the condition containing the 50kDa fragment.

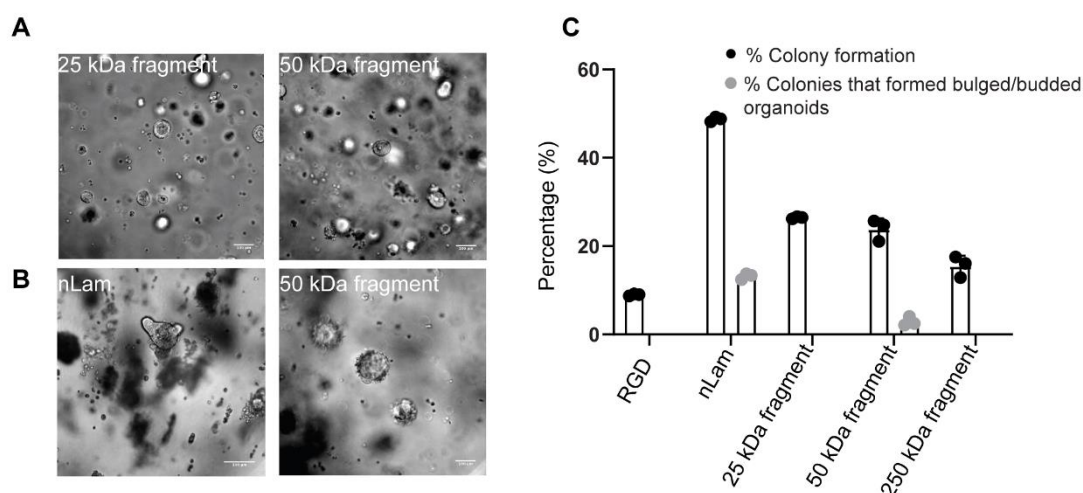


Figure 4. Recovered laminin fragments support intestinal colony formation **A)** Colony formation in LDTM gels containing laminin fragments. **B)** Formation of budded and bulged organoids in LDTM gels containing nLam and 50 kDa laminin fragment. **C)** Colony and organoid formation efficiency in LDTM gels containing RGD, nLam and different laminin fragments. Incorporation of 50 kDa fragment in LDTM gels resulted in only bulge-containing structures.

Recombinant laminin fragment

The importance of the native quaternary structure of laminin for integrin binding has been shown in a number of studies.^{22–25} Most recently, Pulido *et al*²⁶ produced a shortened version (50 residues) of the E8 fragment (globular domain with the terminus of the β and γ chains – 220 residues) and documented the crystal structure of its complex with the integrin-binding region of laminin. As the next step towards a defined matrix for intestinal organoid culture, we thus tried to substitute the

natural fragments with their recombinant counterparts. Protein production and purification are easier for smaller fragments of laminin and these endow recombinant laminin fragments with greater potential for scaled-up applications compared with intact laminin.

Accordingly, we sought to test whether the inclusion of laminin mini-E8 fragment allows intestinal morphogenesis in LDTM hydrogels. As the first step to tether the fragment to the hydrogel, we took advantage of amine and thiol-reactive crosslinking strategies. We thus first PEGylated the mE8 fragment through amine-NHS chemistry. Next, we embedded mISC in a gel containing mE8 fragments only, without any other adhesion cues such as RGD. Colony formation confirmed the bioactivity of the fragment as mISCs do not form colonies in an inert gel (**Supplementary Figure 6**). Next, we cultured mISCs in LDTM gels containing RGD, natural laminin, and crosslinked mE8. After four days of culture, mISCs formed intestinal colonies in all conditions, with the highest efficiency in nLam-containing gels (**Figure 5A**). 2 days after switching to differentiation medium, we observed the appearance of some bulges in nLam- and mE8-containing gels (**Figure 5B**). Yet, the bulged structures further expanded into buds only in the condition containing nLam, and not in the one containing mE8. One of the reasons behind this observation could be that mE8 only carries globular domains required for integrin binding (LG1-3), while α -dystroglycan, heparan sulfates, and sulfated glycolipids (sulfatides) mostly bind to the LG4-5 region of the globular domain of laminin.

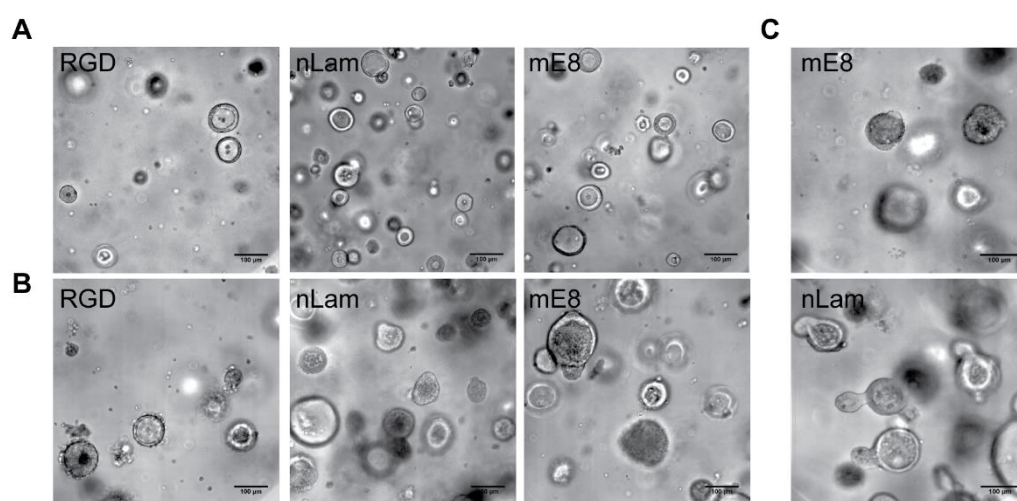


Figure 5. Mouse intestinal organoid culture in LDTM gels containing recombinant laminin mE8 fragment. **A)** colony formation in LDTM gels containing RGD, nLam and mE8 fragment after 4 days of culture in expansion medium. **B)** Appearance of some bulged structures in nLam- and mE8-containing gels after two days of culture in differentiation medium **C)** Formation of budding organoids in the condition containing nLam and not the mE8.

3.4 Conclusion

Multiple studies implicate laminin-111 as an indispensable component for organoid culture, whether as a major constituent of Matrigel or as an addition to synthetic hydrogel matrices^{10,12,13}.

First, we showed that mouse intestinal organoids can be cultured and passaged in laminin gels. Next, we demonstrated the stabilization of the laminin gel at lower protein concentrations by adding FXIIIa as a transglutaminase enzyme, Tris buffer, and providing an amine-donor PEG precursor at 1% (w/v).

Since natural laminin is obtained from a tumor basement membrane and therefore has similar limitations as Matrigel (e.g. batch-to-batch variability, risk of pathogen transfer), to have a fully synthetic organoid culture system we substituted natural laminin with recombinant laminin in LDTM hydrogels. Mouse intestinal organoids could form in presence of recombinant laminin to a lower extent compared to natural laminin. Furthermore, we examined whether fragments within laminin-111 can serve as surrogates for the full protein in supporting organoid growth. These fragments are smaller molecules and have a much higher production yield compared to full-length proteins. Our results indicate that incorporation of mini E8 fragment, the minimum structure harboring the full integrin-binding of laminin-111, could lead to the formation of bulged organoids but was not sufficient for organoid budding.

Tumor-derived natural laminin is not pure, and the presence of other basement membrane proteins such as entactin and collagen-IV could explain the different outcomes between natural and recombinant laminin. Therefore, we postulate that the inclusion of basement membrane proteins, along with laminin, could enhance mouse intestinal organogenesis.

3.5 Materials and methods

Culture of mouse intestinal organoids

Murine intestinal crypts were isolated from 5–10-week-old heterozygous *Lgr5*–eGFP-IRES-CreERT2 mice (Jackson Laboratory), as described previously and embedded in Matrigel (BD Biosciences; growth factor reduced, phenol red-free formulation).¹⁰ Single cells from dissociated mouse intestinal organoids grown in Matrigel were added to the hydrogel precursor solution and cast in 20- μ L droplets at the bottom of wells in PDMS-coated or non-tissue treated 24-well plates. After polymerization (20–30 min, 37°C), the gels were overlaid with 600 μ L of mISC expansion medium (Advanced DMEM/F12 containing Glutamax (Gibco), HEPES, penicillin-streptomycin, B27, N2 (Invitrogen) and 1×10^{-6} M N-acetylcysteine (Sigma)), supplemented with growth factors, including EGF (50×10^{-9} g ml^{-1} ; R&D), Noggin (100×10^{-9} g ml^{-1} ; produced in-house) and R-spondin (1×10^{-6} g ml^{-1} ; produced in-house), and small molecules, including CHIR99021 (3×10^{-6} M; Millipore) and valproic acid (10^{-3} M; Sigma)). For single-cell culture, thiazovivin (2.5 μ M; Stemgent) was included in the medium during the first two days. Broad-spectrum protease inhibitor, GM6001, was added to the medium while embedding the cells in peptide-containing PEG hydrogels. The growth factors were replenished every two days, and the full medium was changed every 4 days. To induce mouse intestinal organoid formation, the medium was removed, and the gels were washed with PBS, and medium containing EGF, Noggin, and R-spondin was added. To digest the gels, gels were detached from the bottom of the plates using the tip of a metal spatula and transferred to 15-ml Falcon tube containing 1 ml of Dispase (1 mg ml^{-1} , Thermo Fisher Scientific). After 10–20 minutes enzymatic digestion, the reaction was quenched using 10% FBS containing 1 mM EDTA, washed with cold basal medium and centrifuged for 3 min at 800 rpm.

Hydrogel Components and formation

Vinylsulfone-functionalized 4-arm PEG (4-arm PEG-VS 20 kDa) was purchased from NOF, and acrylate-functionalized 4-arm PEG (4-arm PEG-Acr 20 kDa) was purchased from Jenkem Technology. The peptide Ac-GCRE-*GPQGIWGQ*-ERCG-NH2 (mol wt 1773.97 g mol^{-1}) with matrix metalloproteinases (MMPs) sensitive sequence (in italics) was obtained from Biomatik. The adhesion peptide Ac-GRCGRGDSPG-NH2 (mol wt 1002.04 g/mol) was purchased from GL Biochem. High concentration natural laminin was purchased from Amsbio, and the recombinant laminin was purchased from BioLamina (concentrated using Amicon Ultra-0.5 Centrifugal Filter Unit). Laminin mE8 fragments were provided by Hohenester lab (Imperial College London). Hydrogel precursor synthesis and hydrogel and formation has been described previously⁹. Briefly, tetra-thiol containing PEG macromer was formed by reaction of 4-arm PEG-Acr and peptides (SH/Acr=10) in triethanolamine (0.3M, pH 8.0) for 2 h at room temperature under inert atmosphere (drop-wise addition of PEG macromers to excess of peptides). The reaction solution was dialyzed (Snake Skin, MWCO 10K, PIERCE) against ultrapure water (pH<7) for 4 days at 4°C, and the final product was lyophilized. The lyophilized product was dissolved in water to make 10% precursor solutions. LDTM PEG-PEP hydrogels were formed by Michael type addition of tetra-thiol containing PEG precursors onto multi-arm PEG-VS. To make hydrogel networks of desired final

PEG content, proper volumes of 10% (w/v) PEG-VS and peptides in 0.3 M triethanolamine, and 10% (w/v) synthesized macromers in water were mixed in stoichiometric ratios.

Quantification of thiol and amine groups in protein fragments

Thiol concentration was measured using Ellman's assay based on the instruction from the supplier (ThermoFisher, 22582). Amine groups were measured using TNBSA assay based on the instruction from the supplier (ThermoFisher, TS-28997).

Thiolation of laminin fragments

Traut's reagent was purchased from ThermoFisher (26101) and the reaction was carried out according to the instruction from the supplier. Briefly, Traut's reagent was dissolved in sodium bicarbonate (pH=8) and added to the protein fragments at 10 times molar excess. The solution was incubated for 1 hour at room temperature and the thiolated protein was separated from excess Traut's Reagent using Zeba spin desalting column (Thermo Scientific, 89882)

PEGylation of laminin mE8 fragment

Protein fragments were conjugated with a maleimide PEG N-hydroxysuccinimide ester (MAL-PEGNHS, mol wt 3.5 kDa, JENKEM TECH., USA). PEG-MAL-NHS was dissolved in PBS at a concentration ~10 mg/mL to minimise protein dilution. NHS solution was spontaneously mixed with the protein of interest at a molar ratio of 4:1 of NHS to protein, targeting 3 to 5 PEG linkers per protein of interest.

Laminin digestion

Laminin (3D cultrex, Amsbio) was dialyzed against 0.05M sodium bicarbonate, pH 7.9 at 4°C for 2 days. Elastase (Worthington Biochemical corporation, 8u/mg protein) was added at a protease: substrate ratio of 1:100 (w/w) ratio and incubated for 24h at 37° C. Reaction was stopped by addition of phenylmethylsulfonylfluoride (PMSF, EDM Millipore Corp. USA) at 50 µg/ml.

Chromatography

Digests of laminin were passed through a 5 ml heparin-Sepharose column equilibrated with 50 mM ammonium bicarbonate pH 7.9. Bound material was eluted with 0.5 M NaCl at 4°C. Bound and unbound materials (eluate and low through) were then lyophilized, resuspended in 1 ml 0.05 M ammonium bicarbonate, and further separated by a size exclusion chromatography (Superose 6 10/300GL).

In-gel sample digestion for LC-MS

Coomassie blue bands of recovered fragments were cut out of a 4–20% gradient polyacrylamide gel (Bio-Rad) and washed twice in 50% Ethanol; 50mM Ammonium Bicarbonate (AB, Sigma-Aldrich) for 20 min. and dried by vacuum centrifugation. Samples were then reduced with 10mM Dithioerythritol (DTE, Merck-Millipore); 50mM AB for 1 h. at 56°C, washed and dried twice as above described prior to alkylation using 55mM Iodoacetamide (IAA, Sigma-Aldrich); 50mM AB for 45 min. at 37°C in the dark. Samples were washed-dried again and digested overnight at 37°C

using either Mass Spectrometry grade Trypsin (Promega) or GluC at a concentration of 12.5ng/μl in 50mM AB with adjunction of 10mM CaCl₂. The resulting peptides were extracted twice in 70% Ethanol; 5% Formic acid for 20 min. with permanent shaking, dried by vacuum centrifugation and desalted on C18 Stage Tips²⁷ prior to storage at -20 °C.

LC-MS2 runs

Each sample was resuspended in 2% Acetonitrile (ACN); 0.1% FA and injected for nano-flow separations on a Dionex Ultimate 3000 RSLC (Thermo Fischer Scientific) nano UPLC system on-line connected to a Q-Exactive HF Mass Spectrometer (Thermo Fischer Scientific). Samples were first trapped on a capillary precolumn (Acclaim Pepmap C18; 3μm-100Å; 2cm x 75μm ID) and analytical separations were performed at 250nl/min over a 90 min. biphasic gradient on a 50cm long in-house packed capillary column (75μm ID; ReproSil-Pur C18-AQ 1.9μm; Dr. Maisch). Data-Dependent acquisition mode was used where top 15 most intense signals were fragmented per cycle. MS scans were acquired with a resolution of 60'000 (at 200 m/z) and fragmentations were performed by High energy Collision Dissociation (HCD) with a Normalized Collision Energy (NCE) of 27% using an isolation window of 1.4 m/z. Fragmented ions were acquired with a resolution 15'000 (at 200m/z) and selected ions were then excluded for the following 20 s.

Data processing

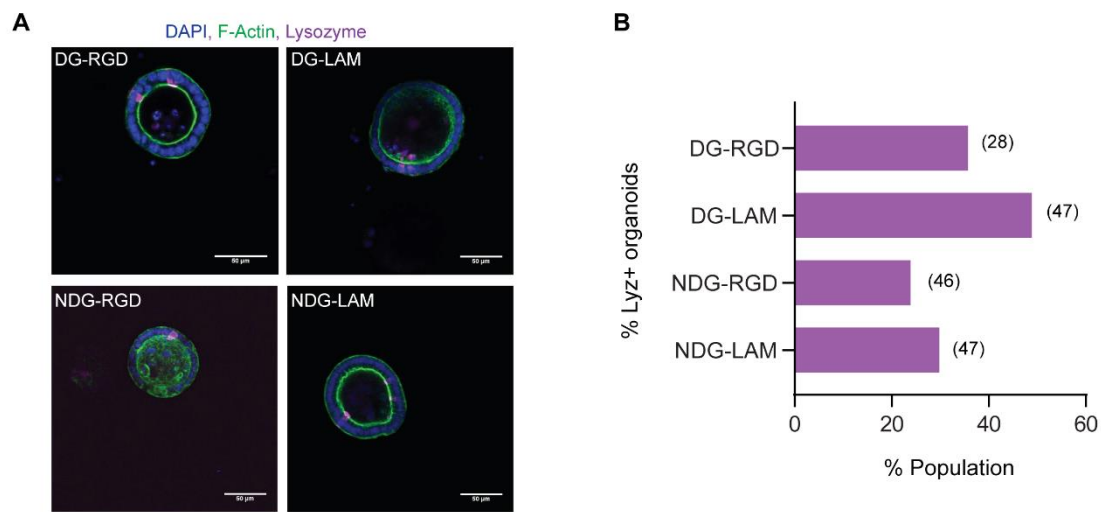
Raw data were processed with Proteome Discoverer v.1.4 using a combination of SEQUEST, Mascot and MS Amanda search engines against the Uniprot Mouse Reference Proteome Database (Release: 2017_01). Enzyme specificity was set either to Trypsin or GluC with a minimum of six amino acids required for peptide identification. A maximum of two missed cleavages were allowed and 1% FDR cut-off was applied both at peptide and protein identification levels. Carbamidomethylation (C) was set as fixed modification while Oxidation (M), Phosphorylation (STY), Acetylation (peptide N-term) were considered as variable ones. Final Data visualization and inspection was performed with Scaffold 3.

3.6 References

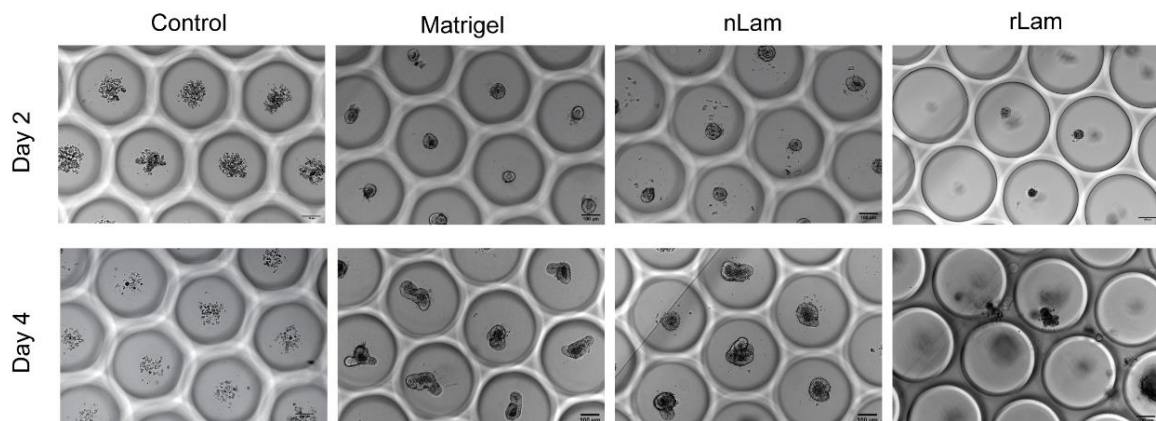
1. Lancaster MA, Knoblich JA. Organogenesis in a dish: Modeling development and disease using organoid technologies. *Science* (80-) 2014;345.
2. Yin X, Mead BE, Safaei H, et al. Engineering Stem Cell Organoids. *Stem Cell* 2016;18:25–38.
3. Moore KA, Lemischka IR. Stem cells and their niches. *Science* (80-) 2006;311:1880–1885.
4. Kleinman HK, Martin GR. Matrigel: Basement membrane matrix with biological activity. 2005;15:378–386.
5. Blondel D, Lutolf MP. Bioinspired hydrogels for 3d organoid culture. *Chimia (Aarau)* 2019;73:81–85.
6. Brassard JA, Lutolf MP. Engineering Stem Cell Self-organization to Build Better Organoids. *Cell Stem Cell* 2019;24:860–876.
7. Kratochvil MJ, Seymour AJ, Li TL, et al. Engineered materials for organoid systems. *Nat Rev Mater* 2019;4:606–622.
8. Enemchukwu NO, Cruz-Acuña R, Bongiorno T, et al. Synthetic matrices reveal contributions of ECM biophysical and biochemical properties to epithelial morphogenesis. *J Cell Biol* 2016;212:113–124.
9. Rezakhani S, Gjorevski N, Lutolf MP. Low-Defect Thiol-Michael Addition Hydrogels as Matrigel Substitutes for Epithelial Organoid Derivation. *Adv Funct Mater* 2020;30:1–12.
10. Gjorevski N, Sachs N, Manfrin A, et al. Designer matrices for intestinal stem cell and organoid culture. *Nature* 2016;539:560–564.
11. Miyazaki T, Futaki S, Hasegawa K, et al. Recombinant human laminin isoforms can support the undifferentiated growth of human embryonic stem cells. *Biochem Biophys Res Commun* 2008;375:27–32.
12. Sorrentino G, Rezakhani S, Yildiz E, et al. Mechano-modulatory synthetic niches for liver organoid derivation. *Nat Commun* 2020;11:1–10.
13. Ye S, Boeter JWB, Mihajlovic M, et al. A Chemically Defined Hydrogel for Human Liver Organoid Culture. *Adv Funct Mater* 2020;30.
14. Serra D, Mayr U, Boni A, et al. Self-organization and symmetry breaking in intestinal organoid development. *Nature* 2019;569:66–72.
15. Paulsson M. The role of Ca²⁺ binding in the self-aggregation of laminin-nidogen complexes. *J Biol Chem* 1988;263:5425–5430.
16. Aeschlimann D, Paulsson M. Cross-linking of laminin-nidogen complexes by tissue transglutaminase: A novel mechanism for basement membrane stabilization. *J Biol Chem* 1991;266:15308–15317.
17. Brandenberg N, Hoehnel S, Kuttler F, et al. High-throughput automated organoid culture via stem-cell aggregation in microcavity arrays. *Nat Biomed Eng* 2020;863–874.
18. Ott U, Odermatt E, Engel J, et al. Protease Resistance and Conformation of Laminin. *Eur J Biochem* 1982;123:63–72.
19. Timpl R, Johanssonlill S, Deldens V Van, et al. Characterization of Protease-resistant Fragments of Laminin Mediating Attachment and Spreading of Rat Hepatocytes. *J Biol Chem*. 1983;8922–8927.
20. Aumailley M, Nurcombe V, Edgar D, et al. The Cellular Interactions of Laminin Fragments. *Biochemistry* 1987;11532–11538.
21. Sonnenberg A, Linders CJT, Modderman PW, et al. Integrin recognition of different cell-binding fragments of laminin (P1, E3, E8) and evidence that $\alpha 6 \beta 1$ but not $\alpha 6 \beta 4$ functions as a major receptor for fragment E8. *J Cell Biol* 1990;110:2145–2155.
22. Deutzmann R, Aumailley M, Wiedemann H, et al. Cell adhesion, spreading and neurite stimulation

- by laminin fragment E8 depends on maintenance of secondary and tertiary structure in its rod and globular domain. *Eur J Biochem* 1990;191:513–522.
23. Ido H, Nakamura A, Kobayashi R, et al. The requirement of the glutamic acid residue at the third position from the carboxyl termini of the laminin γ chains in integrin binding by laminins. *J Biol Chem* 2007;282:11144–11154.
 24. Taniguchi Y, Ido H, Sanzen N, et al. The C-terminal region of laminin β chains modulates the integrin binding affinities of laminins. *J Biol Chem* 2009;284:7820–7831.
 25. Miyazaki T, Futaki S, Suemori H, et al. Laminin E8 fragments support efficient adhesion and expansion of dissociated human pluripotent stem cells. *Nat Commun* 2012;3:1236.
 26. Pulido D, Hussain SA, Hohenester E. Crystal Structure of the Heterotrimeric Integrin-Binding Region of Laminin-111. *Structure* 2017;25:530–535.
 27. Rappsilber J, Mann M, Ishihama Y. Protocol for micro-purification, enrichment, pre-fractionation and storage of peptides for proteomics using StageTips. *Nat Protoc* 2007;2:1896–1906.

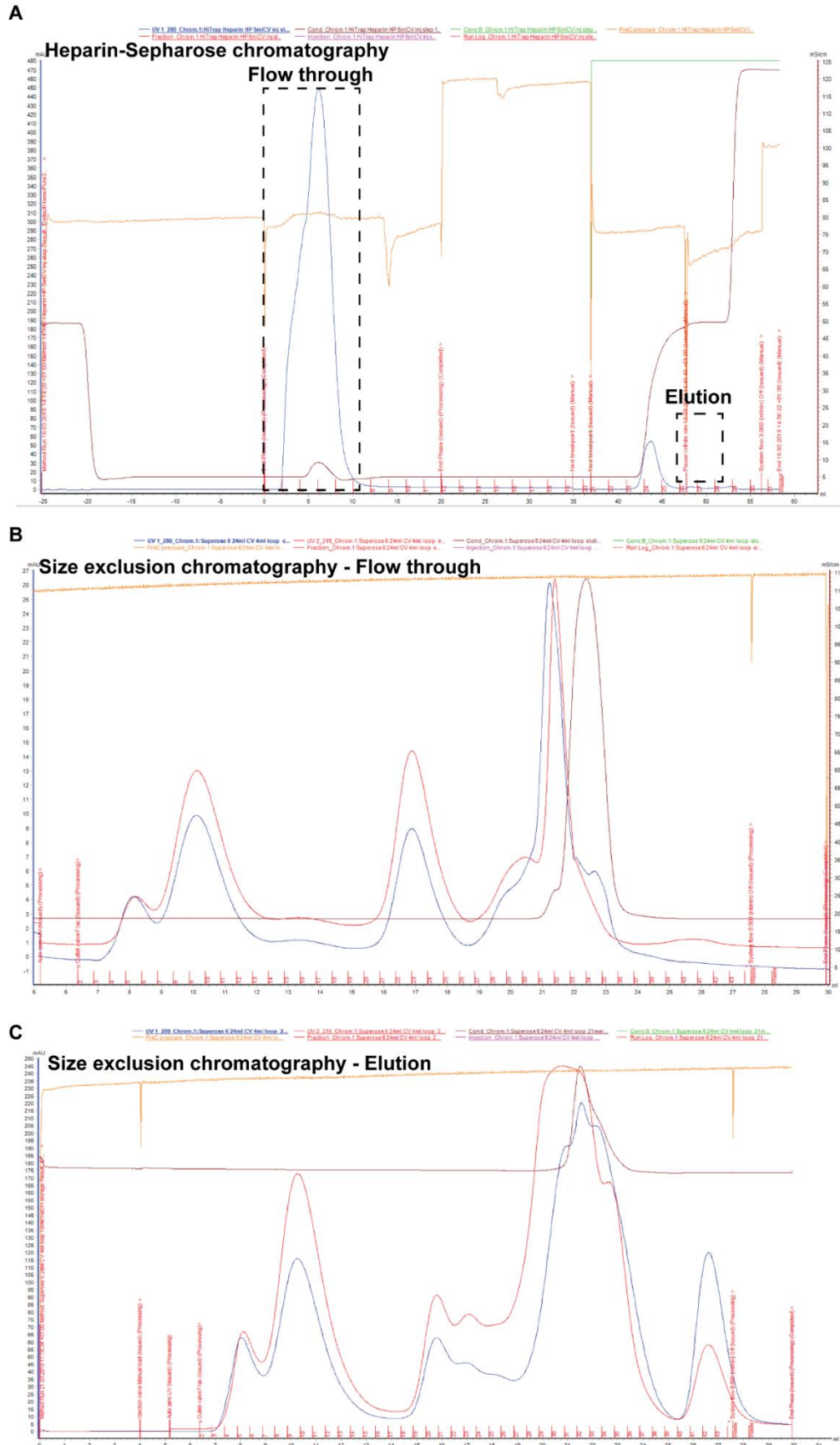
3.7 Supplementary information



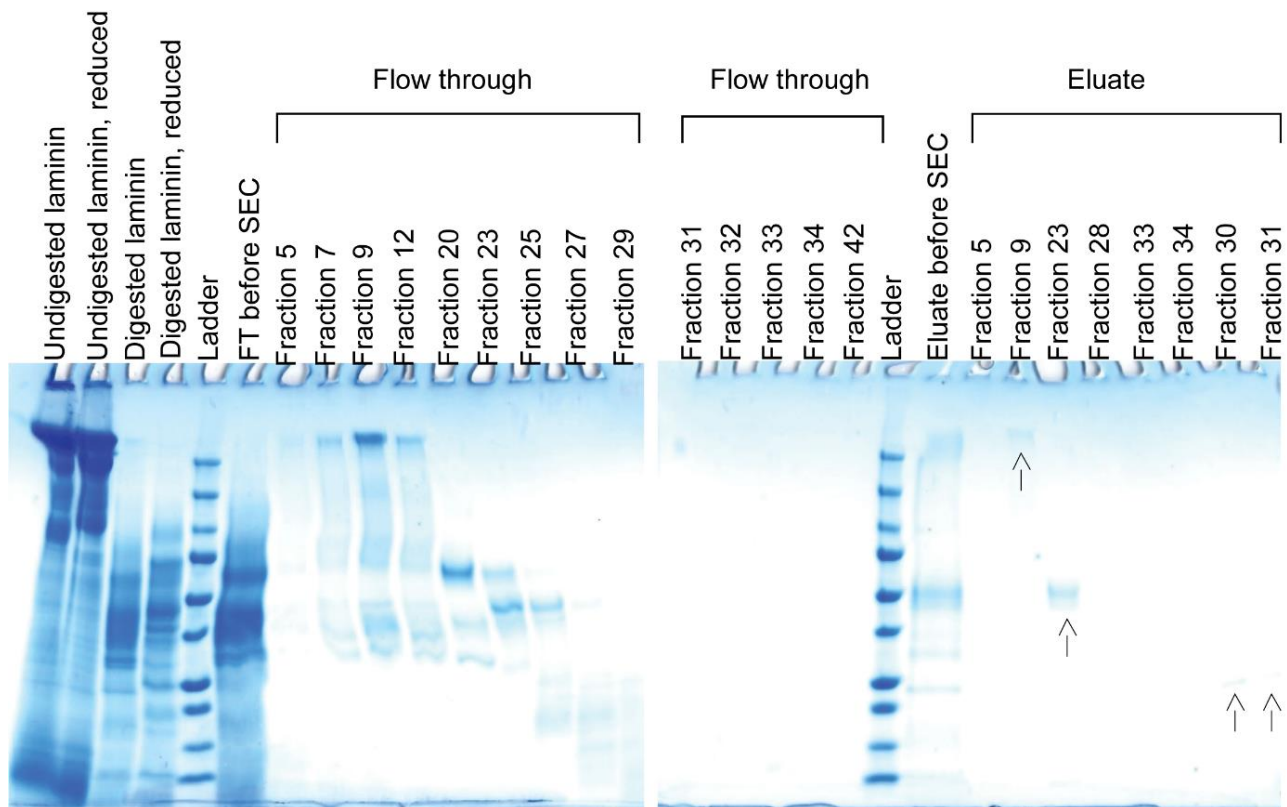
Supplementary Figure 1. Effect of laminin incorporation in the organoid culture at the onset of symmetry breaking. A) Appearance of Paneth cells on day 4 of culture in hydrolytically degradable (DG) and non-hydrolytically degradable (NDG) LDTM gels containing RGD and laminin. **B)** DG gels with laminin results in a higher population of Paneth cells.



Supplementary Figure 2. Mouse intestinal organoid formation in microcavity arrays. Single mISCs were seeded in microcavity arrays in presence of 2% Matrigel or equivalent amount of nLam or rLam.



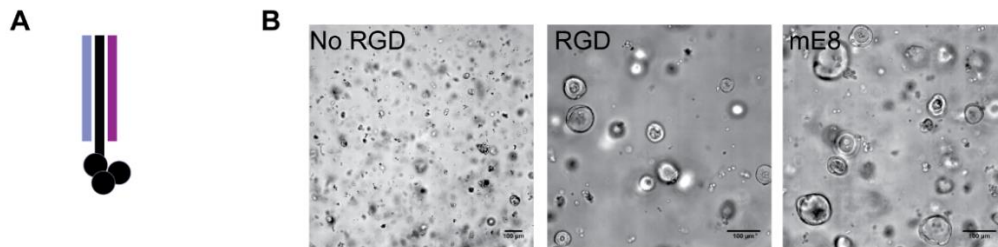
Supplementary Figure 3. Heparin-Sepharose and Size Exclusion chromatography of an elastase digest of laminin. Digests of laminin were passed through a 5 ml heparin-Sepharose column equilibrated with 50 mM ammonium bicarbonate pH 7.9. Bound material was eluted with 0.5 M NaCl at 4°C. Bound and unbound materials (eluate and flow-through) were then lyophilized, resuspended in 1 ml 0.05 M ammonium bicarbonate, and further separated by a size exclusion chromatography (Superose 6 10/300GL).



Supplementary Figure 4. SDS-PAGE (Coomassie blue-stained) of digested laminin, and different fractions recovered from the SEC chromatography. Fractions 9, 23, 30, and 31 correspond to the 250 kDa, 50 kDa, and 25 kDa fragments.

LNVKTQEPDN	LLFYLGSSSS	IKVAVSAD	RDCIRAYQPQ	TSSTNYNTLI
VSINNNRWHS	IYITRFGNMG	SDFLAVEMR	GKVAFLWDLG	SGSTRLEFPE
NSTLMFVGG	GGQIKKSPAV	SLSVKEASAA	ENPPVRTSKS	PGPSKVLDIN
CNGCFGSSQN	EDSSFHFDGS	KVTHFKGCMG	EAFNLGKSIG	LWNYIEREGK
YLASNGTKDF	LSIELVRGRV	GYAMVEKTLR	PTVTQIVILF	STFSPNGLLF
RNRKQGGLLAV	FDAYDTSDE	KVMVDLGS GP	LTLMTDRYN	NGTWYKIAFQ
AVRKGVSRRS	YVGCINKLEI	SRSTFDLLRN	SYGVRKGCAL	IYVGGLPHSK
GGYVEMPPKS	LSPESSLLAT	FATKNSSGIL	LVALGKDAEE	EPIQSVSFLR
FSIMLLEGR	EVHVNSGDGT	SLRKALLHAP	TGSYSDDGQEH	AGGAQAHPVF
ITIQVDENSP	VEMLKGLPTE	GKTIIDISNLY	IGGLPEDKAT	SISLVRNRRV
GCIKNVVLDA	QLLDFTHATG	SEQVELDTCL	LAEPEMQSLH	PMLKMRTSFH
PTLPQPELCA	VDTAPGYVAG	AHQFGLSQNS	HLVLP LNQSD	REHGE L PPEP
IRTFASSGLI	YYVAHQNQMD	YATLQLQEGR	LHFMFDLGKG	VRKRRLQVQLS
SDGKWHTVKT	EYIKRKAFMT	VDGQESP SVT	VVGNAATTLDV	RTKVSHPAL
SHYRARNI GT	ITHSIPACIG	EIMVNGQQLD	KDRPLSASAV	ERKLYLGGLP
TFFEFGSGYAA	LVKEGYKVRL	DLNITLEFRT	TSKNGVLLGI	DRCYVVAQEG
EIVDGVKVLFA	VNNGAGRITA	TYQPR AARAL	CDGK WHTLQA	SSAKVDAIGL
VDGNSVRAES	PHNTHSTSADT	NDPIYVGGYP	AHIKQNC LSS	HKSKHRI VLT
LRLSRGSQVQ	SLDLSRAFDL	QGVFPHSCPG	PEP	RASFRGCVRN

Supplementary Figure 5. LC-MS/MS identification of the 50-kDa laminin-111 fragment. The sequence of the LG1-LG5 domain of the Laminin-111 is shown in black (Uniprot data). The identified peptides after trypsin digestion of the fragment are highlighted in yellow. The image is obtained from the comparison of the fragment peptide sequence with the laminin α chain in the Scaffold software.



Supplementary Figure 6. Recombinant mE8 shows bioactivity in mISC culture. **A)** Schematic of the shortened version (50 residues) of the E8 (globular domain with the terminus of the β and γ chains – 220 residues) fragment of laminin. **B)** Single mISCs form colonies in LDTM gels in presence of biochemical cues such as RGD or mE8.

Chapter 4

Mechano-modulatory synthetic niches for liver organoid derivation

Giovanni Sorrentino^{1,†}, Saba Rezakhani^{2,†}, Ece Yildiz¹, Sandro Nuciforo³, Markus H. Heim^{3,4}, Matthias P. Lutolf^{2,*}, Kristina Schoonjans^{1,*}

¹ Laboratory of Metabolic Signaling, Institute of Bioengineering, School of Life Sciences and School of Engineering, Ecole Polytechnique Fédérale de Lausanne, 1015 Lausanne, Switzerland.

² Laboratory of Stem Cell Bioengineering, Institute of Bioengineering, School of Life Sciences and School of Engineering, École Polytechnique Fédérale de Lausanne (EPFL), 1015 Lausanne, Switzerland.

³ Department of Biomedicine, University Hospital Basel, University of Basel, 4031 Basel, Switzerland.

⁴ Clinic of Gastroenterology and Hepatology, University Hospital Basel, University of Basel, 4031 Basel, Switzerland.

†These authors contributed equally to this work. *Correspondence should be addressed to: M.P.L. (matthias.lutolf@epfl.ch) and K.S. (kristina.schoonjans@epfl.ch).

(Published in Nature Communications 2020,

<https://doi.org/10.1038/s41467-020-17161-0>)

4.1 Abstract

The recent demonstration that primary cells from the liver can be expanded *in vitro* as organoids holds enormous promise for regenerative medicine and disease modelling. The use of three-dimensional (3D) cultures based on ill-defined and potentially immunogenic matrices, however, hampers the translation of liver organoid technology into real-life applications. We here use chemically defined hydrogels for the efficient derivation of both mouse and human hepatic organoids. Organoid growth was found to be highly stiffness-sensitive, a mechanism independent of acto-myosin contractility and requiring instead activation of the Src family of kinases (SFKs) and yes-associated protein 1 (YAP). Aberrant matrix stiffness on the other hand resulted in compromised proliferative capacity. Finally, we demonstrate the unprecedented establishment of biopsy-derived human liver organoids without the use of animal components at any step of the process. Our approach thus opens up exciting perspectives for the establishment of protocols for liver organoid-based regenerative medicine.

4.2 Introduction

Although the liver has a remarkable regenerative potential, chronic inflammation and scarring severely impair liver regeneration¹, making organ transplantation the only treatment option for patients with severe liver failure². This therapeutic approach, however, is limited by the lack of liver donors, emphasizing the urgent need for cell-based therapies³. A promising alternative to liver transplantation comes from the recent breakthrough that liver organoids can be generated *in vitro* within animal-derived matrices (e.g. Matrigel) from mouse and human bile duct-derived bi-potential facultative progenitor cells⁴⁻⁶ or primary hepatocytes^{4,5,7-9}. These organoids are largely composed of progenitor cells that are genetically stable and can be differentiated into functional hepatocyte-like cells, which are able to engraft and increase survival when transplanted in a mouse model of liver disease^{4,5}. However, the batch-to-batch variability of the three-dimensional (3D) matrices currently used for organoid derivation, as well as their mouse tumour-derived origin, makes them unsuited for therapeutic ends. Recent work has suggested that composite matrices of fibrin and laminin-111, optimized for intestinal organoid culture, could also be used for liver organoid growth^{10,11}. Owing to the mouse-tumour derived laminin, these matrices are however incompatible with clinical use, and to the best of our knowledge there is no protocol available to expand and differentiate clinical-grade hepatic organoids^{12,13}.

In this study, we report the establishment of a chemically-defined and mechano-modulatory 3D culture system for mouse and human hepatic progenitors and organoids for basic research and regenerative medicine applications. We optimized the efficiency of liver organoid derivation by tuning the mechanical properties of the synthetic microenvironment to match the physiological stiffness of the mouse liver. Finally, we accurately modelled the stiffness of the fibrotic liver, and demonstrate that aberrant liver mechanics negatively impact liver progenitor proliferation.

4.3 Results and discussion

Generation of a PEG-based synthetic niche for liver organoid culture

We previously reported chemically defined 3D matrices for intestinal stem cell culture and organoid derivation¹², identifying design principles that could be adopted to mimic stem cell niches from different tissues. Here, we sought to develop a synthetic matrix for the efficient proliferation of liver progenitor cells by recapitulating key physical and biochemical characteristics of the hepatic microenvironment as an alternative to the established natural matrices Matrigel and collagen^{4,14} (Supplementary Fig. 1a). To this aim, we first generated inert poly(ethylene glycol) (PEG) hydrogels enzymatically crosslinked by the activated transglutaminase factor XIIIa (FXIIIa)¹⁵. To mimic the mechanical properties of the mouse liver, we tuned the stiffness of PEG gels to physiological values (≈ 1.3 kPa)^{16,17}. Key ECM proteins found in the native liver¹⁸, such as laminin-111, collagen IV and fibronectin, were then incorporated in the PEG network, and soluble factors found in the hepatic niche, such as hepatocyte growth factor (HGF)¹⁹, the Wnt agonist R-

Spondin^{4,20} and fibroblast growth factor 10 (FGF10)²¹, were added to the culture medium, referred to as expansion medium (EM)⁴.

Single dissociated mouse liver progenitor cells derived from Matrigel-expanded liver organoids were embedded into either Matrigel or PEG hydrogels and cultured in EM (Supplementary Fig. 1b). The functionalization of PEG hydrogels with fibronectin and laminin-111 led to efficient organoid generation, comparable to Matrigel (Figs. 1a, b). Replacement of the full-length fibronectin with its minimal integrin recognition peptide RGDSPG (Arg-Gly-Asp-Ser-Pro-Gly) led to similar results, suggesting that the addition of a minimal adhesive moiety to the otherwise inert matrix is sufficient to promote extensive proliferation of liver progenitors (Figs. 1a, b). Cells expanding in PEG hydrogels modified with RGDSPG ('PEG-RGD') generated cystic structures characterized by a central lumen and a surrounding epithelium (Figs. 1c, e). Histology and gene expression analyses showed that these PEG-RGD-derived organoids possess a progenitor phenotype expressing stem/ductal markers such as *Lgr5*, *Epcam*, *Krt19* and *Sox9* (Figs. 1d, e and Supplementary Fig. 1c) and, in terms of morphology and gene expression, are indistinguishable from organoids grown in Matrigel (Figs. 1d, e). As expected, markers of fully differentiated hepatocytes such as *Cyp3a11* were not expressed (Fig. 1d).

A major limitation of all current protocols for culturing epithelial organoids is an obligatory requirement of Matrigel (or similar natural ECM-derived matrices) in the first step of organoid generation. To test whether mouse liver organoids can be established in synthetic matrices without any initial Matrigel culture step, biliary duct fragments were isolated from mouse liver and directly embedded in PEG-RGD hydrogels (Supplementary Fig. 1b). Strikingly, after 6 days of culture, organoids emerged that could be serially passaged in culture (Fig. 1f and Supplementary Fig. 1d). PEG-RGD gels allowed organoid growth for more than 14 days (Supplementary Fig. 1e) without any significant structural deterioration. In contrast, Matrigel softened and no longer provided sufficient mechanical support already after 6 days of culture (Supplementary Fig. 1f), highlighting the importance of having a stably crosslinked matrix for long-term organoid culture.

Liver organoids cultured in PEG hydrogel efficiently differentiate into hepatocyte-like cells

Liver organoids can be partially differentiated *in vitro* into functional hepatocyte-like cells when cultured in the presence of specific differentiation medium (DM) containing inhibitors of Notch and TGF- β pathways^{4,9} (Supplementary Fig. 2a). To test whether organoids derived in the synthetic matrix preserved the capacity for differentiation and hepatocyte maturation, we grew organoids in PEG-RGD gels and replaced the expansion medium with differentiation medium after 6 days, and analysed the expression of differentiated hepatocyte markers after 12 days (Supplementary Fig. 2d)⁴. Similar to Matrigel cultures, synthetic gels promoted a robust increase in the transcript levels of mature hepatocyte markers such as *Cyp3a11*, *Alb*, *Ttr*, *Nr1h4* (*Fxr*), *Slc2a2* (*Glut2*), *Glul* and *Nr1h3* (*Lxr*) (Fig. 2a) and expression of ALB and HNF4 α proteins (Fig. 2b), while markers of stem cells, such as *Lgr5*, disappeared (Supplementary Fig. 2b). As expected, during the differentiation process, cells acquired a characteristic hepatocyte-like morphology, as evidenced by a polygonal shape and expression of junction proteins such as ZO-1 and E-cadherin (Figs. 2c, d).

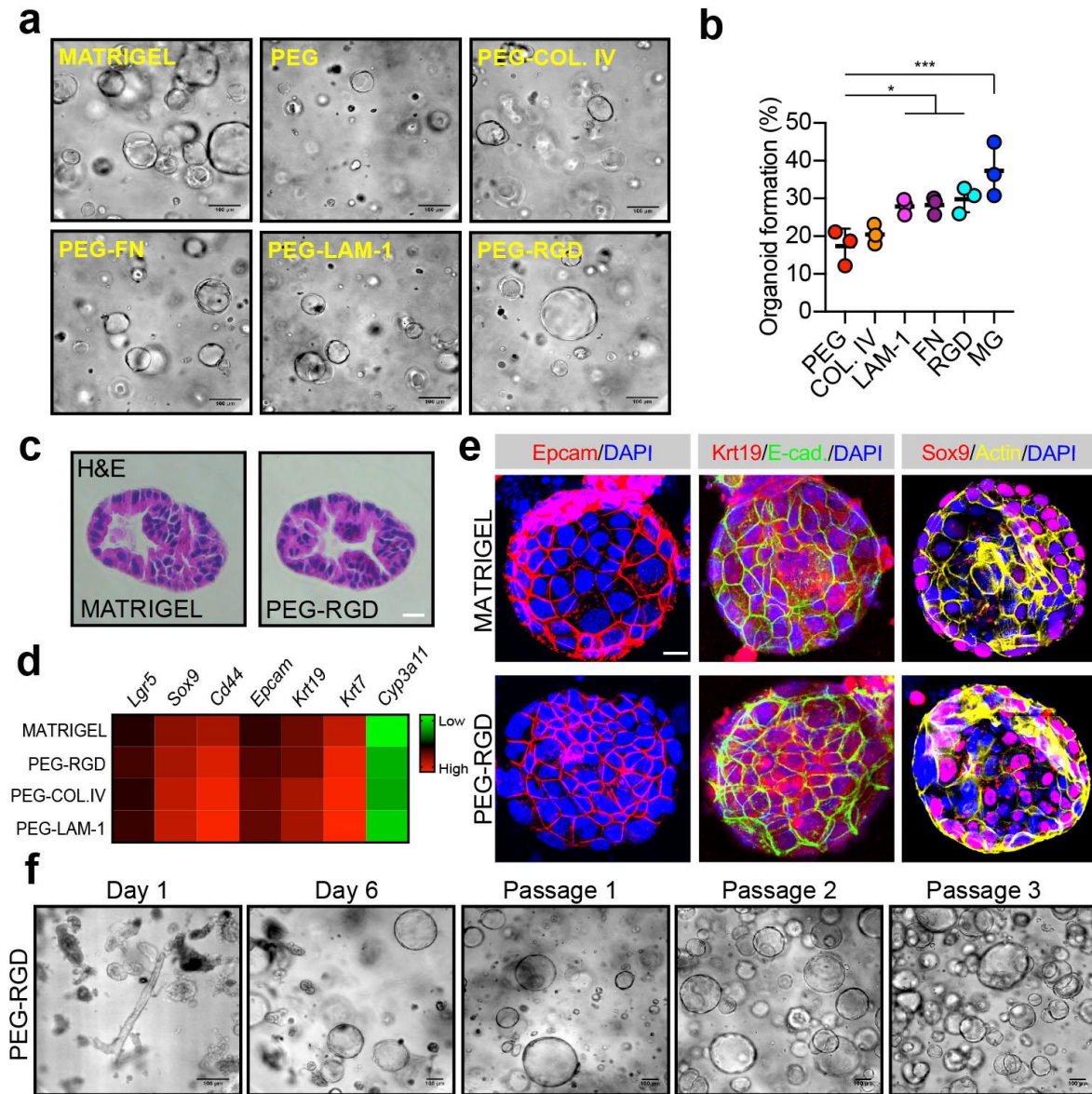


Figure 1. Liver organoid growth in Matrigel and PEG supplemented with ECM components. (a) Mouse liver progenitor cells 3 days after embedding in: Matrigel (MG), plain PEG (PEG) and PEG functionalized with the indicated ECM components: COL.IV (collagen IV), FN (fibronectin), LAM-1 (laminin-1) and RGD-representing peptide (RGD). (b) Quantification of organoid formation efficiency relative to panel a. (c) Hematoxylin and eosin staining of Matrigel- and PEG-derived organoids. Scale bar 25 μ m. (d) Gene expression was analysed by qRT-PCR in liver organoids 6 days after embedding in Matrigel and PEG hydrogels supplemented with different ECM factors. The heatmap represents Δ Ct values as described in the method section. (e) Liver organoid immunostaining was performed 6 days after embedding of liver progenitor cells in Matrigel or PEG-RGD. (f) Liver organoids can be cultured in PEG hydrogels by directly embedding mouse biliary duct fragments. Representative pictures are shown. Graphs show individual data points derived from n=3 independent experiments and means \pm s.d. *P<0.05, ***P<0.001, one way Anova. Source data are provided as a Source Data file.

Occasionally, hepatocyte-like cells showed poly-nucleation, a typical feature of hepatocytes (Figs. 2c, d and Supplementary Fig. 2e).

Next, to test whether hepatocyte-like cells generated in PEG-RGD hydrogels display hepatocyte-specific functions, we monitored albumin secretion. Liver organoids grown in DM showed a marked increase in albumin secretion, as compared to organoids cultured in EM (Fig. 2e). Moreover, hepatocyte-like cells were able to produce and secrete urea, as well as to accumulate glycogen, two enzymatically-regulated processes that occur in mature hepatocytes (Figs. 2f, g). Moreover, the majority of differentiated cells were capable of internalizing low-density lipoproteins (LDL) from the culture medium, indicating that LDL receptor-mediated cholesterol uptake is functional (Fig. 2h). Finally, differentiation of organoids directly derived in PEG-RGD hydrogels was as efficient as in Matrigel (Supplementary Fig. 2c). Altogether, these results demonstrate that liver organoids grown in PEG-RGD hydrogels can be readily differentiated into hepatocyte-like cells that mimic many of the established hepatic functions.

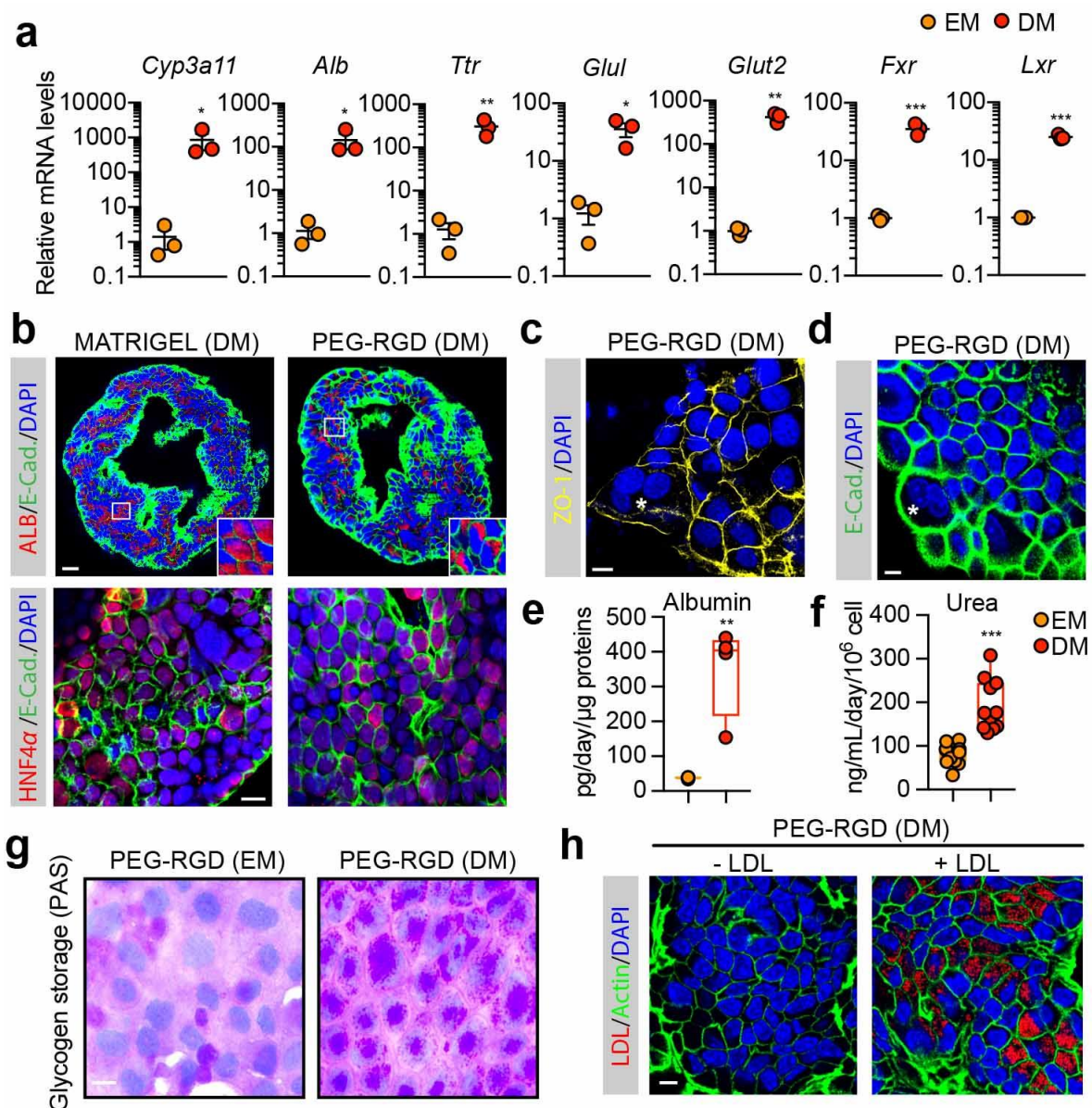


Figure 2. Differentiation of liver organoids into hepatocyte-like cells in PEG-RGD hydrogels. **(a)** Gene expression was analysed by qRT-PCR in liver organoids maintained in expansion medium (EM) or differentiation medium (DM) in PEG-RGD hydrogels. Graphs show individual data points derived from $n=3$ independent experiments and means \pm SEM. * $P<0.05$, ** $P<0.01$ *** $P<0.001$ unpaired Student's one-tailed t-test. **(b)** Representative confocal immunofluorescence images of Albumin (ALB), Hnf4a and E-Cadherin (E-CAD.). Scale bars: 25 μm (top), 10 μm (bottom). **(c)** Representative confocal immunofluorescence images of ZO-1 in liver organoids maintained in differentiation medium (DM) in PEG-RGD hydrogels. The asterisk indicates a bi-nucleated cell. Scale bar 10 μm . **(d)** Liver organoids maintained in differentiation medium (DM) in PEG-RGD hydrogels. E-cadherin was used to visualize cell borders. The asterisk indicates a bi-nucleated cell. Scale bar 10 μm . **(e)** Albumin secretion was quantified in the supernatant of organoids embedded in PEG-RGD hydrogels and maintained in EM or DM. Box plots show min. to max. individual data points derived from $n=4$. ** $P<0.001$, unpaired Student's two-tailed t-test. **(f)** Urea production was quantified in the supernatant of organoids embedded in PEG-RGD hydrogels and maintained in EM or DM. Box plots show min. to max. individual data points derived from $n=11$. ** $P<0.001$, unpaired Student's two-tailed t-test. **(g)** Glycogen accumulation was assessed by PAS (Periodic-Acid Schiff) staining in liver organoids embedded in PEG-RGD hydrogels and maintained in EM or DM. Scale bar 10 μm . **(h)** LDL uptake was monitored by Dil-ac-LDL fluorescent substrate in liver organoids maintained in DM in PEG-RGD hydrogels. Scale bar 10 μm . Source data are provided as a Source Data file.

Matrix stiffness controls liver organoid growth in an acto-myosin-independent manner

Mechanical signals can play a critical role in controlling stem cell behaviour and tissue homeostasis²², but also contribute to the manifestation of diseases^{22–24}. Despite the recent progress in establishing novel 3D liver model systems^{4,7,9}, relatively little is known about the role of mechanics in regulating hepatic stem cell biology. This is mostly due to the fact that current culture systems rely on Matrigel which has batch-to-batch stiffness variability and is not conducive to mechanical modification (Supplementary Fig. 3a). To test whether matrix mechanics affect liver organoid growth, we grew organoids in hydrogel of variable stiffness, ranging from values below the normal mouse liver stiffness (0.3 kPa) to those reaching physiological stiffness (1.3 kPa)^{16,17}. Organoid formation efficiency and proliferation was profoundly affected by the mechanical properties of the matrix, with values mimicking physiological liver stiffness (between 1.3 and 1.7 kPa) being optimal (Figs. 3a, b and Supplementary Fig. 3b). Differentiation capacity however was unaffected by the degree of stiffness as induction of hepatic genes was maintained also when liver organoids were differentiated in soft gels (Supplementary Figs. 2d and 3c). These data demonstrate that optimizing the mechanical properties of the hydrogel represents a critical step in the efficient generation of liver organoids.

Given the pivotal role of the Hippo pathway nuclear effector, Yes associate protein (YAP), in the transduction of micro-environment mechanical cues downstream of integrins²⁵, we next tested whether YAP activation could potentially explain the observed matrix stiffness dependence. We monitored the expression of canonical YAP target genes and YAP subcellular localization in organoids cultured in soft (0.3 kPa) and physiologically-stiff (1.3 kPa) matrices.

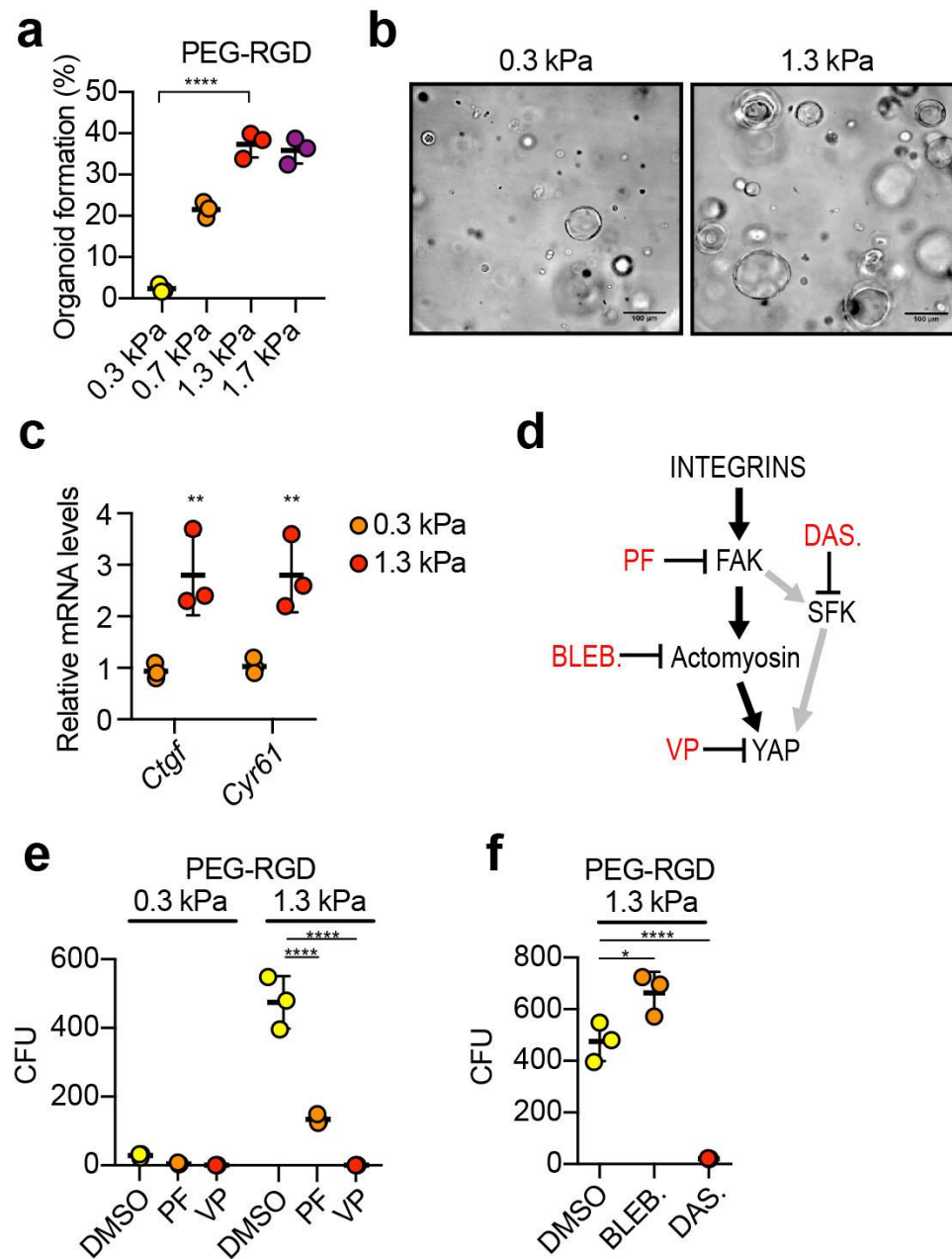


Figure 3. Effect of matrix stiffness on liver organoid formation. **(a)** Effect of matrix stiffness on organoid formation efficiency. **(b)** Representative image of organoids 3 days after embedding in PEG-RGD hydrogels of indicated stiffness. **(c)** Gene expression was analysed by qRT-PCR in liver organoids 6 days after embedding in PEG-RGD hydrogels with indicated stiffness. **(d)** Schematic representation of cellular mechano-signalling pathways. Inhibitors of key elements are depicted in red. **(e)** Effect of indicated inhibitors on organoid formation efficiency in soft (300 Pa) and physiologically-stiff (1.3 kPa) PEG-RGD hydrogels. CFU (colony forming unit). **(f)** Effect of indicated inhibitors on organoid formation efficiency in physiologically-stiff (1.3 kPa) PEG-RGD hydrogels. CFU (colony forming unit). Graphs show individual data points derived from $n=3$ independent experiments and means \pm s.d. * $P<0.05$, ** $P<0.01$ *** $P<0.001$ one way Anova (a, f) or Two way Anova (c, e). Source data are provided as a Source Data file.

Interestingly, in stiffer hydrogels, YAP target genes expression and nuclear accumulation were increased compared to soft matrices (Fig. 3c and Supplementary Fig. 3d). To examine whether an activated integrin/YAP signalling axis is functionally required for organoid derivation in physiologically-stiff matrices, we treated organoid cultures with PF-573228 (PF), an inhibitor of the integrin effector focal adhesion kinase (FAK), or with the YAP inhibitor Verteporfin (VP)²⁶ (Fig. 3d). Both treatments prevented the increase in organoid formation induced in stiffer matrices (Fig. 3e and Supplementary Fig. 3e), indicating that the integrin/YAP module is required in coordinating growth of liver progenitors in response to mechanical stimuli.

We then sought to identify the other components of the FAK-YAP cascade that may play a role in modulating the stiffness response in our system. Since remodelling of the actin cytoskeleton has been identified as a key event upstream of YAP activation^{27–29}, we assessed its putative involvement in physiological stiffness-induced organoid growth by inhibiting acto-myosin contractility with blebbistatin³⁰. Surprisingly, blebbistatin treatment significantly enhanced organoid formation (Fig. 3f) with an efficiency comparable to ROCK inhibitors (Supplementary Fig. 3g), indicating that matrix stiffness promotes organoid growth independently of cytoskeletal dynamics, and that acto-myosin contractility rather interferes with normal liver progenitor expansion. However, tyrosine phosphorylation of YAP by the Src family of kinases (SFK), an alternative route for integrin-dependent and acto-myosin independent YAP activation^{31–39}, was increased by matrix stiffness (Supplementary Fig. 3f). Of interest, treatment with Dasatinib⁴⁰, a FDA-approved SFK inhibitor, fully abolished YAP phosphorylation and organoid growth in physiologically-stiff (1.3 kPa) matrices (Fig. 3f and Supplementary Fig. 3f). These results corroborate the importance of the integrin/SFK/YAP signalling pathway in liver progenitor proliferation in response to differential mechanical inputs.

PEG hydrogels can be tuned to model fibrotic liver mechanics

Liver disease progression is strongly associated with abnormal tissue architecture and mechanotransduction^{16,41,42}. Indeed, as a direct effect of aberrant ECM deposition in the fibrotic liver, tissue stiffness increases in time and severely compromises its function^{43–45}. In fact, the changes in liver stiffness associated with disease are used for diagnostics based on longitudinal non-invasive monitoring⁴⁶. We reasoned that liver organoids grown in defined hydrogels recapitulating the stiffness of fibrotic liver could serve as physiologically relevant 3D model to investigate how stem cells translate aberrant mechanical inputs into disease-relevant phenotypes. To this aim, we generated fibrosis-mimicking hydrogels with a stiffness of 4 kPa^{16,17}. Strikingly, these hydrogels led to a significant impairment of organoid formation (Figs. 4a-b and Supplementary Fig. 3a), demonstrating that an abnormal ECM stiffness is sufficient to decrease the liver progenitor proliferative capacity. In this condition liver organoids showed a reduction in the expression of hepatic progenitor markers (Fig. 4c) and upregulation of genes involved in cellular response to hepatic injury (Fig. 4d and Supplementary Fig. 4a), indicating impaired stemness potential and concomitant induction of a stress response. Finally, fibrosis-mimicking hydrogels led to an increase in the expression of matrix metalloproteases (Fig. 4e), a compensatory phenomenon known to be induced in response to increased ECM stiffness^{47–49}. Surprisingly, in these conditions YAP activation was not affected (Fig. 4f), suggesting the existence of other pathways controlling liver

progenitor growth in response to increased stiffness. These results suggest that synthetic hydrogels may be a useful tool to assess the contribution of mechanical inputs on liver diseases.

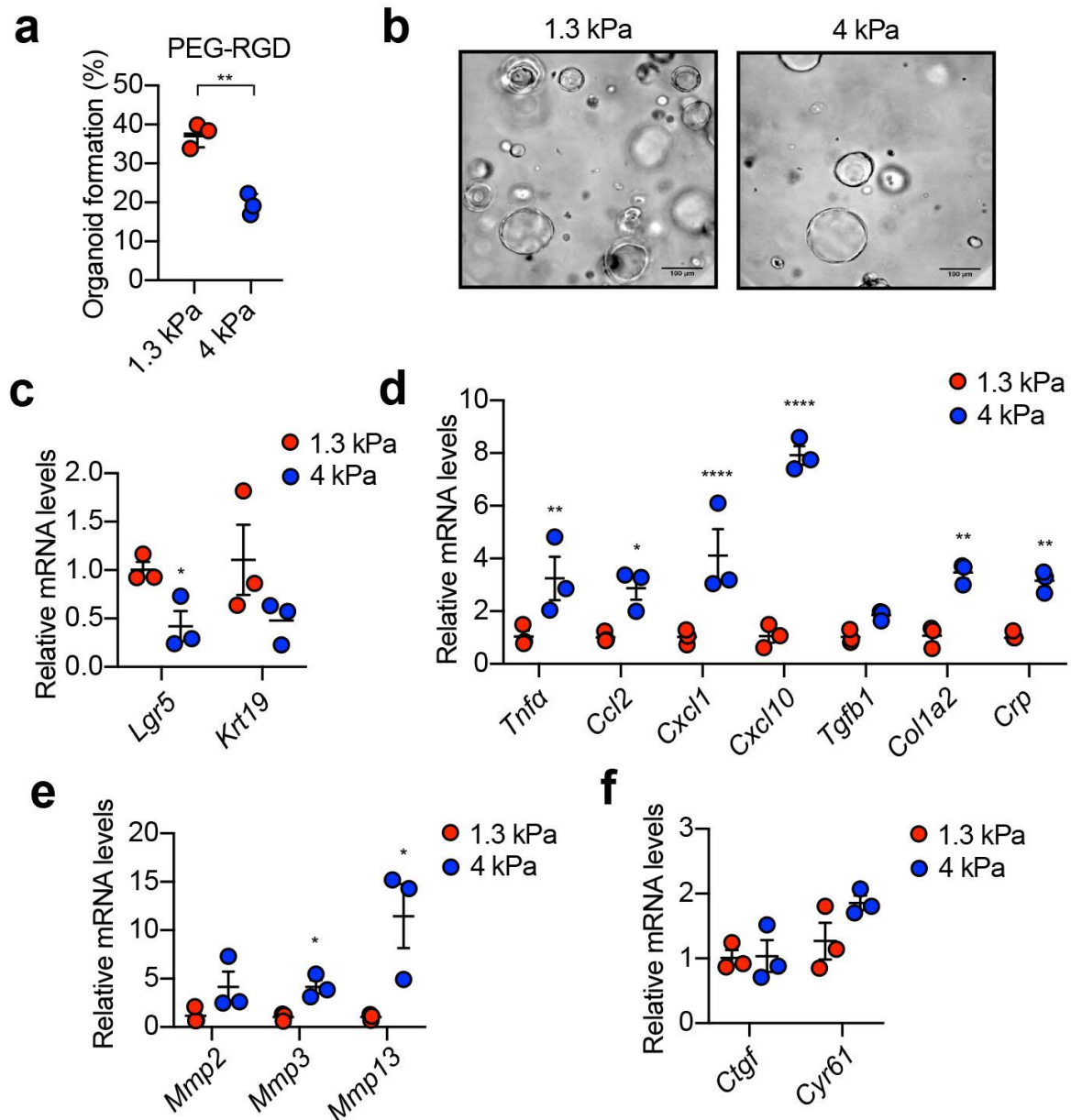


Figure 4. Hydrogels mimicking the stiffness of native fibrotic liver affect the growth of liver organoids and promote a stress response. (a) Effect of matrix stiffness on organoid formation efficiency. Scale bars: 100 μ m. (b) Representative image of organoids 3 days after embedding in PEG-RGD hydrogels of indicated stiffness. (c-f) Gene expression was analysed by qRT-PCR in liver organoids 6 days after embedding in PEG-RGD hydrogels with indicated stiffness. Graphs show individual data points derived from n=3 independent experiments and means \pm SEM *P<0.05, **P<0.01 ***P<0.001 unpaired Student's two-tailed t-test (a) or two way Anova (c-f). Source data are provided as a Source Data file.

PEG hydrogels allow derivation and culture of human liver organoids

To test the potential clinical relevance of our findings, we assessed whether the PEG-RGD hydrogels, initially designed for expansion and differentiation of mouse liver organoids, were also suitable for culturing human organoids. We first generated Matrigel-derived organoids from human non-tumorigenic liver needle biopsies^{5,50}. Human liver progenitor cells were then embedded in PEG-RGD and cultured in human expansion medium (HEM) (Supplementary Fig. 4b). In these conditions human liver progenitor cells generated organoids that could be expanded over multiple passages (Fig. 5a). Similar to mouse, human organoid generation efficiency in PEG-RGD was comparable to Matrigel (Fig. 5a), and was critically dependent on changes in hydrogel stiffness (Fig. 5b). Moreover, when cultured in HEM, human liver organoids grown in PEG-RGD expressed progenitor cell markers, such as KRT19 (Fig. 5c), but readily differentiated into human hepatocyte-like cells when cultured in human differentiation medium (HDM) (Fig. 5d and Supplementary Fig. 4c).

Finally, in order to generate clinically relevant human liver organoids, we tested the possibility of establishing organoids from human patients without the interference of any animal-derived matrices. To this aim, freshly isolated liver biopsies from six patients were digested and directly embedded in PEG-RGD hydrogels (Fig. 5e). Strikingly, after 8 days of culture, organoid formation was scored from progenitor cells of all patients (Fig. 5f) and could be passaged (Fig. 5g) and differentiated (Supplementary Fig. 4d). Moreover, liver organoids could be frozen-thawed in PEG-RGD hydrogels (Supplementary Fig. 4e).

Altogether, these data provide proof-of-concept that human liver progenitor cells can be derived and maintained *in vitro* within synthetic matrices.

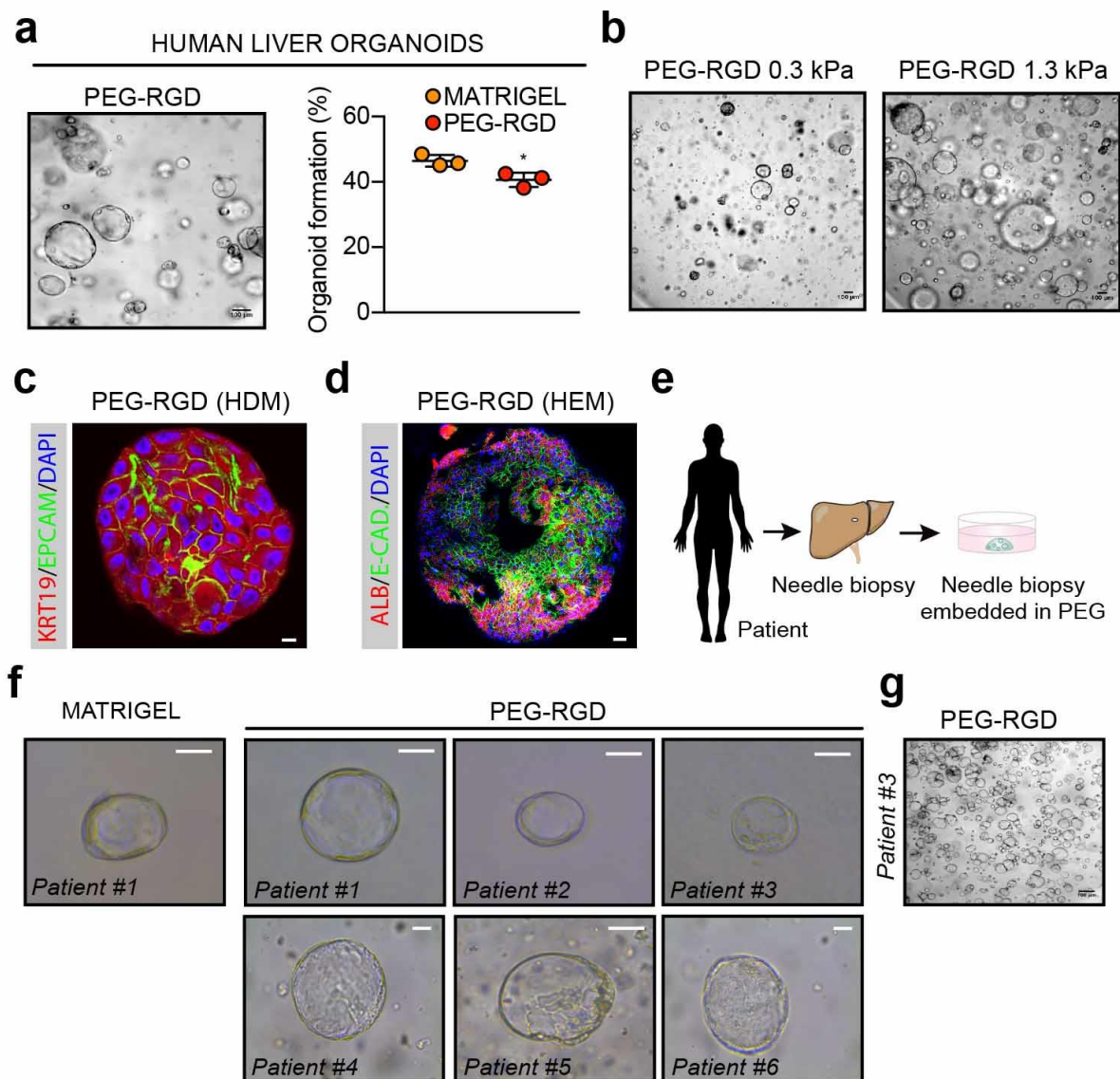


Figure 5. PEG-RGD hydrogels allow for establishment, expansion and differentiation of patient-derived human liver organoids. (a) Matrigel-derived human liver progenitor cells were embedded in physiologically-stiff PEG-RGD hydrogels and passaged in human expansion medium (HEM) with an efficiency comparable to Matrigel. (b) Effect of matrix stiffness on human liver organoid formation. (c) Representative confocal immunofluorescence image of KRT19 and Epcam in liver organoids embedded in physiologically-stiff PEG-RGD hydrogels and cultured in HEM. Scale bar 10 μm . (d) Representative confocal immunofluorescence image of Albumin and E-Cadherin in liver organoids cultured in human differentiation medium (HDM), Scale bar 25 μm . (e, f) Freshly-isolated liver biopsies from six patients were digested and directly embedded in PEG-RGD hydrogels. Scale bar 50 μm . (g) PEG-RGD-derived human liver progenitor cells were embedded in physiologically-stiff hydrogels and passaged in human expansion medium (HEM). Scale bar 100 μm . * $P < 0.05$, unpaired Student's two-tailed t-test. Source data are provided as a Source Data file.

4.4 Conclusion

We report here the establishment of a fully defined 3D culture system for mouse and human hepatic progenitors and organoids. We demonstrated that liver organoids can be expanded and maintained in such minimal environments with an efficiency that is comparable to Matrigel, but without its main disadvantages of structural instability, batch-to-batch variability and clinical incompatibility. By tuning the stiffness of the synthetic networks to match the physiological levels of the liver, we optimized the efficiency of liver organoid derivation, and identified integrin-SFK-YAP as a mechano-sensitive axis that is required for liver organoid growth. Interestingly, in contrast to intestinal organoids¹², we found that liver progenitor cells transduce mechanical signals in an acto-myosin independent manner and instead require activation of the tyrosine kinase Src to support epithelial tissue formation. Moreover, we used PEG hydrogels to accurately model the aberrant mechanical properties of the fibrotic liver, providing evidence that aberrant liver stiffness negatively impacts liver progenitor proliferation. This experimental set-up provides a standardized framework to study hepatic progenitor cells in a defined mechanical environment, which may further our understanding of the underappreciated role of mechanical cues in modulating the molecular properties and signatures of this cell population in healthy and fibrotic liver. Finally, our data showing that clinically relevant human stem/progenitor cells can be grown *in vitro* without any requirement of animal-derived matrices, may open exciting perspectives for the establishment of protocols for liver organoid-based clinical applications.

4.5 Materials and methods

Data reporting

The experiments were not randomized and the investigators were not blinded to allocation during experiments and outcome assessment. No statistical methods were used to determine sample size. The experiments were repeated at least 3 times or with at least 3 different donors to control biological variations.

Animals and ethical approval

Liver tissues were harvested from 8-12 weeks old euthanized C57BL/6J male mice. All the animal experiments were authorized by the Veterinary Office of the Canton of Vaud, Switzerland under the license authorization no. 3263.

Enzymatically crosslinked hydrogel precursor synthesis

Hydrogel precursors were synthesized as previously reported⁵¹. Briefly, vinylsulfone functionalized 8-arm PEG (PEG-VS) was purchased from NOF. The transglutaminase (TG) factor XIII (FXIIIa) substrate peptides *Ac-FKGGGPQGIWQG-ERCG-NH2* with matrix metalloproteinases (MMPs) sensitive sequence (in italics), *Ac-FKGG-GDQGIAGF-ERCG-NH2*, *H-NQEQVSPLERCGNH2* and the RGD-presenting adhesion peptide *H-NQEQVSPLRGDSPG-NH2* were purchased from GL Biochem. FXIIIa substrate peptides and 8-arm PEG-VS were dissolved in triethanolamine (0.3 M, pH 8.0) and mixed at 1.2 stoichiometric excess (peptide-to-VS group), and allowed to react for 2 h under inert atmosphere. The reaction solution was dialysed (Snake Skin, MWCO 10K, PIERCE) against ultrapure water for 3 days at 4 °C, after which the products were lyophilized and dissolved in ultra-pure water to make 13.33% w/v stock solutions.

Formation and dissociation of PEG hydrogels

PEG precursor solutions were mixed in stoichiometrically balanced ratios to form hydrogel networks of a desired final PEG content. Addition of thrombin-activated FXIIIa (10 U ml⁻¹; Galexis) triggered the hydrogel formation in the presence of Tris-buffered saline (TBS; 50 mM, pH 7.6) and 50 mM CaCl₂. The spare reaction volume was used for the incorporation of dissociated liver stem cells, fragments of liver bile ducts, and ECM components: RGD-presenting adhesion peptide, fibronectin (0.5 mg ml⁻¹; R&D systems), laminin-111 (0.2 mg ml⁻¹; Invitrogen), collagen-IV (0.2 mg ml⁻¹; BD Bioscience). Gels cast on PDMS-coated 24 well-plate were allowed to crosslink by incubation at 37°C for 10 min. To release the grown colonies for further processing, gels were detached from the bottom of the plates using a tip of a metal spatula and transferred to 15-ml Falcon tube containing 1 ml of Dispase (1 mg/ml, Thermo Fisher Scientific). After 10 minutes enzymatic digestion, the reaction was quenched using 10% FBS containing 1 mM EDTA, washed with cold basal medium and centrifuged for 3 min at 1000 rpm.

Mechanical characterization of PEG hydrogels

Elastic modulus (G') of hydrogels was measured by performing small-strain oscillatory shear measurements on a Bohlin CVO 120 rheometer with plate-plate geometry. Briefly, 1-1.4 mm thick hydrogel discs were prepared and allowed to swell in water for 24 hrs. The mechanical response of the hydrogels sandwiched between the parallel plates of the rheometer was recorded by performing frequency sweep (0.1-10 Hz) measurements in a constant strain (0.05) mode at 25 °C.

Quantification of liver organoid formation efficiency

Phase contrast z-stacks images were collected through the entire thickness of the PEG gels (every 15 μm) at 4 different locations within the gels (Nikon Eclipse Ti). The Cell Counter plugin in ImageJ (NIH) was used to quantify the percentage of single cells that formed colonies after 3 days of culture in expansion medium.

Culture of mouse and human liver organoids

Mouse liver organoids were established from biliary duct fragments as previously described with some modifications⁴. Briefly, liver tissues were digested in digestion solution (Collagenase type XI 0.012%, dispase 0.012%, FBS 1% in DMEM medium) for 2 hours. When digestion was complete, bile ducts were pelleted by mild centrifugation (200 rpm for 5 min) and washed with PBS. Isolated ducts were then resuspended either in Type I Collagen (8-11 mg/ml prepared following manufacturer's instruction – from Corning), Matrigel (BD Bioscience) or PEG precursor solution and cast in 10 μl droplets in the centre of the wells in a 48-well plate. After the gels were formed, 250 μl of isolation medium was added to each well. Isolation medium was composed of AdDMEM/F12 (Invitrogen) supplemented with B27 and N2 (both GIBCO), 1.25 μM N-acetylcysteine (Sigma-Aldrich), 10 nM gastrin (Sigma-Aldrich) and the following growth factors: 50 ng ml^{-1} EGF (Peprotech), 1 $\mu\text{g ml}^{-1}$ Rspo1 (produced in-house), 100 ng ml^{-1} Fgf10 (Peprotech), 10 mM nicotinamide (Sigma-Aldrich), 50 ng ml^{-1} HGF (Peprotech), Noggin (100 ng ml^{-1} produced in-house), Wnt 3a (1 $\mu\text{g ml}^{-1}$, Peprotech) and Y-27632 (10 μM , Sigma). After the first 4 days, isolation medium was changed with expansion medium (EM) which consists of isolation medium without Noggin, Wnt and Y-27632. One week after seeding, organoids were removed from the Matrigel or PEG hydrogel, dissociated into single cells using TrypLE express (Gibco), and transferred to fresh Matrigel or PEG hydrogels. Passaging was performed in 1:3 split ratio once per week. Plasmids for Rspo1 and Nog production were a kind gift from Joerg Huelsken. Liver progenitor cells were treated with the following compounds for YAP-inhibition experiments: Verteporfin (10 μM , Sigma), Dasatinib (10 μM , Selleckchem), Blebbistatin (10 μM StemCell Technologies), PF 573228 (10 μM Tocris).

Human liver biopsies and generation of human organoids

Human tissues were obtained from patients undergoing diagnostic liver biopsy at the University Hospital Basel. Written informed consent was obtained from all patients. The study was approved by the ethics committee of the northwestern part of Switzerland (Protocol Number EKNZ 2014-099). Ultrasound (US)-guided needle biopsies were obtained with a coaxial liver biopsy technique as described previously⁵⁰. One biopsy cylinder was fixed in formalin and paraffin-embedded for

histopathological diagnosis. Additional cylinders were collected in advanced DMEM/F-12 (GIBCO) for organoid generation. Patient clinical information are shown in Supplementary Table 2. Human liver organoids were generated as previously described with some modifications⁵⁰. Briefly, biopsies were placed in advanced DMEM/F-12 (GIBCO) and transported to the laboratory on ice. Liver samples were then digested to small-cell clusters in basal medium containing 2.5 mg/mL collagenase IV (Sigma) and 0.1 mg/mL DNase (Sigma) at 37°C. Cell clusters were embedded in Matrigel or PEG gels, cast and after the gels were formed, human isolation medium (HIM) was added. HIM is composed of advanced DMEM/F-12 (GIBCO) supplemented with B-27 (GIBCO), N-2 (GIBCO), 10 mM nicotinamide (Sigma), 1.25 mM N-acetyl-L-cysteine (Sigma), 10 nM [Leu15]-gastrin (Sigma), 10 μ M forskolin (Tocris), 5 μ M A83-01 (Tocris), 50 ng/mL EGF (PeproTech), 100 ng/mL FGF10 (PeproTech), 25 ng/mL HGF (PeproTech), 1 μ g mL⁻¹ Rspo1 (produced in-house), Wnt3a (1 μ g mL⁻¹, Peprotech), Y-27632 (10 μ M, Sigma) and Blebbistatin (10 μ M StemCell Technologies). After the first 4 days, isolation medium was changed with human expansion medium (HEM) which consists of HIM without Noggin, Wnt and Y-27632.

Mouse hepatocyte differentiation

Single cells were seeded and kept for 6 days in EM. Then the medium was changed to differentiation medium (DM) which no longer contains Rspo1, HGF and nicotinamide and instead contains A8301 (50 nM, Tocris Bioscience) and DAPT (10 nM, Sigma-Aldrich). Cells were maintained in DM for 12 days. During the last 3 days DM was also supplemented with dexamethasone (Sigma, 3 μ M). Medium was changed every two days.

Human hepatocyte differentiation

Single cells were seeded and kept 6 days in HEM. Then the medium was changed to differentiation medium (HDM) which no longer contains Rspo1, HGF and nicotinamide and instead contains A8301 (50 nM, Tocris Bioscience) and DAPT (10 nM, Sigma-Aldrich), BMP7 (25 ng/mL Peprotech) and human Fgf19 (100 ng/mL, R&D). Cells were maintained in DM for 10 days. During the last 3 days DM was also supplemented with dexamethasone (3 μ M). Medium was changed every two days.

Immunohistochemical analysis of human organoids

Human organoids were fixed in 10% neutral buffered formalin, washed with PBS, dehydrated, and embedded in paraffin. 5 μ m thick sections were made from paraffin-embedded samples and sections were stained with H&E and PAS.

Immunofluorescence analysis

Liver organoids were extracted from Matrigel (with Cell Recovery Solution, Corning) or PEG gels (with 1 mg mL⁻¹ Dispase (Gibco) for 10 min at 37 °C) and fixed with 4% paraformaldehyde (PFA) in PBS (20 min, room temperature). Organoids in suspension were centrifuged (1000 r.p.m., 5 min) to remove the PFA, washed with ultra-pure water and pelleted. The organoids were then spread on glass slides and allowed to attach by drying. Attached organoids were rehydrated with PBS and permeabilized with 0.2% Triton X-100 in PBS (1 h, room temperature) and blocked (1% BSA in

PBS) for 1 h. Samples were then incubated overnight with phalloidin-Alexa 488 (Invitrogen) and primary antibodies against Epcam (1:50, eBioscience, G8.8), Krt19 (1:100, ab15463), E-cadherin (1:100, Cell Signaling, 24E10), Sox9 (1:50, Millipore, AB5535), Albumin (1:50, R&D systems, MAB1455), Hnf4 α (1:50, Santa Cruz, C19), ZO-1 (1:50, Invitrogen, 61-7300); YAP (1:50, Cell Signaling, 4912S). Samples were washed with PBS and incubated for 3 h with secondary antibodies Alexa 488 donkey- α -rabbit, Alexa 568 donkey- α -mouse, Alexa 647 donkey- α -goat (1:1000 in blocking solution; Invitrogen). Following extensive washing, stained organoids were imaged by confocal (Zeiss LSM 710) mode. Dapi was used to stain nuclei.

Western blotting

Samples were lysed in lysis buffer (50 mM Tris (pH 7.4), 150 mM KCl, 1 mM EDTA, 1% NP-40, 5 mM NAM, 1 mM sodium butyrate, protease and phosphatase inhibitors). Proteins were separated by SDS-PAGE and transferred onto nitrocellulose or polyvinylidene difluoride membranes. Blocking (30 min) and antibody incubations (overnight) were performed in 5% BSA in TBST. YAP1 (Santa Cruz sc101199, 1:1000), phospho-YAP1^{Y357} (Abcam ab62751, 1:1000), ACTIN (Santa Cruz sc47778, 1:1000), CXCL10 (RD system AF-466-NA, 1:1000), CCL2 (Novus Biologicals NBP2-22115, 1:1000), COL1A2 (Santa Cruz, 1:1000).

Quantitative real-time qRT-PCR for mRNA quantification

Liver organoids were extracted from Matrigel or PEG gels as previously described¹². RNA was extracted from organoids using the RNAqueous total RNA isolation kit (Thermo Fisher) following manufacturer's instructions. RNA was transcribed to complementary DNA using QuantiTect Reverse Transcription Kit (Qiagen) following manufacturer's instructions. Expression of selected genes was analysed using the LightCycler 480 System (Roche) and SYBR Green chemistry. Quantitative reverse transcription polymerase chain reaction (PCR) results were presented relative to the mean of *Gapdh* ($\Delta\Delta C_t$ method). Expression values shown as heatmap are reported as delta cycle threshold (ΔC_t) values normalized using *Gapdh* (ΔC_t values were calculated as $\Delta C_t = C_t[\text{target gene}] - C_t[\text{Gapdh}]$ and represented by scale colour of ΔC_t values [Green-low expression; Red-high expression])⁵². Primers for qRT-PCR are listed in Supplementary Table 1.

Proliferation assay

Cell proliferation was assessed by EdU assay (Click-iT EdU Alexa Fluor 647) following manufacturer's instructions. Liver organoids were incubated with EdU for 2 hours. For quantification of EdU+ cells, one section per organoid showing the largest dimension of the organoid was analyzed (15 organoid per condition) and from each section EdU+ cells were manually counted and expressed as percentage of cells calculated from nuclear labeling with DAPI.

Functional analysis

LDL uptake was detected with DiI-Ac-LDL (Biomedical Technologies). Mouse albumin secretion was detected with ELISA kit (Abcam, ab108792). Urea secretion was assessed with QuantiChrom™ Urea Assay Kit (BioAssay Systems). All experiments were followed according to the manufacturers' instructions.

Statistical analysis and sample information

Statistically significant differences between the means of two groups were assessed as specified in the legends. All statistical analyses were performed in the GraphPad Prism 7.0 software. A P value of 0.05 or less was considered statistically significant.

Data availability

All summary or representative data generated and supporting the findings of this study are available within the paper. The data underlying Figs 1b, d; 2a, e-f; 3a, c, e-f; 4a, c-f; 5a and Supplementary Figs 1b; 2a-c; 3a-c, g; 4c and uncropped blots are provided as a Source Data file.

Acknowledgments

We thank Andréane Fouassier, Sabrina Bichet, Thibaud Clerc, Laure Vogeleisen-Delpech, Fabiana Fraga, the Phenotyping Unit (UDP) and the Histology core facility (HCF) of EPFL for technical assistance. The work of K.S. was funded by the Swiss National Science Foundation (SNSF 31003A_125487), Sinergia CRSII3_160798/1, the Kristian Gerhard Jebsen Foundation, and the Ecole Polytechnique Fédérale de Lausanne (EPFL). The work of M.P.L. in the area of organoid biology and technology was supported by the Swiss National Science Foundation (grant #310030_179447), the European Union's Horizon 2020 research and innovation programme (INTENS 668294), the Personalized Health and Related Technologies Initiative from the ETH Board, the Vienna Science and Technology Fund and École Polytechnique Fédérale de Lausanne (EPFL). G.S. was funded by a postdoctoral FEBS long-term fellowship.

Author contributions

G.S., S.R., M.L. and K.S. conceived the project and wrote the manuscript. G.S., S.R. and E.Y. planned and performed experiments and analysed data. S.N. and M.H. provided human biopsy samples and critically revised the manuscript.

Competing financial interest

Ecole Polytechnique Fédérale de Lausanne has filed patent applications pertaining to synthetic gels for epithelial stem cell and organoid cultures (with M.P.L.), as well as liver disease modelling (with K.S., M.P.L., G.S., E.Y. and S.R.).

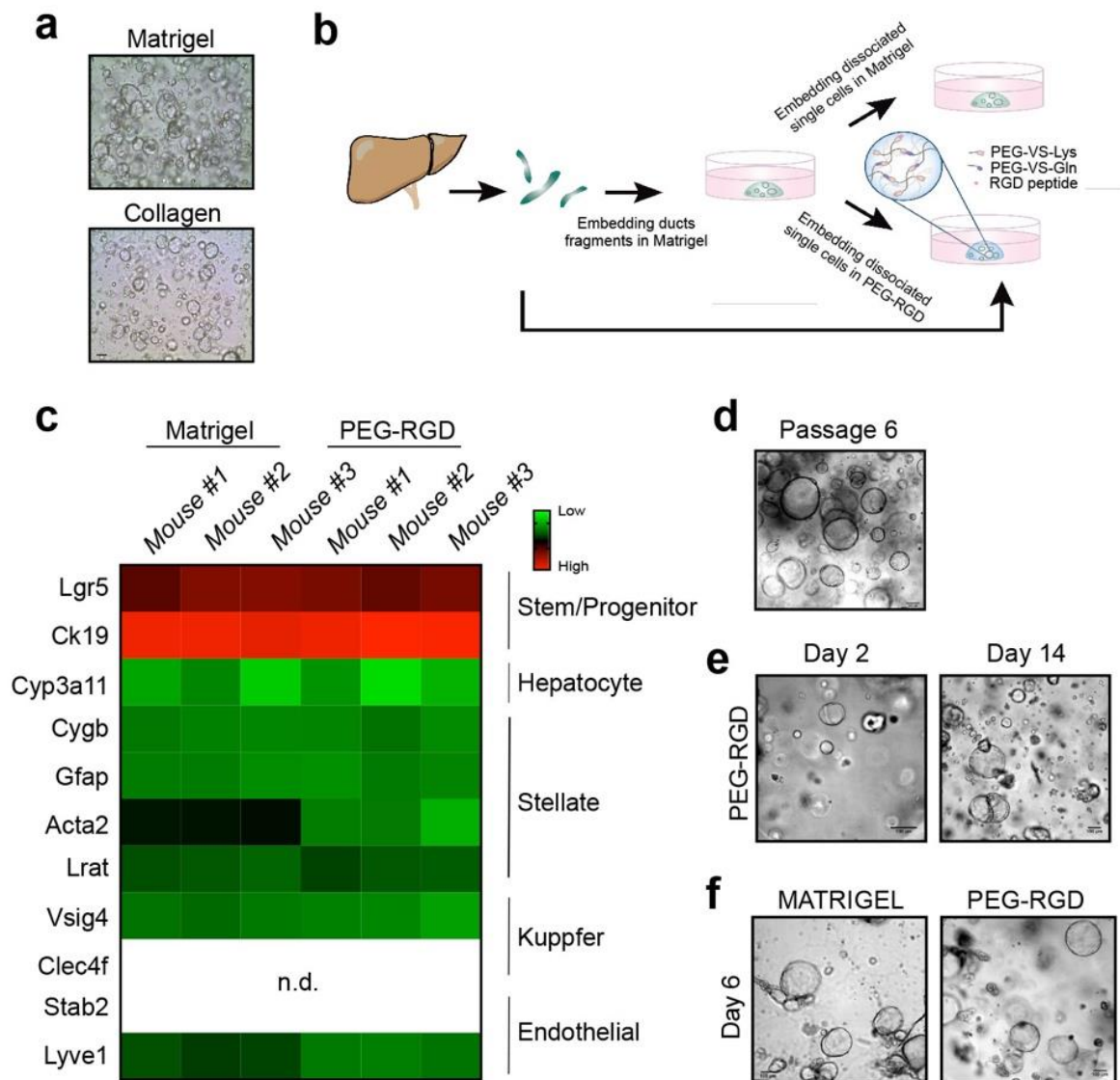
4.6 References

1. Michalopoulos, G. K. Liver regeneration. *J. Cell. Physiol.* **213**, 286-300 (2007).
2. Williams, R., Schalm, S. W. & O'Grady, J. G. Acute liver failure: redefining the syndromes. *Lancet.* **342**, 273–275 (1993).
3. Klein, A. S. *et al.* Organ donation and utilization in the United States, 1999-2008: Special feature. *Am J Transplant.* **10**, 973-986 (2010).
4. Huch, M. *et al.* In vitro expansion of single Lgr5+ liver stem cells induced by Wnt-driven regeneration. *Nature* **494**, 247–250 (2013).
5. Huch, M. *et al.* Long-term culture of genome-stable bipotent stem cells from adult human liver. *Cell* **160**, 299–312 (2015).
6. Evarts, R. P., Nagy, P., Marsden, E. & Thorgeirsson, S. S. A precursor-product relationship exists between oval cells and hepatocytes in rat liver. *Carcinogenesis.* **11**, 1737-1740 (1987).
7. Takebe, T. *et al.* Generation of a vascularized and functional human liver from an iPSC-derived organ bud transplant. *Nat. Protoc.* **9**, 396–409 (2014).
8. Peng, W. C. *et al.* Inflammatory Cytokine TNF α Promotes the Long-Term Expansion of Primary Hepatocytes in 3D Culture. *Cell* **175**, 1607–1619.e15 (2018).
9. Hu, H. *et al.* Long-Term Expansion of Functional Mouse and Human Hepatocytes as 3D Organoids. *Cell* **175**, 1591–1606.e19 (2018).
10. Schneeberger, K. *et al.* Converging biofabrication and organoid technologies: The next frontier in hepatic and intestinal tissue engineering? *Biofabrication.* **9**, 013001 (2017).
11. Broguiere, N. *et al.* Growth of Epithelial Organoids in a Defined Hydrogel. *Adv. Mater.* **30**, 1801621 (2018).
12. Gjorevski, N. *et al.* Designer matrices for intestinal stem cell and organoid culture. *Nature* **539**, 560–564 (2016).
13. Cruz-Acuña, R. *et al.* Synthetic hydrogels for human intestinal organoid generation and colonic wound repair. *Nat Cell Biol* **19**, 1326-1335 (2017).
14. Saheli, M. *et al.* Three-dimensional liver-derived extracellular matrix hydrogel promotes liver organoids function. *J. Cell. Biochem.* **119**, 4320-4333 (2018).
15. Ehrbar, M. *et al.* Biomolecular hydrogels formed and degraded via site-specific enzymatic reactions. *Biomacromolecules* **8**, 3000–3007 (2007).
16. Yin, M. *et al.* Quantitative assessment of hepatic fibrosis in an animal model with magnetic resonance elastography. *Magn. Reson. Med.* **58**, 346–353 (2007).
17. Kumar, P. *et al.* Periostin promotes liver fibrogenesis by activating lysyl oxidase in hepatic stellate cells. *J. Biol. Chem.* **293**, 12781-12792 (2018).
18. Arriazu, E. *et al.* Extracellular matrix and liver disease. *Antioxidants Redox Signal.* **21**, 1078–1097 (2014).
19. Ishikawa, T. *et al.* Hepatocyte growth factor/c-met signaling is required for stem-cell-mediated liver regeneration in mice. *Hepatology* **55**, 1215-1226 (2012).
20. Wang, B., Zhao, L., Fish, M., Logan, C. Y. & Nusse, R. Self-renewing diploid Axin2 + cells fuel homeostatic renewal of the liver. *Nature* **524**, 180-185 (2015).
21. Berg, T. *et al.* Fibroblast growth factor 10 is critical for liver growth during embryogenesis and controls hepatoblast survival via β -catenin activation. *Hepatology* **46**, 1187-1197 (2007).
22. Ingber, D. E. Mechanobiology and diseases of mechanotransduction. *Ann. Med.* **35**, 564–577 (2003).
23. Humphrey, J. D., Dufresne, E. R. & Schwartz, M. A. Mechanotransduction and extracellular matrix homeostasis. *Nat. Rev. Mol. Cell Biol.* **15**, 802-812 (2014).
24. Duscher, D. *et al.* Mechanotransduction and fibrosis. *J. Biomech.* **47**, 1997-2005 (2014).

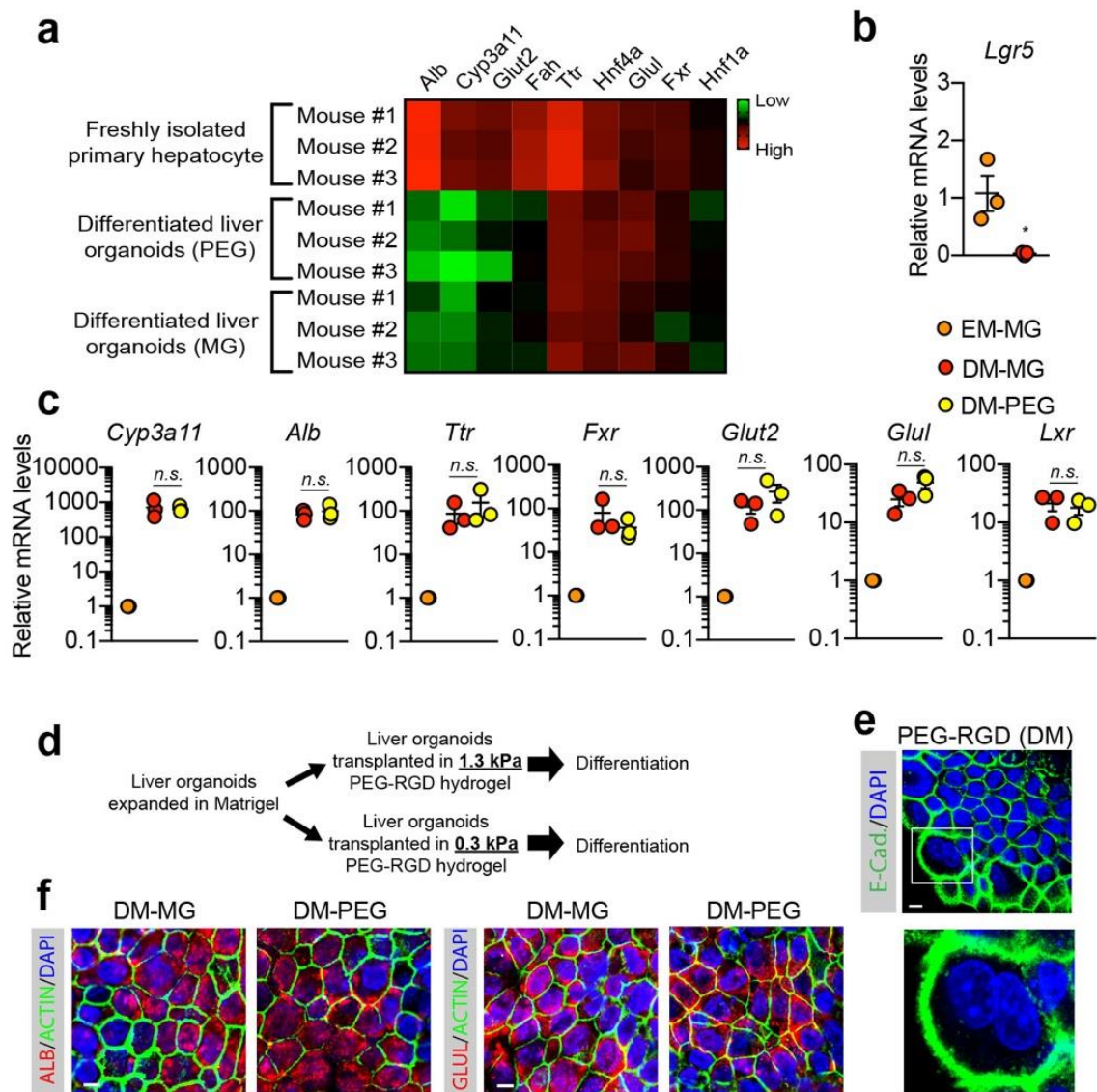
25. Halder, G., Dupont, S. & Piccolo, S. Transduction of mechanical and cytoskeletal cues by YAP and TAZ. *Nat. Rev. Mol. Cell Biol.* **13**, 591–600 (2012).
26. Liu-chittenden, Y. *et al.* Genetic and pharmacological disruption of the TEAD – YAP complex suppresses the oncogenic activity of YAP. *Genes. Dev.* **26** 1300–1305 (2012).
27. Dupont, S. *et al.* Role of YAP/TAZ in mechanotransduction. *Nature* **474**, 179–183 (2011).
28. Sorrentino, G. *et al.* Metabolic control of YAP and TAZ by the mevalonate pathway. *Nat. Cell Biol.* **16**, 357–66 (2014).
29. Sorrentino, G. *et al.* Glucocorticoid receptor signalling activates YAP in breast cancer. *Nat. Commun.* **8**, 14073 (2017).
30. Kovács, M., Tóth, J., Hetényi, C., Málnási-Csizmadia, A. & Seller, J. R. Mechanism of blebbistatin inhibition of myosin II. *J. Biol. Chem.* **279**, 35557–35563 (2004).
31. Taniguchi, K. *et al.* A gp130-Src-YAP module links inflammation to epithelial regeneration. *Nature* **519**, 5–62 (2015).
32. Calvo, F. *et al.* Mechanotransduction and YAP-dependent matrix remodelling is required for the generation and maintenance of cancer-associated fibroblasts. *Nat Cell Biol* **15**, 637–646 (2013).
33. Kim, N.-G. & Gumbiner, B. M. Adhesion to fibronectin regulates Hippo signaling via the FAK-Src-PI3K pathway. *J. Cell Biol.* **210**, 503–515 (2015).
34. Li, P. *et al.* α E-catenin inhibits a Src–YAP1 oncogenic module that couples tyrosine kinases and the effector of hippo signaling pathway. *Genes Dev.* **30**, 798–811 (2016).
35. Lamar, J. M. *et al.* The Hippo pathway target, YAP, promotes metastasis through its TEAD-interaction domain. *Proc. Natl. Acad. Sci. U. S. A.* **109**, 14732–14733 (2012).
36. Abu-Absi, S. F., Hu, W.-S. & Hansen, L. K. Dexamethasone effects on rat hepatocyte spheroid formation and function. *Tissue Eng.* **11**, 415–26 (2005).
37. Smoot, R. L. *et al.* Platelet-derived growth factor regulates YAP transcriptional activity via Src family kinase dependent tyrosine phosphorylation. *J. Cell. Biochem.* **119**, 824–836 (2018).
38. Sugihara, T. *et al.* YAP Tyrosine Phosphorylation and Nuclear Localization in Cholangiocarcinoma Cells is Regulated by LCK and Independent of LATS Activity. *Mol. Cancer Res.* **16**, 1556–1567 (2018).
39. Tamm, C., Bower, N. & Anneren, C. Regulation of mouse embryonic stem cell self-renewal by a Yes-YAP-TEAD2 signaling pathway downstream of LIF. *J. Cell Sci.* **124**, 1136–1144 (2011).
40. Araujo, J. & Logothetis, C. Dasatinib: A potent SRC inhibitor in clinical development for the treatment of solid tumors. *Cancer Treat Rev.* **36**, 492–500 (2010).
41. Tschumperlin, D. J., Ligresti, G., Hilscher, M. B. & Shah, V. H. Mechanosensing and fibrosis. *J Clin Invest* **128**, 74–88 (2018).
42. Mueller, S. & Sandrin, L. Liver stiffness: a novel parameter for the diagnosis of liver disease. *Hepat. Med.* **2**, 49–67 (2010).
43. Herrera, J., Henke, C. A. & Bitterman, P. B. Extracellular matrix as a driver of progressive fibrosis. *J Clin Invest* **128**, 45–53 (2018).
44. Liu, F. *et al.* Mechanosignaling through YAP and TAZ drives fibroblast activation and fibrosis. *Am. J. Physiol. Lung. Cell. Mol. Physiol.* **308**, L344–L357 (2015).
45. Liu, L. *et al.* Mechanotransduction-modulated fibrotic microniches reveal the contribution of angiogenesis in liver fibrosis. *Nat. Mater.* **16**, 1252–1261 (2017).
46. Degos, F. *et al.* Diagnostic accuracy of FibroScan and comparison to liver fibrosis biomarkers in chronic viral hepatitis: A multicenter prospective study (the FIBROSTIC study). *J. Hepatol.* **53**, 1013–1021 (2010).
47. Haage, A. & Schneider, I. C. Cellular contractility and extracellular matrix stiffness regulate matrix metalloproteinase activity in pancreatic cancer cells. *FASEB J.* **28**, 3589–3599 (2014).

48. Xie, J. *et al.* Substrate stiffness-regulated matrix metalloproteinase output in myocardial cells and cardiac fibroblasts: Implications for myocardial fibrosis. *Acta Biomater.* **10**, 2463-2472 (2014).
49. Peeters, S. A. *et al.* Circulating matrix metalloproteinases are associated with arterial stiffness in patients with type 1 diabetes: Pooled analysis of three cohort studies. *Cardiovasc. Diabetol.* **16**, 139 (2017).
50. Nuciforo, S. *et al.* Organoid Models of Human Liver Cancers Derived from Tumor Needle Biopsies. *Cell Rep.* **24**, 1363–1376 (2018).
51. Gjorevski, N. & Lutolf, M. P. Synthesis and characterization of well-defined hydrogel matrices and their application to intestinal stem cell and organoid culture. *Nat. Protoc.* **12**, 2263–2274 (2017).
52. Sebastiani, G. *et al.* Regulatory T-cells from pancreatic lymphnodes of patients with type-1 diabetes express increased levels of microRNA MIR-125a-5p that limits CCR2 expression. *Sci. Rep.* **7**, 6897 (2017) .

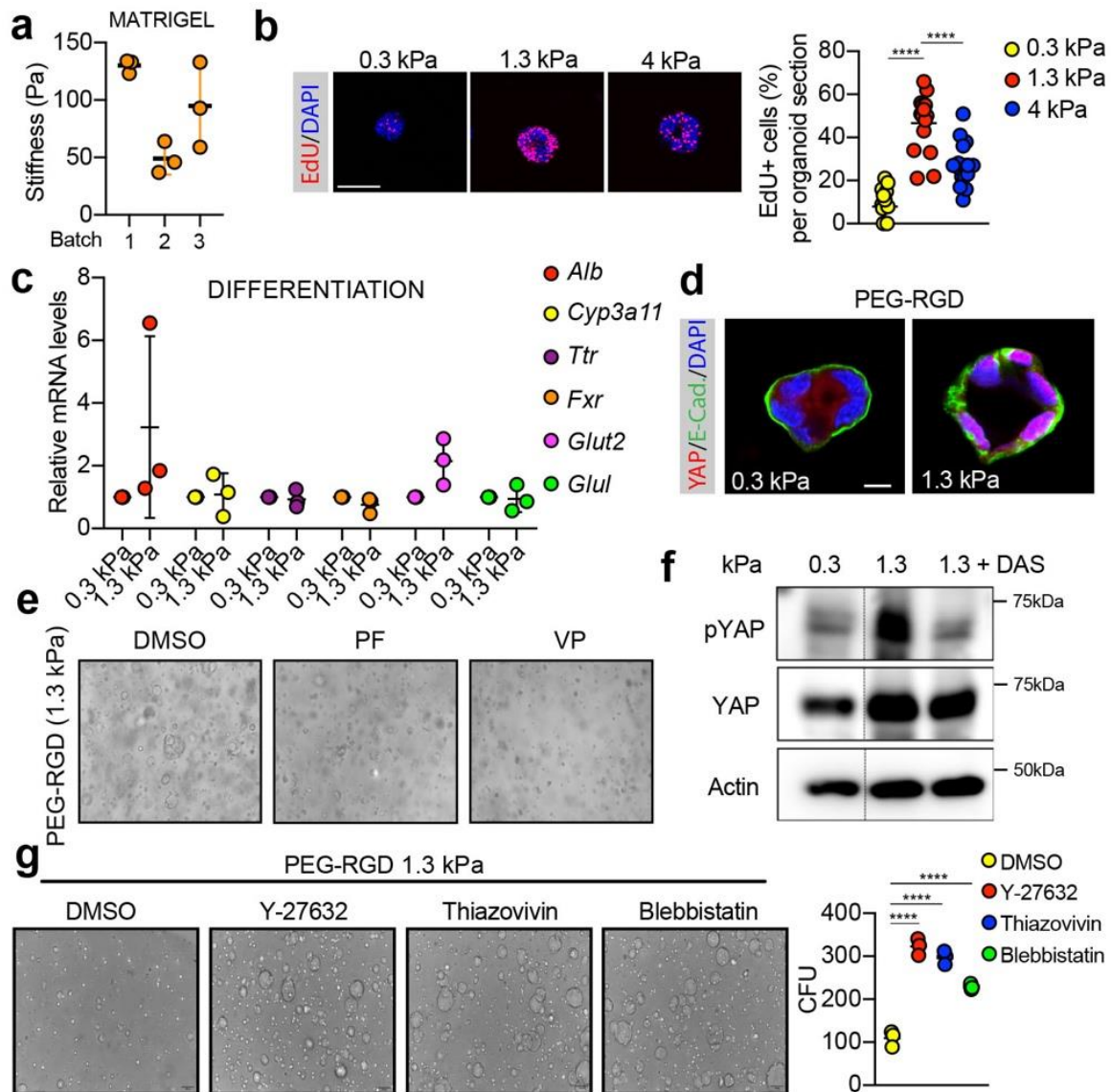
4.7 Supplementary information



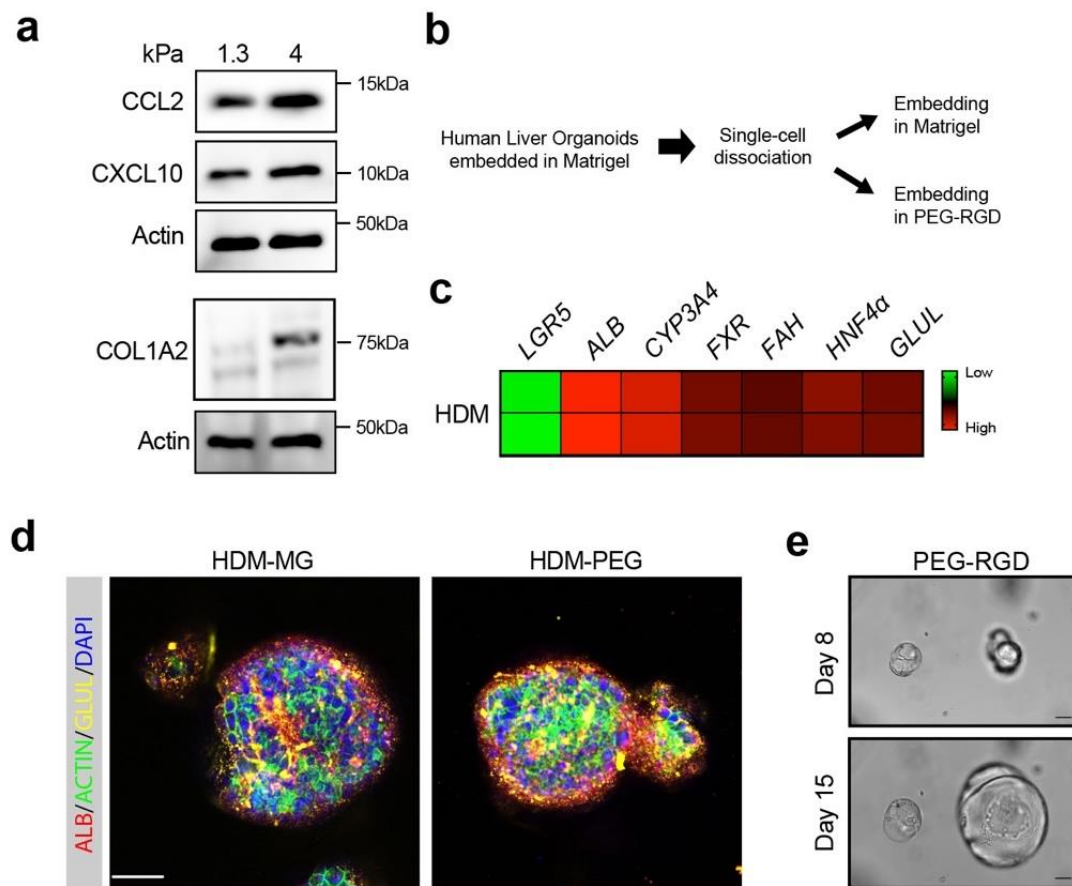
Supplementary Figure 1. Liver organoid growth in Matrigel and PEG | **(a)** Representative picture of mouse liver progenitor cells 6 days after embedding in 10 μ L droplet of Matrigel or Type I Collagen. Scalebar: 100 μ m. **(b)** Schematic of the protocol for generating mouse liver organoid cell lines in Matrigel or, directly, in PEG-RGD hydrogels. **(c)** mRNA levels of markers of different cell types were analysed by qRT-PCR in liver organoids maintained in expansion medium. The heatmap represents Δ Ct values as described in the method section. **(d)** Representative picture of liver organoids embedded in PEG-RGD at the indicated passage. **(e)** Representative picture of liver organoids embedded in PEG-RGD for the indicated times. **(f)** PEG-RGD hydrogel provides a stable matrix for long term culture of hepatic organoids, while Matrigel already softened after 6 days of culture. Scale bars: 100 μ m. Source data are provided as a Source Data file.



Supplementary Figure 2. Differentiation of liver organoids into hepatocyte-like cells | (a) mRNA levels of markers of hepatocyte were analysed by qRT-PCR in freshly isolated hepatocytes or in liver organoids embedded in PEG-RGD (PEG) or matrigel (MG) and maintained in differentiation medium. The heatmap represents Δ Ct values as described in the method section. **(b)** *Lgr5* mRNA levels were analysed by qRT-PCR in liver organoids maintained in differentiation medium (DM). Graph show individual data points derived from $n=3$ independent experiments and means \pm SEM. **(c)** Gene expression was analysed by qRT-PCR in liver organoids derived in Matrigel (MG) or in PEG-RGD (PEG) and maintained in expansion medium (EM) or differentiation medium (DM). Graphs show individual data points derived from $n=3$ independent experiments and means \pm SEM. n.s. (not significant). * $P<0.05$, unpaired Student's two-tailed t-test. **(d)** Liver organoids grown in physiologically-stiff hydrogels were transplanted in soft hydrogels immediately before inducing the differentiation. **(e)** Liver organoids maintained in DM in PEG-RGD hydrogels. E-cadherin was used to visualize cell borders. The square indicates a bi-nucleated cell. Scale bar 10 μ m. **(f)** Representative confocal immunofluorescence images of Albumin (ALB) or Glutamine synthase (GLUL) and Phalloidin (ACTIN). Organoids were derived and maintained as in Supplementary Figure 2c. Scale bar 10 μ m. Source data are provided as a Source Data file.



Supplementary Figure 3. Effect of PEG stiffness on liver organoids | **(a)** Stiffness measurements of three different Matrigel batches. **(b)** Representative images of EdU staining of liver organoids, 3 days after embedding in PEG-RGD hydrogels with indicated stiffness. Scale bar: 100 μ m. **(c)** Gene expression was analysed by qRT-PCR in liver organoids embedded in soft (0.3 kPa) or physiologically-stiff (1.3 kPa) PEG-RGD hydrogels and maintained in DM. Data are shown as relative to the expression in physiologically-stiff hydrogels. **(d)** Representative images of YAP subcellular localization in liver organoids 1 day after embedding in soft (0.3 kPa) or physiologically-stiff (1.3 kPa) PEG-RGD hydrogels. **(e)** Representative images relative to Fig. 3e. **(f)** Western blot showing YAP phosphorylation in mouse liver progenitor cells 6 hours after embedding in soft (0.3 kPa) and physiologically-stiff (1.3 kPa) PEG-RGD hydrogels. **(g)** Matrigel-derived liver progenitor cells were embedded in physiologically-stiff PEG-RGD hydrogels and cultured in expansion medium containing ROCK inhibitors (Y-27632 and Thiazovivin) or Blebbistatin. Colony forming units (CFU) were quantified after 3 days. Graphs show individual data points and means \pm SEM. **** P <0.0001 two way Anova. Source data are provided as a Source Data file.



Supplementary Figure 4. Human liver organoids in PEG hydrogels | **(a)** Western blot of mouse liver progenitor cells 6 days after embedding in PEG-RGD hydrogels with indicated stiffness. **(b)** Schematic representation of the protocol. **(c)** Gene expression was analysed by qRT-PCR in human liver organoids embedded in PEG-RGD hydrogels and maintained in human differentiation medium. The heatmap represents ΔC_t values as described in the method section and shows results from two biological replicates. **(d)** Representative confocal immunofluorescence image of Albumin and GLUL in human liver organoids cultured in human differentiation medium (HDM). **(e)** Human liver organoids were frozen-thawed and monitored in time. Days post-thawing are indicated. Scale bar: 100 μ m. Source data are provided as a Source Data file.

Supplementary Table 1. Primers used for qRT-PCR analysis.

Gene	Species	Forward	Reverse
<i>Cyr61</i>	Mouse	CTGCGCTAAACAACTCAACGA	GCAGATCCCTTTCAGAGCGG
<i>Ctgf</i>	Mouse	GCTTGCGGATTTTAGGTGTC	CAGACTGGAGAAGCAGAGCC
<i>Cyp3a11</i>	Mouse	TGGTCAAACGCCTCTCCTTGCTG	ACTGGGCCAAAATCCCGCCG
<i>Alb</i>	Mouse	GCGCAGATGACAGGGCGGAA	GTGCCGTAGCATGCGGGAGG
<i>Ttr</i>	Mouse	ATGGTCAAAGTCCTGGATGC	AATTCATGGAACGGGGAAAT
<i>Fxr</i>	Mouse	ACAGCTAATGAGGACGACAG	GATTTCTGAGGCATTCTCTG
<i>Glut-2</i>	Mouse	GACCGTGGTGAACCTGCTAT	TGCGGGAATCATAGTCCTTC
<i>Glul</i>	Mouse	CAAGTGTGTGGAAGAGTTACCTGAGT	TGGCAACAGGATGGAGGTACA
<i>Lxr</i>	Mouse	TGCCATCAGCATCTTCTCTG	GGCTCACCAGCTTCATTAGC
<i>Lgr5</i>	Mouse	ATTCGGTGCATTTAGCTTGG	CGAACACCTGCGTGAATATG
<i>Gapdh</i>	Mouse	GGAGAGTGTTTCCTCGTCCC	ACTGTGCCGTTGAATTTGCC
LGR5	Human	GACTTTAACTGGAGCACAGA	AGCTTTATTAGGGATGGCAA
ALB	Human	CTGCCTGCCTGTTGCCAAAGC	GGCAAGGTCCGCCCTGTCATC
CYP3A4	Human	TGTGCCTGAGAACACCAGAG	GTGGTGGAATAGTCCCGTG
FXR	Human	ACAGCTGCGACAGATTGGTT	TCAGAGGGGTTAGACAGCTCA
HNF4A	Human	CGTGCTGCTCCTAGGCAATGAC	ACGGACCTCCCAGCAGCATCT
GLUL	Human	GCTGGTGTAGCCAATCGTAGC	GGCTTCTGTCAACGAAAAGG
GAPDH	Human	TACTAGCGGTTTTACGGGCG	TCGAACAGGAGGAGCAGAGAG
<i>Tnfa</i>	Mouse	GTAGCCACGTCGTAGCAAAC	AGTTGGTTGTCTTTGAGATCCATG
<i>Mmp3</i>	Mouse	GGAAATCAGTTCTGGGCTATACGA	TAGAAATGGCAGCATCGATCTTC
<i>Ccl2</i>	Mouse	AGGTCCCTGTCATGCTTCTG	GCTGCTGGTGATCCTCTTGT
<i>Col1a2</i>	Mouse	AAGGAGTTTCATCTGGCCCT	AGCAGGTCCTTGGAACCTT
<i>Mmp2</i>	Mouse	AACTACGATGATGACCGGAAGTG	TGGCATGGCCGAACCTCA
<i>Tgfb1</i>	Mouse	GAATGACGGTGCGCAACTCT	CAGCCCCAATAACCGTATGAA
<i>Cxcl1</i>	Mouse	TCTCCGTTACTTGGGGACAC	CCACACTCAAGAATGGTCGC
<i>Mmp13</i>	Mouse	ACAAAGATTATCCCCGCCTCATA	CACAATGCGATTACTCCAGATAC TG
<i>Cxcl10</i>	Mouse	CCACGTGTTGAGATCATTGCC	GAGGCTCTCTGCTGTCCATC
<i>Cygb</i>	Mouse	GCTGTATGCCAACTGCGAG	CCTCCATGTGTCTAAACTGGC
<i>Gfap</i>	Mouse	TCGAGATCGCCACCTACAG	GTCTGTACAGGAATGGTGATGC
<i>Acta2</i>	Mouse	GTCCCAGACATCAGGGAGTAA	TCGGATACTTCAGCGTCAGGA
<i>Lrat</i>	Mouse	TACACAGGCCTGGCATCATA	TCCACAAGCAGAATGGGATA
<i>Clec4f</i>	Mouse	ACTGAAGTACCAAATGGACAATGTTA GT	GTCAGCATTACATCCTCCAGA
<i>Vsig4</i>	Mouse	TCACCTATGGCCACCCCACC	AGGCGGCCTCTGTACTTTGCCT
<i>Stab2</i>	Mouse	TGTCCAGACGGCTACATCAA	CCAGGGATATCCAGGACGTA
<i>Lyve1</i>	Mouse	CCTCCAGCCAAAAGTTCAAA	TCCAACACGGGGTAAATGT

Supplementary Table 2. Patient clinical information.

Sex	Age	Diagnosis	Cirrhosis
Male	58	ASH, alcoholic steatohepatitis	YES
Female	36	AFLD, alcoholic fatty liver disease	NO
Male	43	NAFLD, nonalcoholic fatty liver disease	NO
Female	45	NASH, nonalcoholic steatohepatitis	NO
Male	35	NASH, nonalcoholic steatohepatitis	NO
Female	73	Normal	NO
Male	64	ASH/NASH	NO
Male	37	DILI, drug induced liver injury	NO

Chapter 5

Mechanically-controlled cultures of human ductal organoids unveil the role of tissue stiffness in ductular reaction

Saba Rezakhani^{1,2}, Matthias P. Lutolf^{1,2*}

¹Laboratory of Stem Cell Bioengineering, Institute of Bioengineering, School of Life Sciences, Ecole Polytechnique Fédérale de Lausanne (EPFL), 1015 Lausanne, Switzerland.

²Institute of Chemical Sciences and Engineering, School of Basic Sciences, EPFL, 1015 Lausanne, Switzerland.

*E-mail: matthias.lutolf@epfl.ch

(Manuscript in preparation)

5.1 Abstract

Despite the liver's remarkable regenerative capacity, severe injuries can still impair its function. During acute injury, hepatocyte regeneration predominates, while chronic and severe injury lead to emergence of ductular reaction (DR), characterized by the proliferation of reactive bile ducts. A hallmark of all chronic liver injuries is liver fibrosis, in which tissue stiffness increases as a direct effect of aberrant extracellular matrix (ECM) deposition. While the presence of DR during liver fibrosis has been demonstrated, the extent to which DR participates in the regeneration process and the role of the fibrotic environment in this phenomenon is poorly understood. Here we used liver ductal organoids as an *in vitro* model of DR to study the effect of the fibrotic mechanical environment, a feature usually neglected in fibrosis models, on DR. We cultured mouse and human liver ductal organoids in synthetic hydrogels with stiffness values matching those of the fibrotic tissues *in vivo*. Organoids showed reduced proliferation capacity compared to those cultured in matrices of physiological stiffness. Transcriptomic analyses indicated the enrichment of pathways and gene sets associated with inflammatory response, cell-cycle, and metabolism. Furthermore, to validate our assay, a selection of anti-fibrotic drugs was tested for their effect on mouse and human liver organoid formation efficiency. Overall, our results indicate that mechanically-controlled culture of human ductal organoids provides a valuable platform to further understand the important role of mechanics on DR during fibrosis. Identifying molecular mechanisms through which cell-matrix interactions regulate ductular liver regeneration may facilitate strategies to improve this process and develop novel regenerative and antifibrotic therapies.

5.2 Introduction

The liver has a remarkable regenerative potential. Yet, chronic inflammation and scarring can severely impair liver regeneration. In chronic liver injuries, repetitive hepatocyte damage or cell death induces a response involving clearance of the dead hepatocytes by macrophages, stabilization of the hepatic architecture through extracellular matrix (ECM) production by hepatic stellate cells (HSCs) in the perisinusoidal space of the Disse and portal tracts¹, and the emergence of ductular reaction (DR)². DR refers to the proliferation of small cells near the ductal tree and is believed to represent activation of hepatic progenitor cells leading to liver regeneration. Such a regenerative mechanism is compromised in case of severe injuries like liver fibrosis.

Liver fibrosis, characterized by an accumulation of excessive extracellular matrix (ECM) following liver injury, is a major cause of mortality and morbidity worldwide^{3,4}. As a direct effect of aberrant ECM deposition in the fibrotic liver, tissue stiffness increases over time and severely compromises its function⁵.

Due to the complexity of this disease, which involves several cell types and signaling pathways, the development of therapies has been challenging. The main reason for such an unmet clinical need is the lack of reliable and reproducible *in vitro* and *in vivo* models recapitulating the pathophysiology of liver fibrosis. *In vivo* fibrosis models rely mainly on chemical insults to trigger either hepatocyte (CCl₄) or cholangiocyte (bile duct ligation) apoptosis and necrosis, which does not faithfully reflect the natural occurrence of fibrogenesis⁶. Indeed, therapies that have proved potentially effective in animal fibrosis models have failed in clinical trials, highlighting the disparity between animal models and human relevance. Substantial efforts have thus been made, in past years, towards the development of human fibrosis-mimicking bioengineered models, advancing from 2D monocultures/cocultures to 3D spheroids and patient-derived organoids⁷.

The most commonly used 2D models of liver fibrosis are rodent-derived HSC monolayers, in which HSCs spontaneously activate within 10 days of culture on plastic culture dishes¹. Yet, culture-activated HSCs were shown to have a different gene expression profile compared to HSCs activated *in vivo*, indicating that these 2D cell cultures do not recapitulate the pathophysiology of tissue fibrosis⁸. The simplest 3D models are instead based on the aggregation of cells in suspension or in a microwell or hanging drop system¹. Several groups have developed liver spheroid models composed of primary human hepatocytes and nonparenchymal cells⁹, or HepaRG hepatocytes and HSCs¹⁰. Spheroids provide an easy model with relatively high-throughput; however, the lack of a 3D matrix, short period of culture, and difficulty to genetic modification limit their clinical application.

Generally, current 2D and 3D *in vitro* models rely on HSCs and hepatocytes, and the important role of ductular reaction in fibrosis^{11–14} is neglected. Recent breakthroughs have enabled the culture of self-organizing 3D structures, called organoids¹⁵. Liver organoids can be generated *in vitro* within animal-derived matrices (e.g. Matrigel) from mouse and human bile duct-derived bipotential facultative progenitor cells^{16,17}. Ductal organoids mimic liver ductular reaction and are thus a good *in vitro* model to study the role of DR¹⁸ and its association with fibrosis. Yet, current organoid culture relies on animal-derived and non-mechanically tunable matrices such as Matrigel, so that the

effect of matrix stiffness as the overarching aspect of fibrosis cannot be studied. Due to the limited tools available, the role of matrix mechanics on DR and its contribution to tissue repair has not yet been investigated.

To address this shortcoming, we report modeling the mechanical aspects of early-stage liver fibrosis and its effect on DR by culturing human liver ductal organoids in synthetic matrices with stiffness mimicking that of an early-stage fibrotic liver. We showed successful derivation of human liver ductal organoids from patient biopsies, in previously developed Low-Defect Thiol-Michael Addition (LDTM) hydrogels¹⁹. Next, we demonstrated how aberrant matrix mechanics impair liver progenitor proliferation and induce a transcriptional program different from that found at physiological stiffness.

5.3 Results and discussion

Culture of mouse and human liver ductal organoids in LDTM gels

We previously developed LDTM hydrogels for mouse and human intestinal stem cell culture and organoid derivation¹⁹. These matrices do not depend on the use of transglutaminase FXIIIa, which is expensive and thus difficult to translate to the clinic. We thus sought to extend the application of these chemically defined, less expensive matrices with minimal batch-to-batch variability, to liver ductal organoid culture.

To test whether mouse liver organoids can be established in these matrices without any initial Matrigel culture step, biliary duct fragments were isolated from mouse liver and directly embedded in LDTM hydrogels with stiffness mimicking that of the physiological values (~ 1 kPa)²⁰. After 6 days of culture, we observed the formation of cystic organoids that could be serially passaged in culture (**Figure 1A**).

As the next step, we tested whether we could similarly establish organoids from human patients without resorting to animal-derived matrices. To this aim, we embedded a freshly isolated patient liver biopsy in LDTM hydrogels. Strikingly, after 5 days of culture, cystic organoids expressing progenitor KRT19 marker originated from the digested biopsy tissue (**Figure 1 B,C**). Human liver ductal organoids were more heterogeneous in terms of size compared to mouse organoids and could be serially passaged (**Figure 1D**).

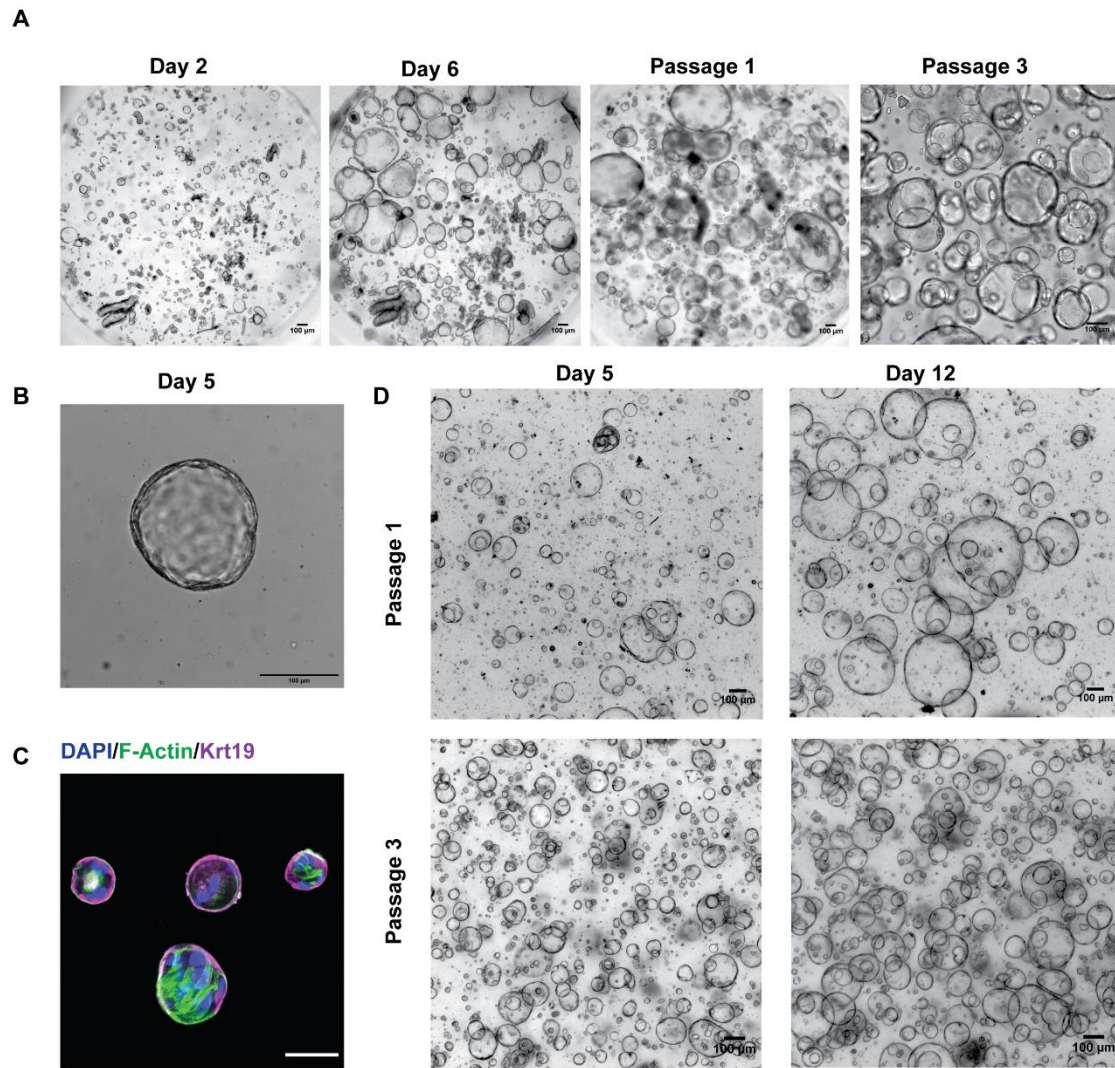


Figure 1- LDTM hydrogels support mouse and human liver ductal organoid culture in absence of any animal-derived component. **A)** Mouse ductal fragments formed cystic ductal organoids 6 days after embedding in LDTM hydrogels and could be serially passaged. **B)** Freshly isolated biopsy from a patient was directly embedded in LDTM hydrogel. **C)** Human ductal liver organoids contain progenitor marker, KRT19. **D)** Human ductal organoids can be serially passaged in LDTM hydrogels. Scale bars: 100 μm.

Effect of matrix stiffness on human ductal liver organoids

Mechanics have been shown to play an integral role in controlling stem cell behavior and tissue homeostasis, and also contribute to the manifestation of diseases^{21,22}. Mechanically-tunable matrices allow to mimick the mechanical properties of fibrotic liver and to assess the biological effects of this pathological environment on DR, an aspect that has not yet been investigated in human models.

We have previously demonstrated that aberrant ECM stiffness negatively impacts liver ductal organoid growth²³. To understand the effect of matrix stiffness on DR, we used organoid formation efficiency as a proxy of progenitor-mediated liver regeneration²⁴. To this aim, we embedded single

cells from dissociated Matrigel-grown liver organoids, in LDTM gels of 1 kPa, and 6 kPa, corresponding respectively to normal and fibrotic liver stiffnesses²⁵. Indeed, and similarly to the effect of matrix stiffness on mouse liver organoid formation, human counterparts also displayed lower organoid formation capacity in the stiffer matrix (**Figure 2 A, B**).

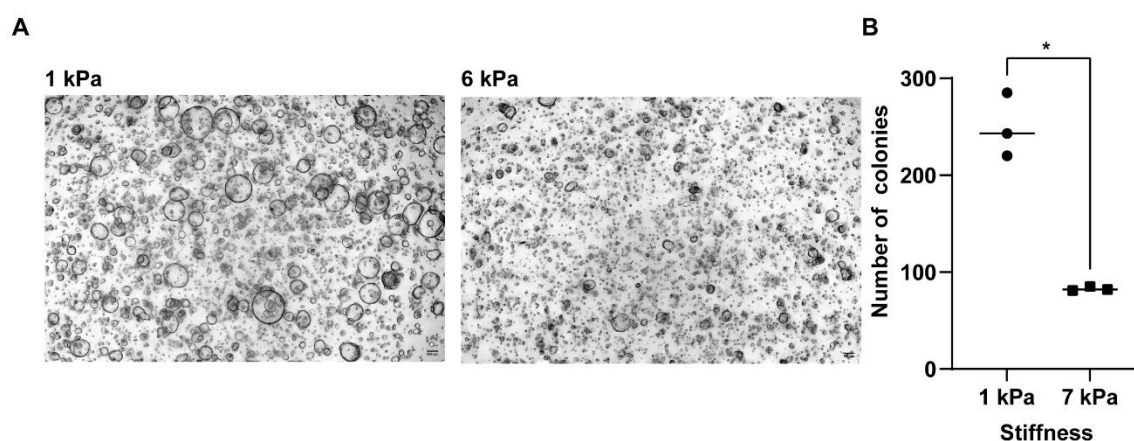


Figure 2. Effect of matrix stiffness on human liver organoid formation. **A)** Single cells derived from human liver ductal organoids previously generated in Matrigel were embedded in LDTM hydrogels of two different stiffness. **B)** Organoid formation efficiency as a function of matrix stiffness. * $P < 0.01$. Scale bars 100 μm .

To shed light on the mechanisms explaining the effect of matrix stiffness on ductal organoid proliferation, we adopted an unbiased approach and performed bulk RNA seq on organoids derived from a patient biopsy in LDTM hydrogels with physiological stiffness and with fibrosis-mimicking stiffness.

Differential expression analyses revealed 965 genes showing an absolute fold change ≥ 1.5 (72 of which with $\text{FDR} < 0.05$) between both stiffness conditions (**Figure 3A**). 45 of the upregulated genes form a network (PPI enrichment p-value: $5.55\text{e-}16$) with clusters related to cell cycle, inflammation, and metabolism (**Supplementary Figure 1**).

Gene ontology (GO) analyses were used to identify the biological processes associated with differentially up and downregulated genes (**Supplementary Figure 2A, B**). Functional annotation of differentially up and downregulated genes revealed three different clusters associated with metabolism, inflammatory response, and cell cycle.

Gene Set Enrichment Analysis (GSEA) also revealed significant enrichment of inflammatory response gene sets (**Figure 3B**). Moreover, Figure 3C, D demonstrate that differentially upregulated genes are involved in pathways such as inflammatory response and bile secretion, while differentially downregulated genes are involved in cell cycle and Wnt signaling pathways (**Figure 3C,D**). These results indicate an impaired stemness and regenerative potential of cholangiocytes, and concomitant induction of a stress response. Our results are in agreement with a study recently published by Aguilar-Bravo, Rodrigo-Torres *et al*¹⁸ describing the expression of profibrogenic and proinflammatory mediators in DR.

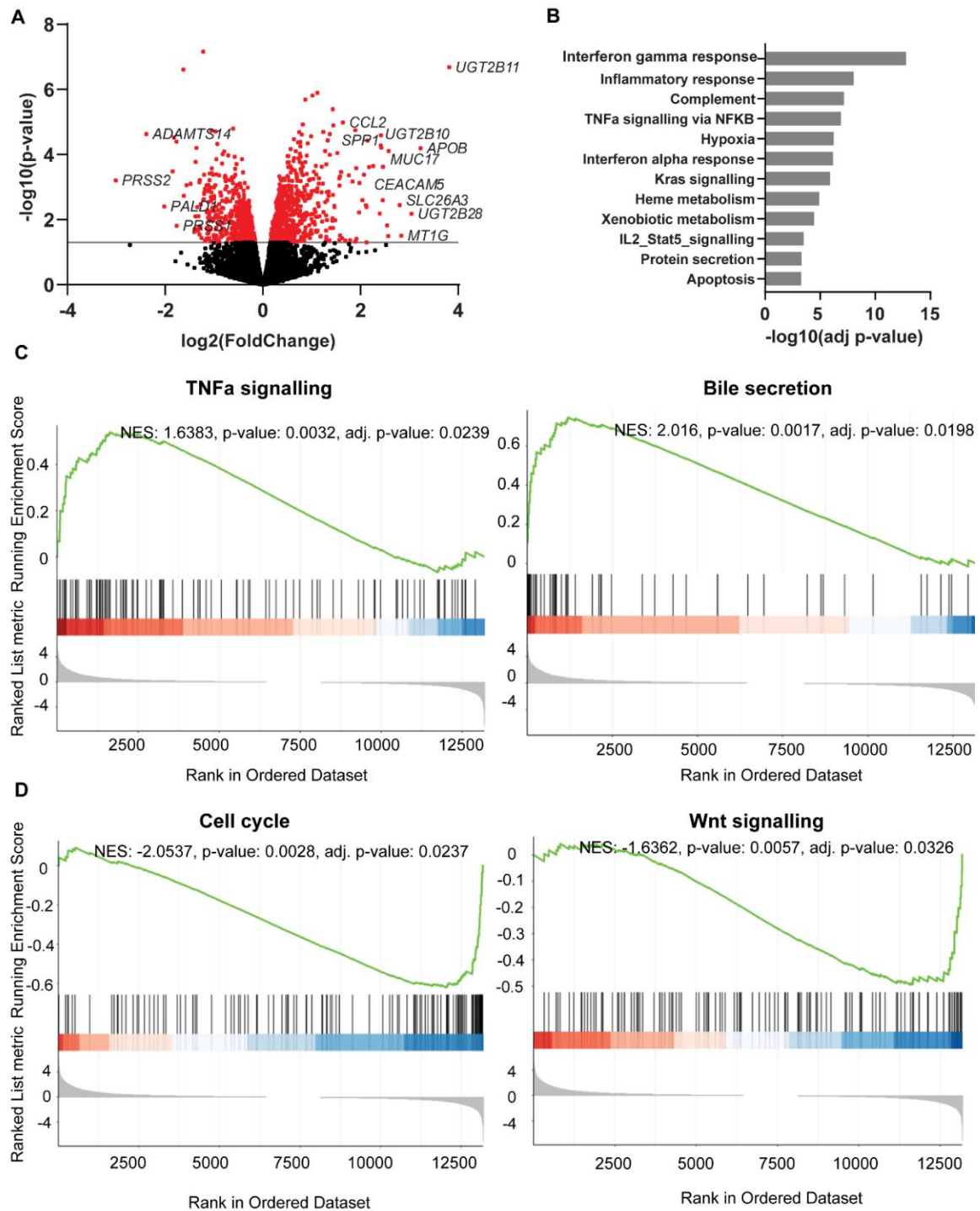


Figure 3. Effect of matrix stiffness on the transcriptome of human ductal organoids. **A)** Volcano plot illustrating genes that are differentially expressed in fibrosis-mimicking vs normal matrix. GSEA of hallmark gene sets (**B**) and pathways (**C,D**) enriched in organoids cultured in the stiff vs normal matrices.

Effect of fibrosis-targeted drugs on organoid-based model of ER

Next, we sought to test the effect on DR of a number of fibrosis-directed, commercially available drugs or small molecules, using organoid formation capacity in the fibrosis-mimicking hydrogels as a proxy of progenitor-mediated regeneration. Some of these drug candidates are currently being tested in clinical trials (Tropifexor²⁶, Aramchol²⁷). Some have shown poor interim results for the last stages of clinical trials (Elafibranor^{28,29}) or were terminated due to the lack of efficacy in treating fibrosis in humans (Selonsertib³⁰, Emricasan³¹). Moreover, since we have shown that Blebbistatin-treated liver progenitor cells have higher organoid formation capacity²³, we included Blebbistatin in the screen as well.

Most of the drugs that show promising results in animal models fail during clinical trials³². To test whether our assay can represent the difference between mouse and human organoids, we first treated the mouse liver organoids (cultured in Matrigel or LDTM hydrogels, stiffness of 6 kPa) with a selection of small molecules. As shown in **Figure 4A** all the drug candidates reduced organoid formation efficiency in Matrigel, while Elafibranor, Aramchol, Olaparib, and Blebbistatin significantly improved the formation of mouse liver organoids in the LDTM hydrogel (**Figure 4B**). The positive effect of these drugs on organoid formation in LDTM hydrogels was completely masked when the organoids were cultured in Matrigel. This observation highlights the importance of modelling the physiological ECM for drug screening purposes.

To test the potential clinical relevance of our finding, we performed the same experiment with human liver organoids. We did not observe any significant effect of drugs and molecules on the organoid culture in Matrigel (**Figure 4C**). Interestingly, among the drugs that showed a positive effect on mouse liver organoid formation in stiff LDTM gels, only Aramchol showed a significant increase in organoid formation (**Figure 4D**). Altogether, these results indicate the relevance of human liver organoid culture in a physiologically-relevant matrix to study DR and to develop novel regenerative and antifibrotic therapies.

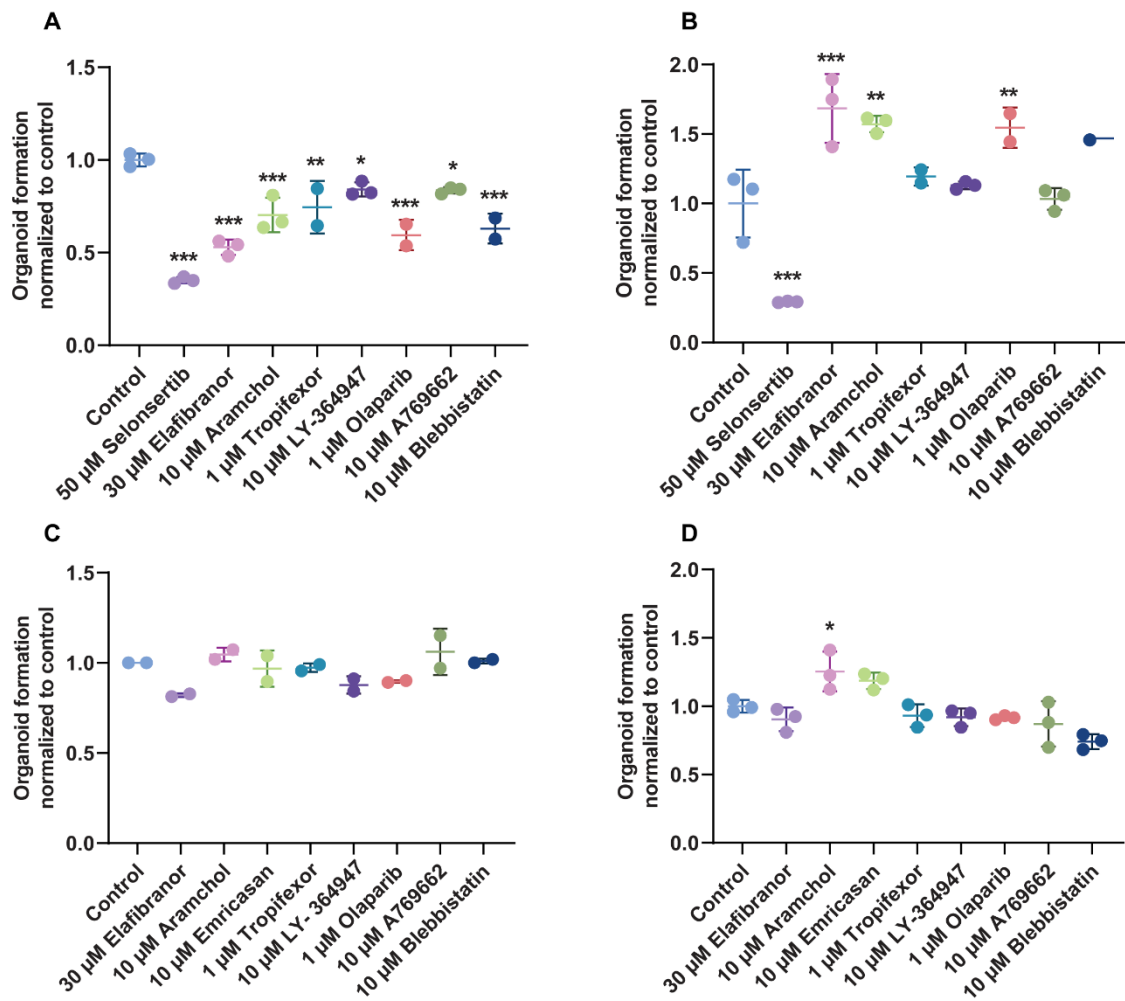


Figure 4. Effect of antifibrotic drugs on the mouse and human liver ductal organoid formation. Single cells derived from mouse (A,B) and human (C,D) liver ductal organoids previously generated in Matrigel were embedded in A,C) Matrigel and B,D) LDTHM hydrogels and treated with different antifibrotic drugs for 6 days.

5.4 Conclusion

Ductular reactions driven by both hepatic progenitor cell activation and non-parenchymal cell-mediated extracellular matrix remodeling are seen in response to acute severe and chronic liver injury¹². Even though organoids have enabled a more physiologically relevant modeling of disease³³, studies on the effect of the pathological microenvironment, such as the extracellular matrix stiffness, remain to be addressed. Here, we modeled the mechanical aspects of the fibrotic environment in organoid cultures derived from mouse and human primary tissues, representing the DR *in vitro*. We cultured mouse and human liver ductal organoids in synthetic Low-Defect Thiol-Michael Addition hydrogels with stiffness values matching those of the fibrotic tissues *in vivo*. Transcriptomic analysis of the human liver ductal organoids cultured in fibrosis-mimicking

matrices revealed enrichment of gene sets related to inflammation and cell cycle. Fibrosis-mimicking hydrogels led to an increase in the expression of proinflammatory genes such as CCL2, SPP1 (osteopontin) and matrix metalloproteases such as MMP10. Osteopontin (OPN) has also been reported to promote inflammatory response and enhance DR during CCl4-induced liver fibrosis³⁴. These findings are aligned with our previous observation that increased stiffness of synthetic hydrogel triggers a profibrotic response in the mouse liver ductal organoids²³. Altogether our results represent an important discovery on how tissue mechanics may contribute to orchestrating the liver immune response during DR and liver fibrosis

Next, we used this model as an *in vitro* platform to test the efficacy of a selection of commercially available fibrosis-related drug candidates in organoid formation efficiency, a phenomenon mimicking DR *in vivo* and whose contribution to liver regeneration is still poorly understood in human diseases. The results of the screening experiments highlighted the importance of mechanically-tunable matrices for mimicking liver physiological stiffness, as Matrigel masked the effect of some of the drugs. Additionally, we highlighted the importance of developing these assays on human organoids, as only one drug showed a positive effect on organoid formation in human liver organoids (Aramchol) compared to the four drugs that showed the same effect in mouse liver organoids

Overall, our results provide a platform to further understand the important role of mechanics on the ductular response in fibrosis. Identifying molecular mechanisms whereby cell-matrix interactions regulate ductular liver regeneration may allow novel strategies to enhance this process and develop novel regenerative and antifibrotic therapies.

5.5 Materials and methods

Synthesis of the hydrogel precursor

Vinylsulfone-functionalized 8-arm PEG (8-arm PEG-VS, molecular weight: 40 kDa) was purchased from NOF, and the bifunctional thiol-containing peptide Ac-GCRE-GPQGIWGQ-ERCG-NH₂ (SH-PEP-SH, molecular weight: 1773.97 g mol⁻¹) with matrix metalloproteinases (MMPs) sensitive sequence (in italics) was purchased from Biomatik. In order to synthesize the thiol-containing PEG macromer, both 8-arm PEG-VS and peptide were first dissolved in 0.3 M triethanolamine (TEA) buffer at pH 8.0. Following that, dissolved PEG macromer was added drop by drop to an excess of the dissolved peptide (with SH to VS functional group stoichiometric ratio of 10), to ensure that intermolecular crosslinking of peptide between functional groups of different PEG molecules is favoured over intramolecular crosslinking between functional groups of the same PEG molecule. The mix was left for 2 hours at room temperature under an inert atmosphere to react. Subsequently, the reaction solution was dialyzed by using Snake Skin with 10000 molecular weight cut-off, against ultrapure water (pH < 7.0) for 4 days at 4 °C, and the final product (PEG-PEP-SH) was lyophilized. The lyophilized product was dissolved in water to make a 10 % hydrogel precursor solution.

Low-Defect Thiol-Michael Addition (LDTM) hydrogel formation

LDTM hydrogels were formed by Michael type addition of octa-thiol containing precursor PEG-PEP-SH onto 8-arm PEG-VS. To make hydrogel networks of desired final PEG content, 10 % (w/v) 8-arm PEG-PEP-SH solution in water and 10 % (w/v) 8-arm PEG-VS solution in TEA were mixed at a stoichiometric ratio of VS to SH functional groups equal to 0.8. Apart from including the PEG precursors in appropriate concentrations (2.5 %, and 7 % (w/v)) to the LDTM gel mixture, dissociated cells, 0.3 M TEA buffer (10 % final concentration), RGD containing peptide (1 mM) were also incorporated, and the spare volume was filled with the base medium. Gels were cast on non-treated tissue culture or polydimethylsiloxane (PDMS)-coated plates and were left to crosslink in the incubator at 37 °C for 30 minutes. After crosslinking, the cell containing hydrogel drops were covered with mouse or liver organoid expansion medium.

Rheological measurements of swollen hydrogels

Shear modulus (G') of hydrogels was measured by performing small-strain oscillatory shear measurements on a Bohlin CVO 120 rheometer with plate-plate geometry. Briefly, 1–1.4 mm thick hydrogel discs were prepared and allowed to swell in water or cell culture medium for 24 h. The mechanical response of the hydrogels sandwiched between the parallel plates of the rheometer was recorded by performing frequency sweep (0.1–10 Hz) measurements in a constant strain (0.05) mode at room temperature.

Cell culture

Mouse and human liver organoids were established from mouse liver biliary duct fragments or patient liver biopsies as previously described²³. Briefly, liver tissues were digested in digestion solution (Collagenase type XI 0.012%, dispase 0.012%, FBS 1% in DMEM medium) for 2 h at 37.

When digestion was complete, bile ducts were pelleted by mild centrifugation (200 rpm for 5 min) and washed with PBS. Isolated ducts were then resuspended either in Type I Collagen (8–11 mg/ml prepared following manufacturer's instruction—from Corning), Matrigel (BD Bioscience) or PEG precursor solution and cast in 10 μ l droplets in the centre of the wells in a 48-well plate. After the gels were formed, 250 μ l of isolation medium was added to each well. Isolation medium was composed of AdDMEM/F-12 (Invitrogen) supplemented with B-27 and N-2 (both GIBCO), 1.25 μ M N-acetylcysteine (Sigma–Aldrich), 10 nM gastrin (Sigma–Aldrich) and the following growth factors: 50 ng ml⁻¹ EGF (Peprotech), 1 μ g ml⁻¹ Rspo1 (produced in-house), 100 ng ml⁻¹ Fgf10 (Peprotech), 10 mM nicotinamide (Sigma–Aldrich), 50 ng ml⁻¹ HGF (Peprotech), Noggin (100 ng ml⁻¹

produced in-house), Wnt 3a (1 μ g ml⁻¹, Peprotech) and Y-27632 (10 μ M, Sigma). After the first 4 days, isolation medium was changed with expansion medium (EM), which consists of isolation medium without Noggin, Wnt and Y-27632. One week after seeding, organoids were removed from the Matrigel or PEG hydrogel, dissociated into single cells using TrypLE express (Gibco), and transferred to fresh Matrigel or PEG hydrogels. Passaging was performed in 1:3 split ratio once per week. For drug screening tests, appropriate volumes of drugs dissolved in dimethyl sulfoxide (DMSO) were added to the expansion medium. The final concentrations of chosen drug candidates in the expansion medium are as below : Selonsertib 50 μ M, Elafibranor 30 μ M, Aramchol 10 μ M, Emricasan 10 μ M, Tropifexor 1 μ M, LY-364947 10 μ M, LY-364947 10 μ M, Olaparib 1 μ M, A769662 10 μ M and Blebbistatin 10 μ M.

Quantification of formed organoids

To identify the number of formed organoids in PEG hydrogels, z-stack images through the entire thickness of the Matrigel and PEG gel drops were acquired using Nikon Eclipse Ti2 microscope with 4x objective. To count the number of formed organoids, series of z-stack images were converted to an all-in-focus image by using Nikon's NIS-Elements software (EDF macro plugin). Finally, the Cell Counter plugin in ImageJ (NIH) was used to quantify the number of lumen-containing organoids within the 2000 μ m \times 2000 μ m specified surface of each image. Alternatively, the same all-in-focus images (2000 μ m \times 2000 μ m) were imported into Cellpose (pre-trained single-cell segmentation algorithm developed in Python) in which the diameter of the organoids were the only inputs and was approximated with the help of the GUI scale disk.

RNA-seq: library preparation, sequencing, data processing, statistical analysis, interpretation

RNA quality was controlled on the TapeStation 4200 (Agilent), confirming that all were of good quality (scores >8.9). Libraries for mRNA-seq were prepared according to the manufacturer's instructions with the TruSeq stranded mRNA kit (Illumina) starting from 500 ng RNA. Libraries, all bearing unique dual indexes, were subsequently loaded at 280 pM in a HiSeq 4000 instrument (Illumina) and sequenced according to manufacturer instructions, yielding paired-end reads of 93 nucleotides. Reads were trimmed of their adapters with bcl2fastq v2.20 (Illumina) and quality-controlled with fastQC v0.11.9. Reads were mapped to Human genome assembly hg38 (GRCh38, Gencode version 36, Ensembl 102), with STAR²⁷ (version 2.7.7a). Gene quantification was done

from uniquely mapped reads (STAR parameter `outFilterMultimapNmax` set to 1) with HTSeq count²⁸ (version 0.12.4, using the following options `-m intersection-nonempty` and `-t exon -r pos -s reverse`). RNA-metrics & Mark Duplicates were collected with Picard, version 2.22.4. Processing of the resulting counts was performed with R, version 4.0, and package EdgeR. Counts Per Million (CPM) were normalized using library sizes. Genes located on non-conventional chromosomes and expressed ($\text{cpm} < 1$) in less than 3 samples were excluded from the rest of the analysis. The Differential expression analysis of stiff vs. soft samples was done on the 14'165 remaining genes applying a Generalised Linear Model with Quasi-Likelihood Test (As Proposed By The GlmQLFit method).

Statistical analysis

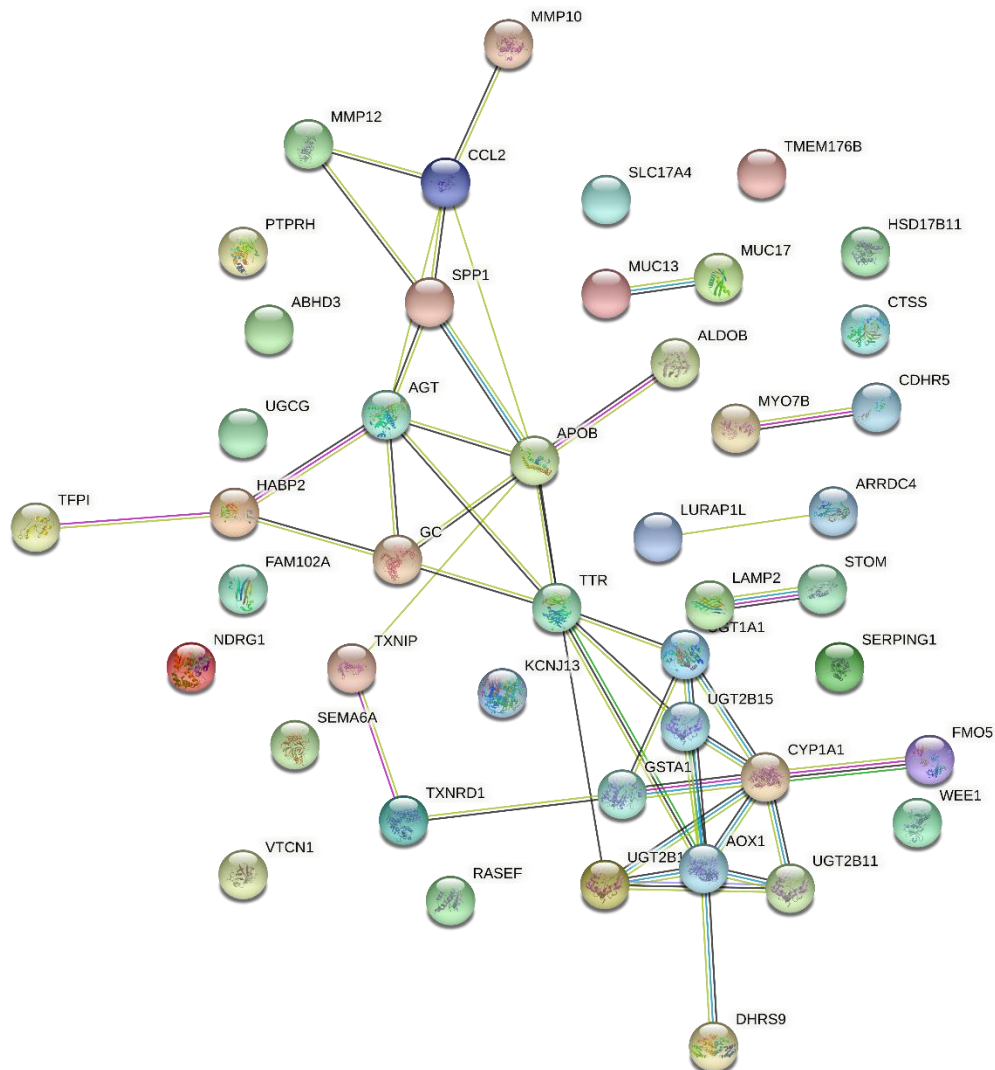
The drug screening test results were statistically analyzed by performing one-way ANOVA followed by a Dunnett's multiple comparisons test.

5.6 References

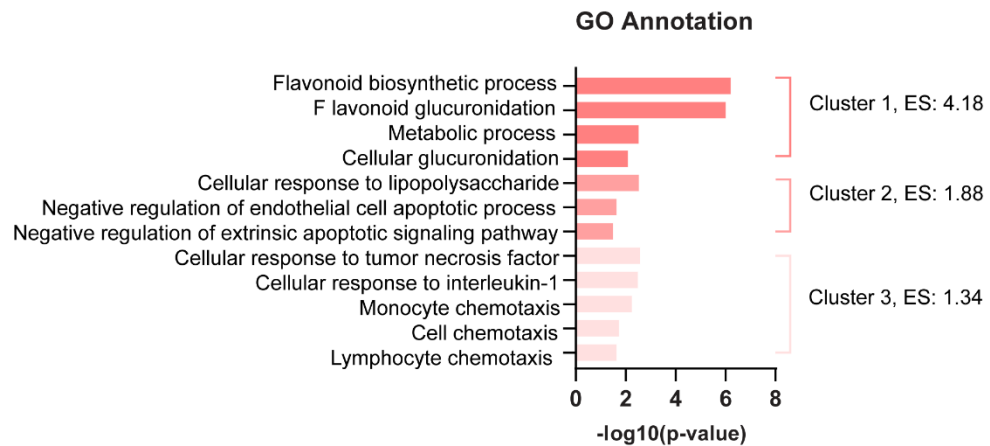
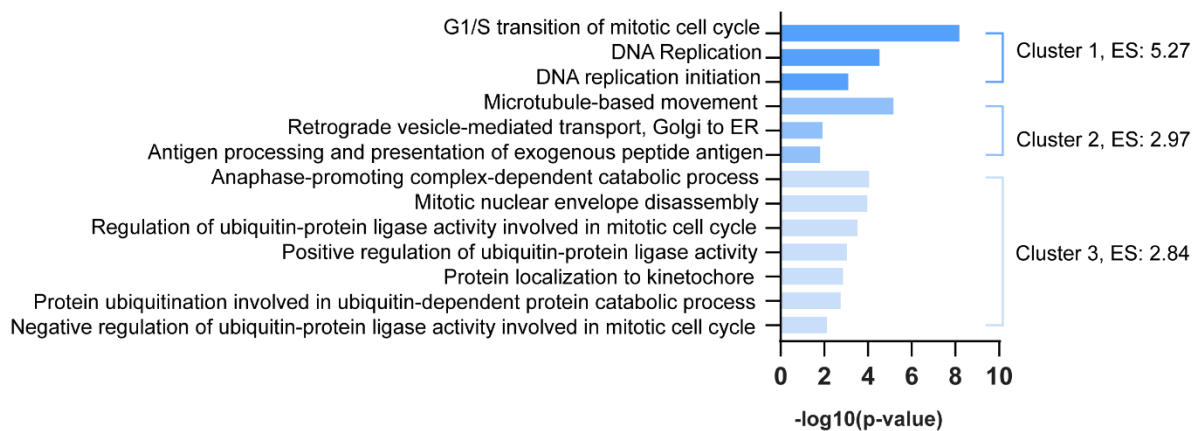
1. Grunsven LA Van. 3D in vitro models of liver fibrosis. 2017;121:133–146.
2. Raven A, Lu WY, Man TY, et al. Cholangiocytes act as facultative liver stem cells during impaired hepatocyte regeneration. *Nature* 2017;547:350–354.
3. Wynn TA, Ramalingam TR. review Mechanisms of fibrosis: therapeutic translation for fibrotic disease. *Nat Med* 2012;18.
4. Hernandez-Gea V, Friedman SL. Pathogenesis of liver fibrosis. *Annu Rev Pathol Mech Dis* 2011;6:425–456.
5. Herrera J, Henke CA, Bitterman PB. Extracellular matrix as a driver of progressive fibrosis. *J Clin Invest* 2018.
6. Nevzorova YA, Boyer-Diaz Z, Cubero FJ, et al. Animal models for liver disease – A practical approach for translational research. *J Hepatol* 2020;73:423–440.
7. Sacchi M, Bansal R. Bioengineered 3D Models to Recapitulate Tissue Fibrosis. *Trends Biotechnol* 2019;38:623–636.
8. Minicis S De, Seki E, Uchinami H, et al. Gene Expression Profiles During Hepatic Stellate Cell Activation in Culture and In Vivo. *Gastroenterology* 2007;132:1937–1946.
9. Bell CC, Hendriks DFG, Moro SML, et al. Characterization of primary human hepatocyte spheroids as a model system for drug-induced liver injury, liver function and disease. *Sci Rep* 2016;6:1–13.
10. Leite SB, Roosens T, Taghdouini A El, et al. Novel human hepatic organoid model enables testing of drug-induced liver fibrosis in vitro. *Biomaterials* 2016;78:1–10.
11. Sato K, Marzioni M, Meng F, et al. Ductular Reaction in Liver Diseases: Pathological Mechanisms and Translational Significances. *Hepatology* 2019;69:420–430.
12. Williams MJ, Clouston AD, Forbes SJ. Links between hepatic fibrosis, ductular reaction, and progenitor cell expansion. *Gastroenterology* 2014;146:349–356.
13. Clouston AD, Powell EE, Walsh MJ, et al. Fibrosis correlates with a ductular reaction in hepatitis C: Roles of impaired replication, progenitor cells and steatosis. *Hepatology* 2005;41:809–818.
14. Richardson MM, Jonsson JR, Powell EE, et al. Progressive Fibrosis in Nonalcoholic Steatohepatitis: Association With Altered Regeneration and a Ductular Reaction. *Gastroenterology* 2007;133:80–90.
15. Lancaster MA, Knoblich JA. Organogenesis in a dish: Modeling development and disease using organoid technologies. *Science* (80-) 2014;345.
16. Huch M, Bonfanti P, Boj SF, et al. Unlimited in vitro expansion of adult bi-potent pancreas progenitors through the Lgr5/R-spondin axis. *EMBO J* 2013;32:2708–2721.
17. Broutier L, Andersson-Rolf A, Hindley CJ, et al. Culture and establishment of self-renewing human and mouse adult liver and pancreas 3D organoids and their genetic manipulation. *Nat Protoc* 2016;11:1724–1743.
18. Aguilar-Bravo B, Rodrigo-Torres D, Ariño S, et al. Ductular Reaction Cells Display an Inflammatory Profile and Recruit Neutrophils in Alcoholic Hepatitis. *Hepatology* 2019;69:2180–2195.
19. Rezakhani S, Gjorevski N, Lutolf MP. Low-Defect Thiol-Michael Addition Hydrogels as Matrigel Substitutes for Epithelial Organoid Derivation. *Adv Funct Mater* 2020;30:1–12.
20. Yin M, Woollard J, Wang X, et al. Quantitative Assessment of Hepatic Fibrosis in an Animal Model With Magnetic Resonance Elastography. 2007;353:346–353.
21. Ingber DE. Mechanobiology and diseases of mechanotransduction. *Ann Med* 2003.
22. Humphrey JD, Dufresne ER, Schwartz MA. Mechanotransduction and extracellular matrix homeostasis. *Nat Rev Mol Cell Biol* 2014.
23. Sorrentino G, Rezakhani S, Yildiz E, et al. Mechano-modulatory synthetic niches for liver organoid derivation. *Nat Commun* 2020;11:1–10.

24. Broutier L, Andersson-Rolf A, Hindley CJ, et al. Culture and establishment of self-renewing human and mouse adult liver and pancreas 3D organoids and their genetic manipulation. *Nat Protoc* 2016;11:1724–1743.
25. Wong VW, Vergniol J, Wong GL, et al. Diagnosis of Fibrosis and Cirrhosis Using Liver Stiffness Measurement in Nonalcoholic Fatty Liver Disease. 2009:454–462.
26. Alper PB, Mutnick D, Bursulaya B, et al. Discovery of Tropifexor (LJN452), a Highly Potent Non-bile Acid FXR Agonist for the Treatment of Cholestatic Liver Diseases and Nonalcoholic Steatohepatitis (NASH). 2017.
27. Iruarizaga-lejarreta M, Varela-rey M, Fern D, et al. Role of Aramchol in Steatohepatitis and Fibrosis in Mice. 2017;1:911–927.
28. Staels B, Rubenstrunk A, Noel B, et al. Hepatoprotective Effects of the Dual Peroxisome Proliferator-Activated Receptor Alpha/Delta Agonist, GFT505, in Rodent Models of Nonalcoholic Fatty Liver Disease/Nonalcoholic Steatohepatitis. 2013;305707:1941–1952.
29. Ratziu V, Harrison SA, et al. Elafibranor, an Agonist of the Peroxisome Proliferator-Activated Receptor- α and $-\delta$, Induces Resolution of Nonalcoholic Steatohepatitis Without Fibrosis Worsening. *Gastroenterology* 2016;150:1147–1159.
30. Harrison SA, Wong VWS, Okanoue T, et al. Selonsertib for patients with bridging fibrosis or compensated cirrhosis due to NASH: Results from randomized phase III STELLAR trials. *J Hepatol* 2020;73:26–39.
31. Frenette CT, Morelli G, Shiffman ML, et al. Emricasan Improves Liver Function in Patients With Cirrhosis and High Model for End-Stage Liver Disease Scores Compared With Placebo. *Clin Gastroenterol Hepatol* 2019;17:774-783.e4.
32. Denayer T, Stöhrn T, Roy M Van. Animal models in translational medicine: Validation and prediction. *New Horizons Transl Med* 2014.
33. Kim J, Koo B. Human organoids: model systems for human biology and medicine. *Nat Rev Mol Cell Biol* 2020;21.
34. Wen Y, Jeong S, Xia Q, et al. Role of osteopontin in liver diseases. *Int J Biol Sci* 2016.
35. Dobin A, Davis CA, Schlesinger F, et al. STAR: Ultrafast universal RNA-seq aligner. *Bioinformatics* 2013.
36. Anders S, Pyl PT, Huber W. HTSeq-A Python framework to work with high-throughput sequencing data. *Bioinformatics* 2015.

5.7 Supplementary information



Supplementary Figure 1. Gene interaction network. Interaction network of differentially upregulated genes in the stiff matrix (fold change >1.5, FDR < 0.05) was generated with STRING. The network comprises 45 nodes and connected with 43 edges (PPI enrichment p-value:5.55e-16).

A**B**

Supplementary Figure 2. GO annotation of differentially expressed genes. Differentially upregulated (A) and downregulated (B) expressed genes in the stiff matrix (fold change>1.5, FDR<0.25) were processed for GO BP annotation enrichment using DAVID. Different clusters are marked with enrichment score (ES).

Extended Data Table 1. Functional annotation of genes significantly upregulated in stiff matrices versus normal matrices, in terms of signaling pathways.

ID	Description	setSize	enrichmentScor	NES	pvalue	p.adjust	qvalues	rank
hsa00830	Retinol metabolism	38	0.8619	2.2417	0.0017	0.0198	0.0141	840
hsa04142	Lysosome	116	0.7083	2.2053	0.0016	0.0198	0.0141	2072
hsa00140	Steroid hormone biosynthesis	32	0.8592	2.1934	0.0017	0.0198	0.0141	840
hsa04976	Bile secretion	48	0.7444	2.016	0.0017	0.0198	0.0141	1191
hsa00040	Pentose and glucuronate interconversions	20	0.8514	1.9748	0.0018	0.0198	0.0141	1066
hsa04978	Mineral absorption	40	0.7524	1.9715	0.0017	0.0198	0.0141	1441
hsa05204	Chemical carcinogenesis	47	0.7305	1.968	0.0017	0.0198	0.0141	1892
hsa00053	Ascorbate and aldarate metabolism	17	0.8602	1.9251	0.0018	0.0198	0.0141	949
hsa00982	Drug metabolism - cytochrome P450	38	0.7352	1.9122	0.0017	0.0198	0.0141	1543
hsa04610	Complement and coagulation cascades	38	0.7326	1.9054	0.0017	0.0198	0.0141	1472
hsa00980	Metabolism of xenobiotics by cytochrome P450	42	0.717	1.8955	0.0017	0.0198	0.0141	1543
hsa04140	Autophagy - animal	131	0.5958	1.8946	0.0015	0.0198	0.0141	1676
hsa00860	Porphyrin and chlorophyll metabolism	29	0.7555	1.8814	0.0018	0.0198	0.0141	1140
hsa04514	Cell adhesion molecules	78	0.6362	1.8636	0.0016	0.0198	0.0141	1248
hsa00601	Glycosphingolipid biosynthesis - lacto and neolacto series	19	0.8052	1.8483	0.0018	0.0198	0.0141	658
hsa04621	NOD-like receptor signaling pathway	125	0.5831	1.8417	0.0015	0.0198	0.0141	1530
hsa04145	Phagosome	98	0.5989	1.8143	0.0016	0.0198	0.0141	1969
hsa04137	Mitophagy - animal	67	0.6292	1.7951	0.0017	0.0198	0.0141	1640
hsa00052	Galactose metabolism	24	0.7372	1.7836	0.0018	0.0198	0.0141	1124
hsa05323	Rheumatoid arthritis	59	0.6266	1.748	0.0017	0.0198	0.0141	1830
hsa04060	Cytokine-cytokine receptor interaction	111	0.5567	1.7269	0.0016	0.0198	0.0141	1109
hsa05142	Chagas disease	75	0.5891	1.7173	0.0016	0.0198	0.0141	2135
hsa05144	Malaria	20	0.7368	1.7089	0.0018	0.0198	0.0141	2119
hsa00760	Nicotinate and nicotinamide metabolism	27	0.6922	1.7081	0.0018	0.0198	0.0141	165
hsa05152	Tuberculosis	120	0.5452	1.706	0.0015	0.0198	0.0141	1969
hsa04612	Antigen processing and presentation	48	0.6288	1.7029	0.0033	0.0239	0.017	1422
hsa04061	Viral protein interaction with cytokine and cytokine receptor	35	0.6631	1.6932	0.0035	0.0239	0.017	1484
hsa05321	Inflammatory bowel disease	36	0.6579	1.6924	0.0034	0.0239	0.017	2101
hsa04979	Cholesterol metabolism	29	0.6766	1.6849	0.0018	0.0198	0.0141	1096
hsa04062	Chemokine signaling pathway	112	0.539	1.677	0.0015	0.0198	0.0141	2096
hsa00600	Sphingolipid metabolism	42	0.6338	1.6755	0.0034	0.0239	0.017	1627
hsa04966	Collecting duct acid secretion	17	0.7481	1.6744	0.0092	0.0461	0.0328	1830
hsa04913	Ovarian steroidogenesis	26	0.6725	1.6524	0.0088	0.0451	0.0321	1261
hsa05120	Epithelial cell signaling in Helicobacter pylori infection	57	0.5923	1.641	0.0034	0.0239	0.017	2135
hsa04216	Ferroptosis	35	0.6425	1.6407	0.0052	0.0306	0.0218	1441
hsa04668	TNF signaling pathway	100	0.5391	1.6383	0.0032	0.0239	0.017	1631
hsa04650	Natural killer cell mediated cytotoxicity	71	0.5644	1.6363	0.0065	0.0347	0.0248	1604
hsa04721	Synaptic vesicle cycle	47	0.6054	1.631	0.0067	0.0347	0.0248	1936
hsa04380	Osteoclast differentiation	92	0.5441	1.6288	0.0032	0.0239	0.017	1966
hsa05211	Renal cell carcinoma	66	0.5665	1.6103	0.0067	0.0347	0.0248	2334
hsa04931	Insulin resistance	94	0.5336	1.6059	0.0047	0.0304	0.0216	1619
hsa05131	Shigellosis	209	0.4762	1.5926	0.0015	0.0198	0.0141	1975
hsa04670	Leukocyte transendothelial migration	77	0.5411	1.5813	0.0049	0.0304	0.0216	1604
hsa04659	Th17 cell differentiation	74	0.5416	1.5793	0.0064	0.0347	0.0248	2135
hsa04012	ErbB signaling pathway	76	0.5339	1.557	0.0065	0.0347	0.0248	2179
hsa04144	Endocytosis	227	0.4554	1.5255	0.0015	0.0198	0.0141	2604
hsa04217	Necroptosis	111	0.4815	1.4937	0.0093	0.0461	0.0328	1521
hsa05132	Salmonella infection	216	0.4393	1.4738	0.0015	0.0198	0.0141	2135
hsa05168	Herpes simplex virus 1 infection	407	0.395	1.3948	0.004	0.0271	0.0193	3800
hsa04310	Wnt signaling pathway	118	-0.4955	-1.6362	0.0057	0.0326	0.0232	1596
hsa04115	p53 signaling pathway	68	-0.5328	-1.6384	0.0051	0.0306	0.0218	2149
hsa03008	Ribosome biogenesis in eukaryotes	71	-0.5342	-1.6501	0.0052	0.0306	0.0218	3778
hsa00240	Pyrimidine metabolism	49	-0.6024	-1.7315	0.0049	0.0304	0.0216	717
hsa03420	Nucleotide excision repair	45	-0.6328	-1.7857	0.0025	0.0229	0.0164	2345
hsa03460	Fanconi anemia pathway	50	-0.6191	-1.7957	0.0049	0.0304	0.0216	2384
hsa00670	One carbon pool by folate	17	-0.7952	-1.8703	0.0065	0.0347	0.0248	1633
hsa03440	Homologous recombination	39	-0.6823	-1.8888	0.0024	0.0229	0.0164	1904
hsa03410	Base excision repair	33	-0.7142	-1.8912	0.0024	0.0229	0.0164	1767
hsa03430	Mismatch repair	22	-0.7764	-1.9242	0.0022	0.0227	0.0162	2154
hsa03013	RNA transport	150	-0.5721	-1.9629	0.0029	0.0237	0.0169	3062
hsa03040	Spliceosome	130	-0.5974	-2.0174	0.0029	0.0237	0.0169	3105
hsa04110	Cell cycle	119	-0.6207	-2.0537	0.0028	0.0237	0.0169	1137
hsa03030	DNA replication	35	-0.8023	-2.1739	0.0023	0.0229	0.0164	1804
hsa05171	Coronavirus disease - COVID-19	180	-0.6439	-2.2559	0.0029	0.0237	0.0169	906
hsa03010	Ribosome	130	-0.8549	-2.887	0.0029	0.0237	0.0169	906

Chapter 6 Conclusion and perspective

Organoids, 3D structures that can self-organize under specific microenvironmental cues, are a new class of biological model systems that have garnered significant interest for their application in disease modeling, drug screening, and regenerative medicine^{1,2}. Current organoid systems models rely on animal-derived Matrigel—an ill-defined gelatinous basement-membrane protein mixture composed of laminin, collagen IV, entactin, heparan sulfate, and numerous growth factors³—as the 3D matrix. The batch-to-batch variability, the risk of pathogen carryover, and the inability to modify its key physical and biochemical properties make this matrix unsuitable for clinical applications. Although these culture systems have been important for identifying molecules and niche signals (such as Wnt/R-spondin, regulating stem cell maintenance and differentiation), they do not allow manipulation of ECM components and, accordingly, of their effect on specific tissues. Instead, synthetic matrices with minimal batch to batch variation, that provide better control over their components, allow control of organoid formation efficiency and proliferation, and thus expedite the organoid production and disease modeling⁴⁻⁷.

Our laboratory has demonstrated successful derivation of mouse intestinal organoids within PEG hydrogels crosslinked *via* human Factor XIIIa, a natural transglutaminase⁸. These enzymatically crosslinked PEG matrices have served as an important starting point to characterize the growth requirements of mouse intestinal stem cells (ISCs) and of the organoids generated from them, revealing for example the important role of gel stiffness in controlling multiple steps of *in vitro* organogenesis. Yet, the complexity of the hydrogel crosslinking chemistry, as well as the high costs and batch-to-batch variability associated with the crosslinking enzyme FXIIIa, arguably limit the broader applicability of these gels. Accordingly, I adopted a similar rationale to design a simpler and more robust hydrogel crosslinking chemistry based on Michael addition reactions between thiols and vinyl sulfone - a highly modular “click” reaction⁹. To this end, I modified the conventional crosslinking strategy of PEG-co-peptide hydrogels formed by Michael addition of bis-cysteine peptides and vinyl sulfone (VS)-terminated PEG macromers¹⁰ to substantially reduce network defects and thus enhance the gel’s physicochemical properties at low solid content. These hydrogels, named Low Defect Thiol-Michael Addition (LDTM) hydrogels, could form at unusually low solid content and with higher bioactive ligand concentration than what was achievable with previously existing systems. Indeed, hydrolytically degradable LDTM gels (2.5% (w/v)) with an initial stiffness of ~ 1kPa allowed mISC colony formation, and, through gradual softening over 4 days of culture and switching to differentiation medium, they promoted budding of the colonies and organoid formation. Furthermore, I demonstrated successful derivation of human intestinal organoids in these matrices in the absence of any animal-derived laminin. Inclusion of laminin-111 further improved organoid formation capacity.

In agreement with other studies^{8,11,12}, we found laminin as an indispensable component of organoid cultures. Yet, the animal origin of the laminin used in these studies hampers successful translation

of organoid technology from the lab to the clinic. In Chapter 3, I thus explored the possibility of replacing animal-derived laminin with its recombinant counterpart. I demonstrated that incorporation of recombinant full-length laminin in LDTM matrices permits mouse intestinal organoid formation, albeit to a lower extent than natural laminin. Yet, the minimal fragment of laminin conferring integrin-binding properties was not sufficient to induce organoid budding alone. In addition to direct laminin-receptor interactions, another important interaction is provided by connection of agrin to laminin. Agrin, has indeed been shown to augment laminin anchorage both *in vitro* and *in vivo*¹³. Therefore, inclusion of agrin may enhance the effect of laminin fragments on intestinal organogenesis. Moreover, laminin is the major component of basement membranes, and its role in promoting organogenesis may span beyond mere integrin binding. Indeed, the basement membrane is known to be formed by laminin and collagen networks linked by entactin and heparan sulfates¹³. Future studies should thus target laminin in concert with other basement membrane proteins, mainly entactin and collagen IV. Importantly, future experiments need to address the intracellular events triggered by laminin-based adhesion in the optics of organoid biology, which underly the crucial role of this protein. Outstanding questions remain, for instance, on why RGD/fibronectin-based adhesion is sufficient for expanding mouse ISCs in the presence of strong Wnt and Notch signals, whereas laminin-111 is essential for mouse ISC differentiation and morphogenesis into intestinal organoids. Could such differential requirements be explained by engagement with different integrin receptors? If so, could the effects of the full proteins be replaced by selective stimulation of integrins, perhaps even using synthetic ligands?

In Chapter 4, I applied a strategy similar to the one used for intestinal organoids, to hepatic organoids. I cultured ductal organoids in synthetic matrices with a stiffness that matched the physiological stiffness of the liver (≈ 1.3 kPa¹⁴) and included RGDSCPG peptides, the minimal integrin recognition motif of fibronectin. The organoids derived in such PEG-RGD gels could be differentiated towards hepatocytes; yet, their development still fell short of reaching full maturity (primary hepatocyte identity, even in Matrigel culture). I speculate that the inclusion of collagen to mimic the physiological hepatocyte niche would enhance hepatocyte differentiation. Moreover, organoid growth was found to be highly stiffness-sensitive and dependent on yes-associated protein 1 (YAP) activity. However, and in contrast to intestinal organoids⁸, stiffness sensitivity was independent of acto-myosin contractility and required instead activation of the Src family of kinases (SFKs)/YAP axis. Finally, I showed the successful derivation of biopsy-derived human liver organoids in these hydrogels without any animal-derived components, thus making this approach fully compatible with clinical applications. A recent study from Sampaziotis *et al*¹⁵, showed that liver ductal organoids can repair bile ducts after transplantation in the human liver. This proof of principle, along with our method to generate clinical grade organoids, opens up exciting opportunities for cell-based therapy as a therapeutic alternative for adult liver transplantation.

In Chapter 2 and 4, I discussed how to leverage the modularity of synthetic matrices to mimic physiological ECMs. Similarly, the ECM also plays a key role in the progression of disease, and its composition, structure, and mechanical properties change during pathological processes. In fact, the importance of developing organoid disease models based on the ECM and the manipulation of its mechanobiological properties is highlighted by the fact that developing therapies *via* strategies

based on soluble factor signaling pathway inhibitors has been mostly unsuccessful, especially for what concerns fibrosis in epithelial tissues¹⁶. To this aim, in Chapter 5, I demonstrated the role of tissue stiffness on a regenerative mechanism in the liver, namely ductular reaction (DR). I used liver ductal organoids as an *in vitro* model of DR to study the effect of the fibrotic mechanical environment, a feature most often neglected in fibrosis models. Culture of human liver ductal organoids in LDTM gels with stiffness values matching those of fibrotic liver led to reduced organoid proliferation compared to growth in hydrogels with physiological stiffness. Transcriptomic analysis of these organoids revealed enrichment of gene sets related to inflammation and cell cycle. Indeed, differentially upregulated genes were involved in pathways such as inflammatory response and bile secretion, while differentially downregulated genes were involved in cell cycle and Wnt signaling pathways. These results indicated impaired stemness and regenerative potential of cholangiocytes, and concomitant induction of stress responses. Targeting affected pathways and identifying molecular mechanisms through which cell-matrix interactions regulate ductular liver regeneration may allow new strategies to enhance this process and, as such, inform novel regenerative and antifibrotic therapies. Incorporating hepatic stellate cells and portal fibroblasts, the major cells contributing to fibrogenesis, would further increase the complexity and accuracy of the model.

In chapters 2, 4 and 5, I discussed the importance of the mechanical properties of ECM in intestinal and hepatic organoid formation, as well as the use of modular hydrogel systems to probe their effects. However, stiffness is not sufficient to capture all cell-relevant aspects of ECM mechanics. The native ECM and natural ECM-based gels such as collagen and Matrigel, are not linearly elastic. Rather, they exhibit more complex mechanical behaviors, such as viscoelasticity, shown to be important regulators of a range of cellular phenomena^{18,19}. Incorporating viscoelastic responses into next-generation synthetic matrices for organoid culture would make them more physiologically realistic, and thus potentially improve the growth and maturation of epithelial organoids. Indeed, the necessity of mechanical softening of PEG hydrogels for the formation of intestinal organoids^{8,20} likely stems from the need to dissipate the compressive stresses that occur due to the growth of ISC colonies within such purely elastic environments. Engineered viscoelastic, stress-dissipative behavior would likely permit organoid formation within matrices of a constant stiffness, thus eliminating the need for complex, mechanically dynamic hydrogels. Moreover, the recapitulation of the spatiotemporal aspects of ECM changes during fibrosis would benefit from biomaterials capable of dynamic changes in mechanical properties, or from the ability to spatially pattern their stiffness¹⁷.

Overall, using novel bioengineering platforms to define the role of the ECM on organoid culture would shed light on a crucial yet previously overlooked facet of intestinal and hepatic niches. Departing from one-size-fits-all animal-derived gels and moving toward well-defined designer matrices tailored to the needs of a specific model system will likely further enhance the maturation and functionality of tissues grown *in vitro* and expedite their application to cell-based therapies and regenerative medicine. Comprehensive knowledge of ECM requirements for the growth of organoids will also provide clues on how the ECM contributes to developmental and

regenerative programs *in vivo* and will help us understand how ECM regulation is coopted and circumvented in the context of malignant and inflammatory disease.

References

1. Clevers H. Modeling Development and Disease with Organoids. *Cell* 2016;165:1586–1597.
2. Rossi G, Manfrin A, Lutolf MP. Progress and potential in organoid research. *Nat Rev Genet* 2018;19:671–687.
3. Kleinman HK, Martin GR. Matrigel: Basement membrane matrix with biological activity. *2005*;15:378–386.
4. Gjorevski N, Ranga A, Lutolf MP. Bioengineering approaches to guide stem cell-based organogenesis. *Development* 2014;141:1794–804.
5. Yin X, Mead BE, Safaei H, et al. Engineering Stem Cell Organoids. *Stem Cell* 2016;18:25–38.
6. Murrow LM, Weber RJ, Gartner ZJ. Dissecting the stem cell niche with organoid models: an engineering-based approach. *Development* 2017;144:998–1007.
7. Kim J, Koo B. Human organoids: model systems for human biology and medicine. *Nat Rev Mol Cell Biol* 2020;21.
8. Gjorevski N, Sachs N, Manfrin A, et al. Designer matrices for intestinal stem cell and organoid culture. *Nature* 2016;539:560–564.
9. Cruz-Acuña R, Quirós M, Farkas AE, et al. Synthetic hydrogels for human intestinal organoid generation and colonic wound repair. *Nat Cell Biol* 2017;1–6.
10. Lutolf MP, Hubbell J a. Synthesis and Physicochemical Characterization of End-Linked Poly (ethylene glycol) -co-peptide Hydrogels Formed by Michael-Type Addition. *Biomacromolecules* 2003;4:713–722.
11. Brogiere N, Isenmann L, Hirt C, et al. Growth of Epithelial Organoids in a Defined Hydrogel. *Adv Mater* 2018;30.
12. Ye S, Boeter JWB, Mihajlovic M, et al. A Chemically Defined Hydrogel for Human Liver Organoid Culture. *Adv Funct Mater* 2020;30.
13. Hohenester E, Yurchenco PD. Laminins in basement membrane assembly. *Cell Adhes Migr* 2013;7:56–63.
14. Yin M, Woollard J, Wang X, et al. Quantitative assessment of hepatic fibrosis in an animal model with magnetic resonance elastography. *Magn Reson Med* 2007;58:346–353.
15. Sampaziotis F, Muraro D, Tysoe OC, et al. Cholangiocyte organoids can repair bile ducts after transplantation in the human liver. *2021*;846:839–846.
16. Lampi MC, Reinhart-king CA. Targeting extracellular matrix stiffness to attenuate disease: From molecular mechanisms to clinical trials. *2018*;0475:1–15.
17. Davidson MD, Burdick JA, Wells RG. Engineered Biomaterial Platforms to Study Fibrosis. *Adv Healthc Mater* 2020;9:1–20.
18. Chaudhuri O, Gu L, Klumpers D, et al. stem cell fate and activity. *Nat Mater* 2016;15:326–334.
19. Chaudhuri O. Viscoelastic hydrogels for 3D cell culture. *Biomater Sci* 2017;5:1480–1490.
20. Rezakhani S, Gjorevski N, Lutolf MP. Low-Defect Thiol-Michael Addition Hydrogels as Matrigel Substitutes for Epithelial Organoid Derivation. *Adv Funct Mater* 2020;30:1–12.

Curriculum Vitae



- **Motivated and dedicated researcher**
- **Experienced in developing stem cell- and organoid-based assays**
- **Good collaboration and communication skills**

EDUCATION

MAY 2016- MAY 2021

PhD in Chemistry and Chemical Engineering
EPFL, Lausanne, Switzerland

SEP 2012 - APR 2015

M.Sc in Chemical Engineering and Biotechnology,
EPFL, Lausanne, Switzerland GPA: 5.5/6

SEP 2007 - SEP 2011

B.Sc in Chemical Engineering
University of Tehran, Tehran, Iran GPA: 17.46/20

SKILLS

Lab Skills

- Assay development ((stem)-cell- or organoid-based)
- Cell Culture (adult stem cells, iPSC, cancer cells, immune cells)
- Organoid culture (mouse and human intestinal, pancreatic and hepatic organoids)
- Performing cellular assays: ELISA, proliferation, etc.
- Polymer synthesis and hydrogel preparation
- Polymer chemical and mechanical characterization (NMR, rheometry)
- Microscopy (Brightfield, Confocal)
- Immunohistochemistry (IHC)
- Flow cytometry
- qPCR, bulk RNA-seq analysis
- Bioreactor design and operation

IT Skills

Image processing (ImageJ)
Project Management: Trello, Slack
Graphpad Prism
Adobe Illustrator
Programming languages: C++, Matlab, R (Basic)

Engineering Softwares

Aspen Hysys
Aspen Plus
Gambit and fluent

SABA REZAKHANI

Phone : +41-78-8372636 **Email :** rezakhani.saba@gmail.com **LinkedIn :** sabarezakhani

Address : Rue de la Borde 33, 1018 Lausanne, Switzerland **Date of Birth :** 04.04.1989

Marital status : Single **Residence Permit :** B

ABOUT

I am a chemical engineer by training, and currently doing research in the interface of biology and engineering to improve human systems. My research is focused on developing models and 3D culture systems to facilitate translational applications of organoids. I am a motivated researcher who is driven by direct impact on the human health. I am aspired to bring my expertise into real life applications and impact directly the research of future therapies.

PROFESSIONAL EXPERIENCE

MAY 2016 - MAY 2021

Doctoral assistant | EPFL | Switzerland

Laboratory of Stem Cell Bioengineering, Supervisor: Prof. Matthias Lutolf

- Developed synthetic hydrogels for clinically-relevant epithelial organoid culture
- 3D culture of human intestinal and hepatic organoids in synthetic hydrogels in the absence of any animal-derived components
- Developing epithelial organoid-based disease models for drug screening
- Supervised 3 students for their Master's thesis

SEP 2014 - SEP 2015

Research assistant | Harvard Medical School | USA

Karp Lab, Supervisor: Prof. Jeff Karp

- Developed cellular assays for quantifying potency of mesenchymal stem cell-derived extracellular vesicles (MSC-EVs).
- Optimized a filtration technique for extracellular vesicle isolation
- Systematic review and meta-analysis of therapeutic extracellular vesicles

FEB 2014 - AUG 2014

Research assistant | EPFL | Switzerland

Laboratory of Stem Cell Bioengineering

Identified a 3D hydrogel-based culture environment for mesenchymal stem cell culture and established a perfusion co culture with hematopoietic stem cells on a microfluidic chip

AUG 2013 - FEB 2014

Intern | Merck Serono | Switzerland

Manufacturing Technical Support, Supervisor: Dr. Veronique Deparis

Evaluation of a new small scale perfusion bioreactor for Rebif (interferon beta-1a) production

AUG 2013 - FEB 2014

Research assistant | EPFL | Switzerland

Cellular Biotechnology Laboratory, Supervisor: Prof. Florian Wurm

CHO culture in bioreactor

HONORS & AWARDS

JAN 2019

Selected as a representative of EPFL for Global Young Scientist Summit, Singapore

FEB 2018

Awarded a grant from Swiss Federal Institutes of Technology board to organize a summer school: New Frontiers in Extracellular Matrix Research, Zurich, Switzerland

AUG 2015

Selected among several hundred applicants to participate at Novartis international Biocamp, Basel, Switzerland

JUL 2015

Selected as Lab member of the month, Karp Lab, Harvard Medical School, Boston, US

SEP 2011

Ranked 7th among over 100 students in the Chemical Engineering Department at the end of 8th semester; awarded full scholarship, graduate Program, University of Tehran, Tehran, Iran

SEP 2010

Awarded the FOE Award (Faculty of Engineering Award, an award given to recognize top-ranked students) at the end of 6th semester; University of Tehran, Tehran, Iran

LANGUAGES

English: Fluent
French: B1
German: A1
Farsi: Mother tongue

HOBBIES / INTERESTS

Learning a new language
Humanitarian volunteering
Poetry
Playing piano
Swimming

REFERENCES

- Prof. Matthias Lutolf
Head of Laboratory of Stem Cell Bioengineering, EPFL
matthias.lutolf@epfl.ch
- Dr. Giovanni Sorrentino
Head of Laboratory of Cancer and Stem Cell Biology,
University of Trieste
giovanni.sorrentino@units.it
- Dr. Kelvin Songyu Ng
Head of Strategic Innovation, A*STAR, Singapore
kelvinnng.mit@gmail.com

ADDITIONAL COMPETENCIES

Teaching and supervising

- Teaching assistant for graduate courses:
Advanced separation processes
Pharmaceutical Biotechnology
Biomaterials
- Supervised three students for their Master's theses

Project Management

Managing an EU-funded project (Intestinal Tissue ENgineering Solution, www.intens.ino) for which I had to write progress reports, collaborate with other partners, attend the meetings and present the project progress.

Fundraising and networking

Awarded a grant, and got sponsors for organizing an international summer school (<https://archiveweb.epfl.ch/ecmatrix.epfl.ch/>)

Leadership

Managing the team of organizers for an international summer school, and as a vice president of Iranian student association, organized several multicultural events

PATENTS

Three-dimensional models of tissue fibrosis. S. Reza khani, G. Sorrentino, E. Yildiz, K. Schoonjans, M. Lutolf. . EP Patent Application Nr 19177445.4

PUBLICATIONS

S. Reza khani, N. Gjorevski, M. Lutolf. Low-Defect Thiol-Michael Addition Hydrogels as Matrigel Substitutes for Epithelial Organoid Derivation. *Adv. Func. Mater.* 2020, 2000761.

S. Reza khani, **G. Sorrentino**, et al. Mechano-modulatory synthetic niches for liver organoid derivation. *Nat Commun* 11, 3416 (2020).

J. Buess, M. Biocanin, J. Pezoldt, R. Dainese, **S. Reza khani**, et al. Deterministic scRNA-seq of individual intestinal organoids reveals new subtypes and coexisting distinct stem cell pools. *BioRxiv* 103812.

D. Blondel, A. Chrisnandy, **S. Reza khani**, et al. Synthetic dynamic hydrogels promote degradation-independent in vitro organogenesis. *Nat. Mater.* In revision.

PRESENTATIONS

OCT 2020

Poster presentation

EMBL Symposium, Organoids: Modelling Organ Development and Disease in 3D
Mechano-modulatory synthetic niches for liver organoid derivation

MAY 2019

Oral presentation

6th IBI Symposium, Rostock, Germany
Mechano-modulatory synthetic niches for liver organoid culture

JAN 2019

Poster presentation

Global Young Scientist Summit, Singapore
Synthetic hydrogels for epithelial organoid culture

"Now this is not the end. It is not even the beginning of the end.

But it is, perhaps, the end of the beginning."

- Winston Churchill

